Investigating the Role of Oligomeric State in Chimeric Antigen Receptor Function Using *de novo* Designed Transmembrane Structures.

PhD Thesis

Nicholas Chandler

ORCID: 0000-0003-4093-7503

Supervisors:

Associate Professor Dr Matthew E. Call and Dr Melissa J. Call

March 2021

The Walter and Eliza Hall Institute of Medical Research

Department of Medical Biology

Faculty of Medicine, Dentistry and Health Sciences The University of Melbourne

Thesis submitted in total fulfilment of the requirements for the degree of Doctor of Philosophy

Table of Contents

Declaration

This is to certify that:

1. I) This thesis comprises only my original work except where indicated in the Preface.
2. II) Due acknowledgements have been made in the text to all other materials used.
3. III) The thesis is less than 100,000 words in length, exclusive of tables, bibliographies, figures and appendices.

Nicholas Chandler

March 2021

Acknowledgements

I first owe a huge amount of gratitude to Matt and Mel for their supervision and support over the last 5 years of my PhD and honours studies. The Calls were the absolute perfect fit for me as an incredibly unpolished student at the beginning of my honour's year and I truly don't think any other combination of supervisors could have fostered my growth as a scientist like they have. I still remember the moment in the first week of my honours year when I innocently asked them if they 'wanted a hand in the lab so that they could leave by 5:00pm?', only to be met with raucous laughter. While perhaps a red flag in any other workplace, I soon realised the cruel trap laid by the Calls for me and other students in the lab, was to ignite a passion for science and then set us free in pursuit of answers.

To my partner Annie: thank you for the unconditional love and support you've given me through thick and thin of this PhD, effortlessly distracting me from my science failures and equally preventing me from getting a big head when science is going well. To Mum, Dad and Bonnie thank you for the years and years of support you've shown for me as the weird nerd of the family. It's incredibly comforting how I've never felt an ounce of pressure to do anything but follow my interests, because of that I've enjoyed every minute of my studies and I'm glad I'll get to celebrate soon with you all! I also owe a huge thanks to undoubtedly my biggest fans Gran, Nan and Pa. I'm certain that everyone at Watergardens shopping centre knows I'm doing a PhD and it spurs me on every day knowing how proud you all are.

The past and present members of the Call lab are huge contributors to the enjoyment I've experienced during the course of my PhD. The Turf-era Call lab of Cyrus, Raph and Loges taught me the unofficial ropes of science during tissue culture and late nights at the pub and played an instrumental role in convincing me that a PhD could be rewarding and still enjoyable. I consider myself fortunate that with the changing of the guard the post-Turf era Call lab of Sam, Ash, Julie, Anna, Jess, Daniel, Josh, Margareta have continued to provide a workplace that is a joy to come into every day. I owe huge thanks to Ash and Julie for joining the CAR project seamlessly and being incredibly humble teachers, mentors and work mates. Special mention also to Sam who I've been lucky enough to share the experience of doing a

PhD with, I still remember the relief I felt in my first week in the lab with you when I realized your dark sense of humour outpaced even mine or Raph's.

Acknowledgement is also owed to the structural biology division as a whole for providing such a fantastic environment to work in every day. It's a testament to the culture of our division that we decide to spend so much time socialising together, from joker poker at the turf to the shaving of heads at the Christmas party, it's hard to forget the amazing times I've shared with you all – Jase, Katrina, Liau, Angus, Cal, Rich, Rhiannon, Katherine, Ruth, Catia, Kaiseal, Nick Kirk, Kristen, Michelle. A special nod also to the honorary structural biology members and my scientific elders Christoph, Erin and Margs. Given you're all leaving the country soon you'll sadly miss my repayment of post-doc beers, but I can't wait to meet up with you all overseas and repay the favour (with favourable exchange rates)!

Thanks to each and every one of my friends for the support they've given me and the memories we've shared over the past 4 years. Thanks to my Tennyson St housemates G, Cal, Laurie, Steen, Anna, Katherine, Katlin, Andres, Rik and Inge who were always there to cheer me up and share a drink after 12-hour days in the lab. A huge thanks to Tsig, Claudia, Mick, Leo, Rox, Will, Sair, Tanya, Greg, Zoe, Lucy and Max, you've all embraced the joy of T cells as well as millions of my other enthusiastic, half-baked social adventures and I'm incredibly grateful to count you all as my closest friends.

A big thanks to Sarel Fleishman, Assaf Elazar and Jonathan Weinstein from the Weizmann institute in Israel, a unique group of extremely talented yet eternally modest collaborators. Without them this project would never have been possible.

The work of the C3 crystallization facility in Parkville was essential to this work, in particular Janet Newman and Bevan Marshall and their infectious love of protein crystallography. The same thanks are owed to the MX beamline scientists at the Australian synchrotron as well as Mike Mlodzianoski and Stephen Mieruszynski for their assistance with microscopy experiments.

Thanks also to Amanda Voudouris, Keely Bumstead-O'brien and Sue Hardy for everything they do behind the scenes and for their calm help during my inevitable annual panic dealing with PhD candidature administration.

I would like to acknowledge also the support and advice from me PhD committee Phil Hodgkin, Mike Lawrence and Misty Jenkins. The scientific support of Misty and her lab members has been particularly important for this project and their willingness to answer CAR T cell questions and assist in the establishment of experiments was instrumental to our success.

I'm also eternally grateful for the willingness of Doug Hilton and WEHI to provide me with a PhD scholarship after my honours year. I've never taken my position at WEHI for granted and I hope my contributions to the WEHI science and social community have justified that decision.

Last but not least, I would like to acknowledge the traditional owners of the land on which WEHI lies, the land of the Wurundjeri people of the Kulin nation. I pay my respects to elders past, present and emerging and acknowledge their continued connection to this country.

Preface

In accordance with the regulations of the University of Melbourne, I acknowledge the following contributions by past and current members of the Call laboratory, by researchers of the Walter and Eliza Hall Institute of Medical Research and by collaborators at the Weizmann Institute of Science, Israel. Acknowledgement is also made through-out the text where relevant.

I) All proMP sequences were designed by Sarel Fleishman and colleagues Assaf Elezar and Jonathon Weinstein at the Weizmann Institute of Science.

II) Cloning of proMP2.1 and proMP2.2 sequences into the pTrpLE bacterial expression vector was conducted by Raphael Trenker, a former PhD student within the Call lab.

III) The crystal structures of proMP2.1 and proMP2.2 were solved and refined with assistance from Melissa Call.

IV) Cloning, expression, purification and crystallisation of proMP3.2 and proMP4.1 was conducted by Julie Ngyuen. X-ray crystallography and structure determination of these peptides was conducted by Julie Ngyuen and Melissa Call.

V) Isolation of CD8+ primary mouse T cells and generation of primary mouse CAR T cells was carried out by Ashleigh Davey, a post-doctoral researcher within the Call lab. Primary CAR T cell cytotoxicity and cytokine release assays were conducted by Ashleigh Davey, with assistance provided by Nicholas Chandler acknowledged in place within the text.

VI) A section of text on page 21-22, section 1.1, was adapted from published work previously written by Nicholas Chandler and Matthew Call (Chandler et al., 2020). This published work was written by Nicholas Chandler, with proof-reading and editing contributed to by Nicholas Chandler, Matthew Call and Melissa Call.

Publications

[2,4*]**Chandler, N. J.**, [2,4*]Call, M. J. & Call, [2,4*]M. E. 2020. T Cell Activation Machinery: Form and Function in Natural and Engineered Immune Receptors. *Int J Mol Sci,* 21.

Assaf Elazar[1,*], **Nicholas J. Chandler[2,4,*],** Ashleigh S. Davey[2,4,*], Jonathan Y. Weinstein[1] , Julie V. Nguyen[2] , Raphael Trenker[2,4], Misty R. Jenkins[3,4, 5], Melissa J. Call[2,4,#,] Matthew E. Call[2,4,#] and Sarel J. Fleishman[1,#], 2020. *De novo* designed receptor transmembrane domains enhance CAR-T cell cytotoxicity and attenuate cytokine release. *BioRxiv*. (Non-peer-reviewed)

1. Department of Biomolecular Sciences, Weizmann Institute of Science, Rehovot, Israel.
2. Structural Biology Division, The Walter and Eliza Hall Institute of Medical Research, Parkville, Victoria 3052, Australia
3. Immunology Division, The Walter and Eliza Hall Institute of Medical Research, Parkville, Victoria 3052, Australia
4. Department of Medical Biology, The University of Melbourne, Parkville, Victoria 3052, Australia
5. La Trobe Institute of Molecular Science, La Trobe University, Bundoora, Victoria 3083, Australia

*Equal first authors
#Equal senior and corresponding authors

List of Figures

List of Tables

Acronyms and Abbreviations

AICD	Activation-induced Cell death
ADCC	Antibody-dependent cell-mediated cytotoxicity
APC	Allophycocyanin
ATP	Adenosine tri-phosphate
B-ALL	B-cell Acute Lymphoblastic Leukemia
BCR	B-cell receptor
BTLA	B- and T-lymphocyte attenuator
CAR	Chimeric antigen receptor
CBA	Cytokine bead array
CD	Cluster of differentiation
CRISPR	Clustered Regularly Interspaced Short Palindromic Repeats
CRS	Cytokine release syndrome
Cryo-EM	Cryogenic electron microscopy
Csk	C-terminal Src kinase
CTLA-4	Cytotoxic T-lymphocyte-associated protein 4
CNBR	Cyanogen Bromide
DAP	DNAX-activating protein
DMEM	Dulbecco's modified eagle medium
DNA	Deoxynucleic acid
dsTbL	deep sequencing ToxR-b-lactamase
EC	Extracellular
ER	Endoplasmic reticulum
ERK	Extracellular signal-regulated kinase
EGFR	Epidermal growth factor receptor
FACS	Fluorescence-activated cell sorting
FcRg	Fc receptor gamma
FDA	Food and Drug Administration
GADS	GRB2-related adaptor protein 2
eGFP	enhanced Green fluorescent protein
GM-CSF	Granulocyte-macrophage colony-stimulating factor
GpA	Glycophorin A
Grb2	Growth factor receptor-bound protein 2
HBS	Hepes buffered saline

HEK293T	Human embryonic kidney 293T cells
HER2	Human epidermal growth factor receptor 2
HFIP	Hexafluoroisopropanol
HPLC	High performance liquid chromatography
HRP	Horseradish peroxidase
HVEM	Herpes virus entry mediator
ICOS	Inducible T-cell costimulatory
IFN	Interferon
IgSF	Immunoglobulin superfamily
IL	Interleukin
IPTG	Isopropyl β-D-1-thiogalactopyranoside
IRES	Internal ribosomal entry site
IS	Immune Synapse
ITAM	Immunoreceptor tyrosine-based activation motif
Itk	Interleukin-2-inducible T-cell kinase
IVT	*In vitro* translation
JAK	Janus kinase
kDa	Kilodalton
KIR	Killer Ig-like receptor
KIR2DS2	Killer Ig-like receptor two Ig domains and short cytoplasmic tail 2
LFA-1	Lymphocyte function-associated antigen 1
Lck	Lymphocyte-specific protein tyrosine kinase
LCP	Lipidic cubic phase
LDS	Lithium dodecyl sulfate
MHC	Major histocompatibility complex
mRNA	Messenger RNA
MSCV	Murine stem cell virus
MC38	Mouse colon 38
MCF7	Michigan Cancer Foundation 7
mTCM	mouse T cell media
MMTS	methyl methanethiosulfonate
NK	Natural killer
NKG2D	Natural killer group 2 member D
NOD	Non-obese diabetic

N&B	Numbers and brightness
Nck	Non-catalytic region of tyrosine kinase adaptor protein 1
NFκB	Nuclear factor kappa B
NKG2D	Natural Killer Group 2D
NMR	Nuclear Magnetic Resonance
OD_{600}	Optical density at 600 nm
PDB	Protein Data Bank
PD-1	Programmed death receptor 1
PI3K	Phosphoinositide 3-kinase
PKC	Protein kinase C
PBS	Phosphate buffered saline
pMHC	Peptide-bound major histocompatibility complex
proCAR	programmed Chimeric Antigen Receptor
proMP	programmed Membrane Protein
PVDF	Polyvinylidene fluoride
QSOX2	Human sulfhydryl oxidase 2
RPMI	Roswell park memorial institute
RMSD	Root mean square deviation
scFv	Single-chain variable fragment
SCID	Severe combined immune deficiency
SDS	Sodium dodecyl sulfate
SH2	Src-homology 2
SHP-1	Src homology 2 domain-containing protein tyrosine phosphatase 1
STAT	Signal Transducer and Activator of Transcription protein
TbL	ToxR-b-lactamase
TBSt	Tris buffered saline tween-20
TCR	T cell receptor
THEMIS	Thymocyte-expressed-molecule
TIRF	Total internal reflection fluorescence
TM	Transmembrane
TMD	Transmembrane domain
TNF	Tumor necrosis factor
TNFR	Tumor necrosis factor receptor
TNFRSF	Tumor necrosis factor receptor Superfamily

TRAF	TNF receptor associated factor
TFA	Trifluoro-acetic acid
ZAP-70	Zeta-associated protein 70

Abstract

Chimeric antigen receptor (CAR) T cell therapy has revolutionized the treatment of B cell malignancies by redirecting patient T cells to destroy cancer cells using engineered receptors. While CAR T cell therapies hold enormous potential as treatments in a wide range of tumour settings, treatments for non-B cell cancers have largely failed to significantly improve patient outcomes thus far. Furthermore, CAR therapies carry significant risk of inducing cytokine release syndrome (CRS), a potentially deadly toxicity caused by excessive release of inflammatory cytokines. The ability to minimize toxicity whilst maintaining adequate tumour cell-killing is therefore vital to the continued improvement of CAR therapies. We aimed to investigate the currently ill-defined relationship between CAR oligomeric state and potency using a novel protein engineering approach, with the aim of leveraging this knowledge to predictably modulate CAR activity.

With *de-novo* protein design collaborators we identified synthetic transmembrane domain (TM) sequences that predictably formed defined homo-oligomeric structures. In addition to a previously validated trimeric TM sequence, I used X-ray protein crystallography to determine the structure of a dimeric TM peptide that agreed closely with its predicted structure. I inserted these novel oligomeric TM sequences into a well-established anti-HER2 CAR construct (comprising an anti-HER2 scFv attached via stalk/TM to costimulatory and stimulatory tail sequences) and validated their oligomeric state and signalling capacity in a mouse T cell line. When expressed in primary mouse T cells and incubated with HER2+ target cells, dimeric and trimeric CARs exhibited enhanced target cell killing compared to a reference anti-HER2 CAR. Using an *in vivo* mouse tumour model it was subsequently demonstrated that CAR oligomeric state correlates positively with CAR T cell anti-tumour efficacy. CARs encoding synthetic oligomeric TM's also demonstrated a dramatic reduction in the release of inflammatory, CRS-associated cytokines within *in vitro* experiments. Using rational TM sequence mutations I identified lateral interactions between CARs and the endogenous T cell costimulatory molecule CD28 in primary mouse T cells as the key determinant of CAR cytokine release. These findings present an opportunity to improve efficacy and safety of CAR T cell therapies and warrant further validation in other clinically relevant CAR T cell disease models.

Chapter 1 Chimeric Antigen Receptor (CAR)-T Cell Immunotherapy and the CAR Structure/Function Relationship

The adaptive immune system provides highly specific and efficient protection from infectious agents. However, the development of cancer is inextricably linked to an inability of immune cells to recognise tumour cells and/or launch a sufficiently strong immune response. From the very earliest discoveries outlining the biological mechanisms underlying immune evasion in tumorigenesis it was evident that modulation of these processes would have enormous therapeutic potential. Many avenues of therapeutic intervention have been explored, with great success coming in the form of approaches that harness the potent anti-tumour activity of T cells. One of the earliest therapeutic approaches to achieve success was known as checkpoint inhibition, where antibodies are used to block T cell inhibitory molecules such as PD-L1 and CTLA-4, expressed on the surface of tumours or T cells, respectively, that are upregulated to prevent immune clearance (Ishida et al., 1992, Dong et al., 1999, Brahmer et al., 2012, Hodi et al., 2010). In addition to checkpoint inhibition, autologous T cell therapies have also emerged as a powerful immunotherapeutic tool in certain disease settings. These therapies involved extracting T cells from tumour biopsies, activating and expanding them *ex vivo* before readministering them to the patient with high doses of the mitogenic cytokine IL-2 (Rosenberg et al., 1988, Rosenberg et al., 1994). This approach achieved remarkable success in the treatment of metastatic melanoma, which has a high burden of tumour antigens, however the application of this approach to other tumour settings has proved largely unsuccessful.

Chimeric antigen receptor (CAR) T cell therapy was developed to extend and improve upon these early autologous T cell therapies, as a means of redirecting and enhancing a patient's immune response to a specific, chosen cancer antigen. Fundamentally, this therapy involves the ectopic expression of a cancer-antigen-specific CAR gene in patient T cells. These T cells undergo expansion and hyper-activation *ex vivo* and when re-introduced to the patient they can drive potent anti-tumour cytotoxicity (Fig 1.1A). First-generation CAR designs built upon the observation that exchanging the variable domains of TCR$\alpha\beta$ with those of a monoclonal antibody could successfully redirect T cell activation towards a desired antigen (Gross et al., 1989). Subsequently it was demonstrated that the CD3ζ tail sequence in the absence of

CD3ε, δ and γ was capable of eliciting powerful T cell activation (Irving and Weiss, 1991). The distillation of these dual observations resulted in the design of what are now referred to as first-generation CARs, which consisted of a high-affinity cancer-specific antibody single-chain variable fragment (scFV) fused in frame with the N-terminus of the CD3ζ immune signalling chain (Fig1.1B) (Eshhar et al., 1993). Engagement of a CAR scFv with its cognate ligand resulted in the phosphorylation of immunoreceptor tyrosine-based activation motifs (ITAMs) within the CD3ζ tail of the CAR, thus initiating downstream T cell signalling and T cell effector functions (Eshhar et al., 1993, Stancovski et al., 1993). These first-generation designs showed significant activity *in vitro*, however two key improvements were instrumental in translating this concept into a clinical success. Firstly, the inclusion of a flexible stalk region connecting the transmembrane (TM) domain to the scFv significantly improved antigen sensitivity (Finney et al., 1998, Moritz and Groner, 1995), presumably due to better reach and ability to bind different epitopes. Secondly, the inclusion of an auxiliary signalling tail adapted from an endogenous T cell costimulatory molecule (generally either CD28 or 4-1BB) greatly improved the quality and duration of the T cell response in patients (Maude et al., 2015, Savoldo et al., 2011b, Brentjens et al., 2013). These key advancements were instrumental in the clinical success of the first two FDA-approved anti-CD19 CAR T cell therapies, axicabtagene ciloleucel and tisagenlecleucel (trade names Yescarta® and Kymriah®, respectively), now recommended for the treatment of a range of advanced and refractory B cell leukemias (Geyer, 2019, Bouchkouj et al., 2019).

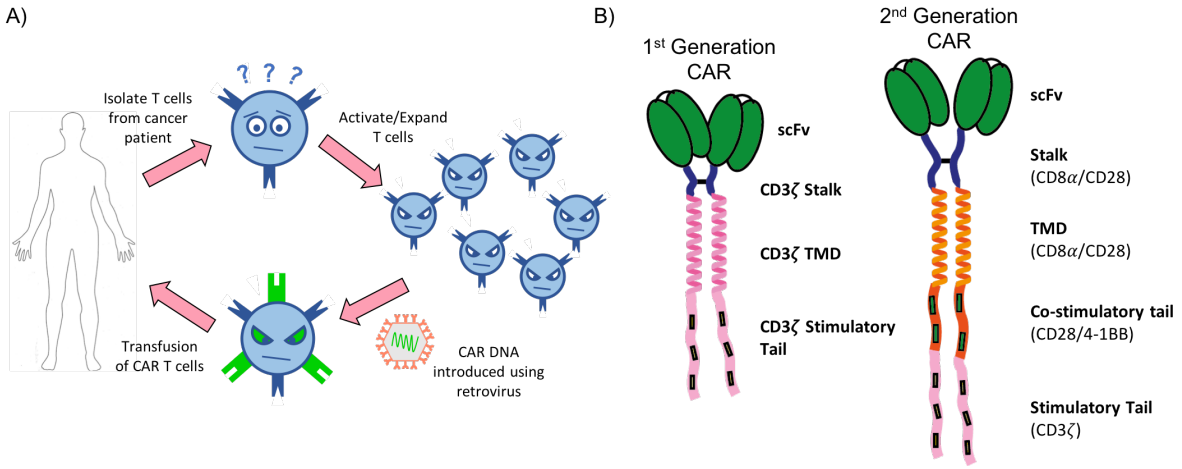

Figure 1.1 CAR T cell therapy *A) Flowchart detailing the process involved in clinically approved CAR therapies. Briefly, T cells are isolated from patient blood, activated and expanded, retrovirally transduced with a desired CAR and then further expanded to yield a pure population of CAR+ T cells. T cells are then readministered to the patient, resulting in rapid tumour clearance. B) domain architecture of a 1st and 2nd generation CAR. Inclusion of CD28/4-1BB costimulatory tail sequences and CD8α/CD28 stalk/TM sequences were instrumental in achieving clinical success of CAR T cell therapy. Listed in brackets are the native proteins from which conventional CAR domains are derived. Receptor is depicted as a disulfide linked homodimer, black line linking stalk sequences indicates presence of disulfide linkage. Boxes within tail segments indicate signalling motifs.*

However, the success of CAR-T therapies in other cancer contexts has been limited, and a significant technical hurdle is the optimization of the quality and potency of CAR signalling (reviewed in (June et al., 2018)). For example, insufficient CAR potency may be responsible for the lack of success in targeting tumours expressing relatively low levels of antigen (Majzner et al., 2020). Additionally, if CAR signalling is too weak, the expansion and persistence of CAR-T cells within the body is reduced, resulting in ineffective treatment. Conversely, CAR-T cells that are too sensitive or delivered at too high a dose can release harmful levels of inflammatory cytokines such as IL-2, IL-6, IFN-γ and GM-CSF, subsequently stimulating bystander immune cell cytokine release resulting in potentially life-threatening neurotoxicity or systemic Cytokine Release Syndrome (CRS) (Neelapu et al., 2018). In the clinic, IL-6 blocking monoclonal antibody (tocilizumab, Roche) treatment and reduced T cell number per dose has mitigated these toxicities, however these remain a major limitation in

CAR safety. Excessive CAR signalling can also result in T cell exhaustion and apoptosis (Long et al., 2015), which is a significant concern given the strong correlation between T cell persistence and clinical efficacy in the treatment of haematological malignancies (Porter et al., 2015). Thus, it has become clear that the ability to modulate CAR potency may hold the key to improving the safety of currently available treatments and broadening the scope of treatable cancers moving forward. Whilst additional layers of control have been afforded to CAR activity in recent years thanks to several novel and extravagant engineering approaches, the broad utility of these approaches is hampered by the requirement for complex re-engineering of CAR constructs and T cells, often involving delivery of multiple transgenes and/or CRISPR deletion of endogenous T cell genes (Lim and June, 2017, Roybal and Lim, 2017, Labanieh et al., 2018).

In contrast, several recent studies have elegantly detailed how improving the understanding of the fundamental receptor biology of CARs can guide optimization of their structural features and signalling domains. Such efforts have resulted not only in findings with potential to provide immediate clinical benefit, but also act to strengthen our understanding of fundamental receptor biology and offer an insight into immune receptor engineering rules with broad scope to improve not just CARs, but receptor engineering efforts in general.

1.1 Controlling CAR function through signalling domain number/configuration and affinity tuning

The inclusion of costimulatory tail sequences to first-generation CAR designs was central to achieving the improved in-vivo expansion and persistence required for anti-tumor efficacy in patients (Maude et al., 2014, Savoldo et al., 2011a, Brentjens et al., 2013). Preclinical comparisons of CD19 CARs containing CD28, DAP10, 4-1BB or OX40 costimulatory sequences in a single study (Brentjens et al., 2007) found that the CD28 tail uniquely supported antigen-specific *in vitro* T cell expansion and strong cytokine production. In the context of a mesothelin-targeted CAR, CD28 and 4-1BB tails both supported effective tumor control in mice, but CD28 yielded faster eradication and 4-1BB uniquely supported long-term CAR-T cell persistence (Carpenito et al., 2009).

These results have generally been borne out in the context of the FDA-approved CD19 CARs, for which there is now a great deal of patient data showing that while overall response rates are similar, 4-1BB-containing CARs mediate slower tumor rejection but cause less cytokine toxicity and persist for longer (Majzner and Mackall, 2019). However, the molecular mechanisms underpinning these functional differences have only recently begun to be systematically dissected. While there exists an extensive body of preclinical work comparing the functionality of CAR costimulatory sequences, determining the precise contribution of these domains has been confounded by the varied use of hinge and TM domains between CAR constructs. This was primarily because spacer and/or TM domains were often (but not always) transferred along with the costimulatory tails (Brentjens et al., 2007, Finney et al., 1998, Maher et al., 2002, Zhao et al., 2015b). As described in detail in section 5.1, there is a growing appreciation of the relevance of hinge and TM sequences to CAR function, and this is a significant confounding factor when not accounted for systematically.
Such a systematic approach was undertaken in a recent study comparing signaling downstream of CD28 and 4-1BB tail sequences in the context of otherwise identical CD19 CARs (Sun et al., 2020). They found that enhanced Lck recruitment amplifies both basal and antigen-induced phosphorylation in the CD28-containing CAR, while the unique ability to recruit phosphatase SHP1 (in a THEMIS-SHP1 complex) suppresses basal phosphorylation and attenuates antigen-induced phosphorylation in the 4-1BB-containing CAR. Importantly, the authors went on to show that engineering SHP1 recruitment into the CD28-containing CAR could ameliorate cytokine toxicity without sacrificing overall efficacy, emphasizing the utility of gaining detailed mechanistic understanding for engineering better therapies.

In addition to the optimization of CAR costimulatory domains, various other novel engineering approaches have been utilized to tackle challenges presented by cancers characterized by over-expression of endogenous growth receptors such as HER2. In this case the targeting of a cancer antigen that is also present on healthy tissue can result in potentially life-threating off-tumour cytotoxicity (Morgan et al., 2010). It was recently shown that by deliberately reducing the affinity of a HER2-specific scFv, selectivity could be achieved for tumours expressing high levels of HER2 while sparing healthy cells that express low levels of HER2 (Fig 1.2A) (Liu et al., 2015). Furthermore, it has recently been shown that reducing the affinity of an anti-CD19 CAR could reduce the frequency and severity of toxic

side-effects (Ghorashian et al., 2019) without losing cytotoxic potency as long as antigen levels on tumour cells are high.

In addition to affinity tuning approaches, a handful of studies have sought to untangle the relationship between CAR potency and the number of stimulatory Immunoreceptor Tyrosine-based Activation Motifs (ITAMs) present within the CAR CD3ζ tail (Fig 1) (James, 2018). The CD3ζ tail which contains 3 ITAMs, was compared in early studies to a number of single ITAM-containing stimulatory tails, such as that of FcRIg. CD3ζ was consistently shown to be the most potent activator of cytotoxicity (Haynes et al., 2001) and for this reason the CD3ζ tail is now used almost ubiquitously within the CAR field. However, one recent study has cast doubt over the 'one size fits all' use of the native CD3ζ sequence. Feucht *et al.* (2020) used an anti-CD19 CAR design currently used in the clinic (comprising a CD28 stalk, TM and tail followed by CD3ζ) and via point mutations generated constructs leaving only certain combinations of the CD3ζ ITAMs functionally intact (Fig 1.2B). They found that the use of a single intact ITAM at the membrane-proximal position possessed the greatest *in vivo* efficacy in a mouse tumour model in comparison to single ITAMs at more membrane distal positions and even a traditional CAR containing all 3 ITAMs. Upon further investigation, improved efficacy was attributed to the acquisition of a clinically favourable memory T cell phenotype and reduced T cell exhaustion in CARs containing only the membrane-proximal ITAM. Importantly, this study used the nalm6 tumour cell line which expresses very high levels of CD19 relative to other documented CD19+ cell lines.

While indications currently approved for treatment by CAR therapy also exhibit high CD19 expression, there are a number of B cell cancers that express significantly lower levels and may not support optimal responses from conventional CAR T cells. For this reason, a more recent study by Majzner et al (2020) investigated the relationship between CAR potency and ITAM number in the context of a range of CD19 expression levels. Nalm6 cell lines were generated with a wide range of CD19 expression levels, and low CD19 expression correlated with significantly reduced cytotoxicity *in vitro*. Additionally, it was observed that CARs with a single membrane-proximal ITAM were capable of killing $CD19^{high}$ targets, but these were significantly less effective when targeting $CD19^{low}$ tumour targets. Extending these findings,

it was also shown that the linear insertion of an additional CD3ζ chain increased the potency of a previously ineffective CAR in against $CD19^{low}$ targets. These studies provide a strong fundamental basis for the modulation of ITAM number and membrane proximity as a means of controlling CAR T cell quality and potency. Furthermore, they imply that there are significant clinical benefits to be attained if potency can be matched to the requirements of a given tumour setting. However, an aspect of CAR design which may impact the broader application of these findings, and yet has received very little systematic investigation, is the effect of oligomeric state upon CAR signalling output.

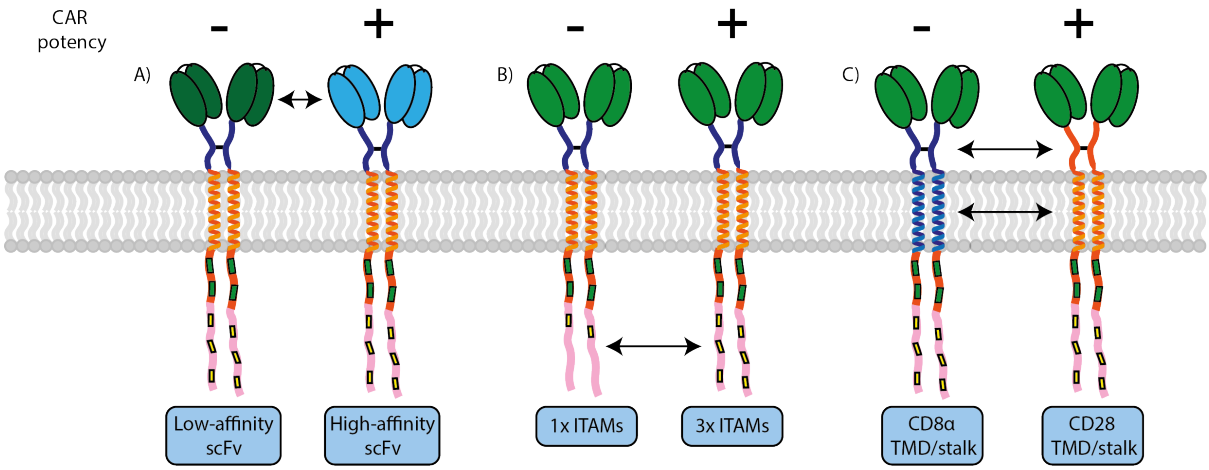

Figure 1.2. Leveraging fundamental biology of 2nd generation CAR design to control potency. *Affinity tuning of scFv affinity (A), titration of CD3ζ ITAMs encoded per CAR (B) and CD8a vs. CD28 stalk/TM selection (C) are all approaches demonstrated capable of controlling CAR T cell potency. Both increases and decreases to CAR T cell potency can provide therapeutic benefit in specific tumour contexts. Black line linking stalk sequences indicates presence of disulfide linkage.*

1.2 Higher-order structures in CARs and the influence of stalk/TM sequences

In each of the aforementioned studies, either a CD8a or CD28 stalk were used, both of which contain cysteine residues responsible for the stabilisation of covalent dimers within their respective source proteins. Rigorous functional comparisons of CAR stalk sequences (where nothing else is varied) are lacking in the literature, however there is circumstantial evidence to suggest that stalk-cysteine-mediated CAR dimerization is positively correlated with CAR potency (Fitzer-Attas et al., 1998, Bridgeman et al., 2010). It was only recently,

however, that this phenomenon was more directly investigated in the context of current-generation CAR designs. Salzer et al. (2020) observed when covalent dimerization was prevented via mutation of the CD8a stalk cysteine, both cytotoxic potential and cytokine release were diminished compared to cysteine-sufficient dimeric CAR designs. There are two candidate explanations for this observation. Firstly, the key T cell activating kinase ZAP-70 is known to display enhanced activity due to transautophosphorylation when bound to CD3ζ tails arranged as dimers compared to single tail chains in experiments using purified proteins *in vitro* (Hatada et al., 1995). Hence, it may would be expected that CARs, in which CD3ζ tails are presented as dimers, may provide the most favourable binding scaffold for ZAP-70 activity. A second and non-mutually exclusive explanation for increased potency of dimeric CARs is that an increase in the oligomeric state of a receptor at the cell surface proportionally increases the number of signalling tails able to be engaged by a single ligand. In the case of the CARs described by Salzer et al (Salzer et al., 2020), a single ligand engaging a monomeric CAR would engage one signalling tail encoding 3 CD3ζ ITAMS, whereas a single ligand engaging a dimeric CAR would engage 2 signalling tails encoding 6 CD3ζ ITAMs. Interestingly, natural immune receptors seem to have evolved to harness this concept as a means of modulating receptor potency according to ligand availability (Fig 1.3). For example, the TCR, which is responsible for signalling in response to pMHC molecules at potentially vanishingly low densities (Irvine et al., 2002, Purbhoo et al., 2004, Huang et al., 2013), assembles as an octameric complex encoding 10 ITAMs (Fig 1.3A) (Dong et al., 2019, Call et al., 2002). By comparison, other immune receptors such as NKG2D and KIR, responsible for binding far more abundant ligands, assemble as hexameric or trimeric complexes, respectively, that contain only 4 or 2 signalling motifs (Fig 1.3A) (Garrity et al., 2005, Feng et al., 2005). This underscores once again the power of using oligomeric assemblies to control the number of signalling tails that are available to be engaged by a single ligand.

In addition to the role of stalk dimerization on CAR function, there is growing evidence of a broader, sequence-specific influence of stalk/TM domains on CAR function. This was emphasized recently by several studies determining that replacing the CD8α stalk/TM domain of the commercial CAR tisagenlecleucel with that of CD28 dramatically improved

CAR potency in response to low-density ligand (Brudno et al., 2020, Alabanza et al., 2017, Majzner et al., 2020) (Stalk sequences listed in table 1, depicted Fig 1.2C)). The molecular mechanisms underlying this phenotype were not addressed in this study, and the independent contributions of TM versus stalk sequences were not investigated. However, given that both CD8α and CD28 stalk/TM domains drive equivalent degrees of receptor dimerization (Fujiwara 2020) it appears likely that this observed effect may derive from an alternative biological mechanism. These findings highlight the urgent need to disentangle the roles of stalk and TM sequences in CAR structure and function, which will inevitably provide a more nuanced, empirical understanding of the relationship between oligomeric state and CAR potency.

Table 1.1. Native human stalk and transmembrane domain sequences commonly used in 2nd generation CARs.

Native protein	Stalk sequence/Transmembrane sequence
CD8α	ALSNSIMYFSHFVPVFLPAKPTTTPAPRPPTPAPTIASQPLSLRPEA**C**R PAAGGAVHTRGLDFA**C**DIYIWAPLAGTCGVLLLSLVITLYC
CD28	**C**KIEVMYPPPYLDNEKSNGTIIHVKGKHL**C**PSPLFPGPSKPFWVLVVVG GVLACYSLLVTVAFIIF

** Stalk cysteine residues capable of disulfide bonding marked in bold/underlined.*

1.3 Developing tools to control CAR oligomerisation through TM domains

We predicted that by controlling CAR oligomeric state, we could modulate signalling output and expand the dynamic range of CAR signalling. Successfully achieving this goal of encoding deliberate and predictable control over CAR potency would consequently have the potential to enhance CAR therapies in two clinically relevant scenarios. Firstly, the ability to reduce CAR potency by expressing a monomeric CAR presents an opportunity to reduce the severity and incidence of harmful toxicities such as CRS. Additionally, combining oligomeric state manipulation with other engineering approaches has the potential to enable fine tuning of other low-potency CAR designs (Feucht et al., 2019, Brudno et al., 2020). The goal of the field is to pursue CAR therapies capable of achieving the lowest degree of toxicity while still eliciting maximal anti-tumour efficacy.

There are also several scenarios where an increase in CAR potency may be clinically desirable. For example, for a new antigen to be targeted by CAR T cell therapy, an scFv with sufficiently high binding affinity to induce cytotoxicity is required. If existing anti-tumour scFvs possess affinity below this empirical threshold, then the process of sufficiently improving affinity can be time-consuming and not guaranteed to succeed. Improving receptor potency by increasing the oligomeric state of the receptor could provide a simple means of overcoming this potency threshold. Furthermore, there has been significant interest in designing CARs capable of targeting oncogenic peptide targets presented by MHC molecules on the surface of tumour cells. While some pMHC-targeted CAR designs have shown promise using *in vivo* mouse models, none of these have entered clinical trials (Akatsuka, 2020) as of the time or writing this thesis. These peptide:MHC target molecules may exist at low concentrations on the cell surface and therefore CARs targeting these antigens could benefit significantly from the increased potency afforded by increased oligomeric state.

The natural assembly of modular immune receptor complexes such as the TCR through TM interactions highlights the possibility of using these domains to control CAR oligomeric state (Berry and Call, 2017, Call and Wucherpfennig, 2007). However, the direct use of natural receptor TM domains as a means of directing CAR oligomerization is potentially problematic due to their competing interactions with other proteins that are expressed in T cells. For example, first generation CAR designs including the CD3□TM and tail were incorporated into endogenous TCR complexes, an interaction facilitated by paired interactions of charged residues within the CD3□TM and TCRa (Bridgeman et al., 2010, Call et al., 2002). We therefore proposed to develop completely synthetic TM sequences capable of forming highly specific and highly stable oligomeric structures in cellular membranes through *de novo* protein design (Fig 1.3B). To achieve this goal, our lab collaborated with protein design expert Sarel Fleishman (Weizmann Institute, Israel), whose recent work on helical membrane protein energetics (Elazar et al., 2016a, Elazar et al., 2016b, Weinstein et al., 2019) forms the basis of improved membrane protein structure prediction and design tools. The aim of this collaboration was to generate a panel of transmembrane domain sequences capable of forming homotypic, oligomeric structures to be inserted into CAR constructs,

thereby encoding control of CAR oligomeric state. We termed this approach the 'programmed CAR' system (shortened herein to proCAR), referring to the act of programming CAR oligomeric state through TM domain design.

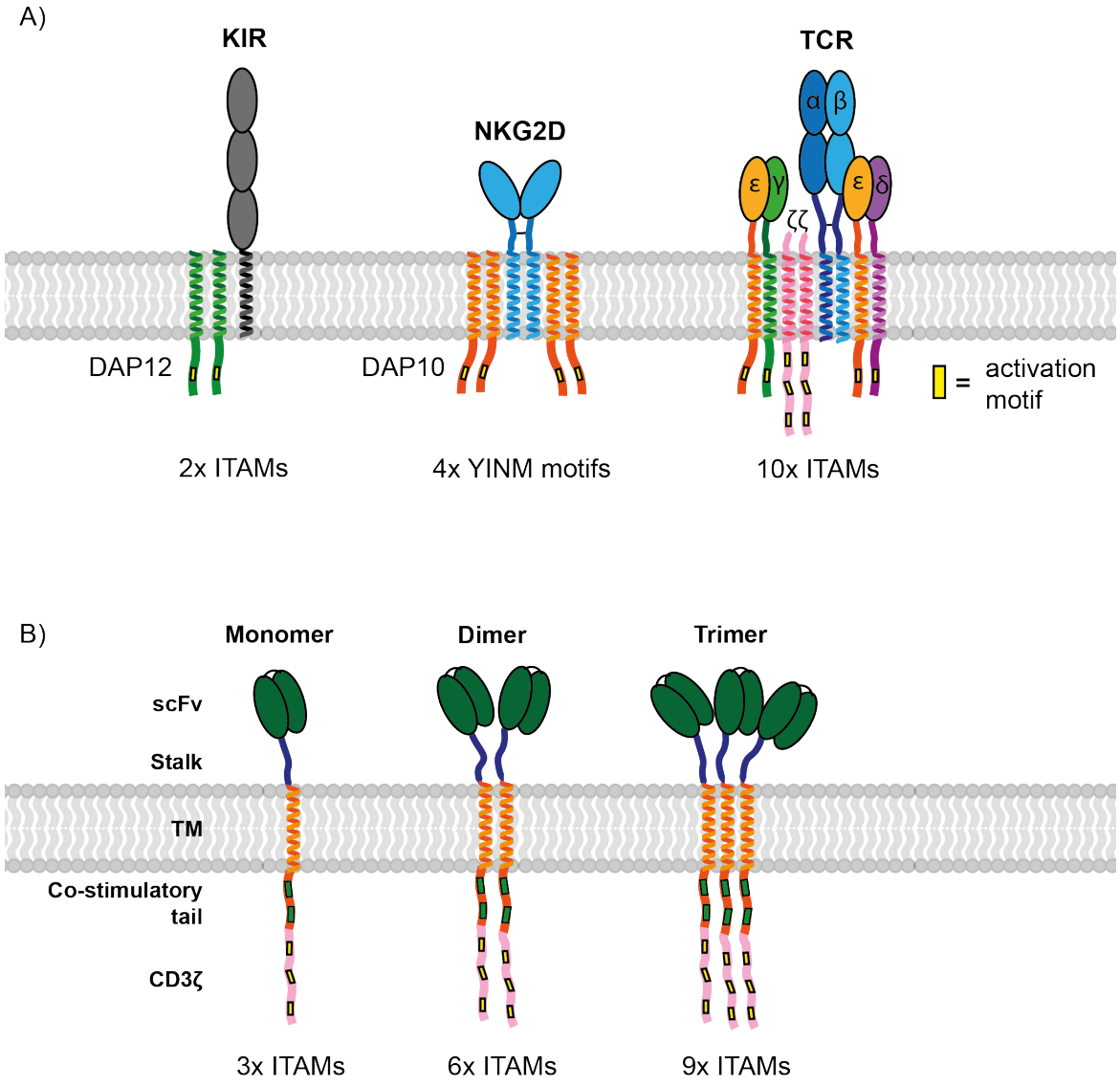

Figure 1.3. Controlling natural and engineered receptor potency via lateral recruitment of signalling tails. *A) Immune receptor potency is approximately correlated with the number of ITAMs found in native receptors. The TCR is capable of responding to single ligands on the cell surface, whereas KIR family receptors bind MHC ligands expressed abundantly at the cell surface. B) Our hypothesis is that by mirroring native immune receptor organisation, increasing the number of ITAMs per receptor complex will result in an increase in receptor potency.*

Encoding CAR oligomeric state via TM domain alterations also presented us with an opportunity to ask an important secondary question: do commonly used TM sequences influence CAR function? Despite the established relevance of TM sequence in native immune receptor structure and function (discussed in detail in chapter 3), the functional relevance of these same TM sequences in the context of CAR constructs remains poorly defined. However, several recent publications have suggested an important functional role for these 'framework' regions of CAR, with functional differences observed between CARs possessing CD8α vs. CD28 TM/stalk regions (Brudno et al., 2020, Majzner et al., 2020). However, the independent contributions of the TM and stalk sequences are yet to be empirically tested. The design of CAR constructs possessing TM domains capable of replacing commonly used native receptor TM domains whilst maintaining receptor oligomerisation presents an opportunity to independently determine the contribution of native TM sequence to CAR function.

1.4 Hypothesis and Aims

Given the relative lack of basic structure-function studies in the CAR design field, the hypotheses which defined my PhD studies were as follows:

1. CAR function is influenced by receptor oligomeric state.
2. Commonly used CAR TM domains have sequence-specific functional influence.

To adequately address these hypotheses several experimental aims were established, some of which were conducted by collaborators both within our Lab and elsewhere, and others which formed the core of my PhD studies and the work presented in this thesis. These aims are summarised below (visually represented in Fig 1.4), with reference made to aims where experimental contributions were made by other researchers within our team:

1. Validate candidate oligomeric sequences through experimental structure determination. (*De novo* TM domain design conducted by Sarel Fleishman, Assaf Elazar)

2. Characterise the expression, oligomeric state and function of a panel of oligomeric proCAR constructs *in vitro* using T cell lines.
3. Determine the ability of proCAR designs to drive cytotoxicity and cytokine release in primary mouse T cells. (Experiments conducted by Ashleigh Davey, assistance provided by Nicholas Chandler).

These experimental aims provided a framework for the work described herein. My role within this research team was to initiate structural investigations of *de novo* designed dimeric transmembrane domain (TMD) peptides and subsequently establish a robust *in vitro* experimental system capable of characterising an initial panel of oligomeric proCAR designs both biochemically and functionally using T cell lines. Inherent in these aims was the potential for observations of proCAR behaviour *in vitro* to inform the refinement of *de novo* TM design. Additionally, the establishment of a robust experimental system using mouse T cell lines presented an opportunity to elucidate mechanisms underlying proCAR phenotype in primary mouse T cells. In this regard, the ability of observations of proCAR phenotype in primary T cells to inform new CAR constructs capable of refining fundamental mechanisms of CAR function formed the basis for chapter 5 of this thesis.

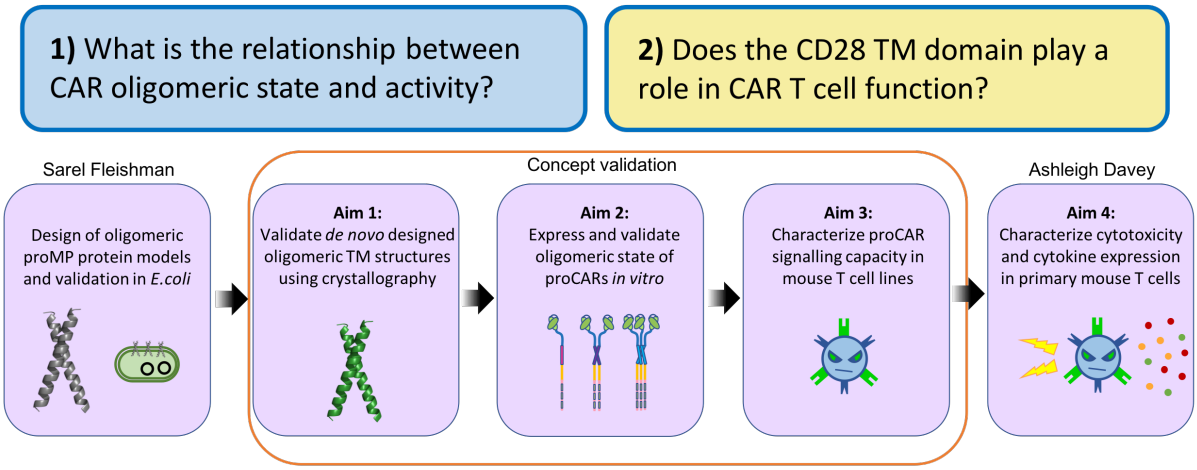

Figure 1.4. Visual presentation of hypotheses and aims. *Outline of the hypotheses and experimental outline of this project. Concept validation represented the portion of this project conducted by me. Collaborators who contributed significantly to aspects of this research pipeline are listed above their relevant experimental aim. Prof Sarel Fleishman was assisted by Dr. Assaf Elazar and Jonathan Weinstein.*

Chapter 2 Materials & Methods

General Cloning Procedures

Where necessary DNA sequences were constructed by overlap PCR or designed as synthetic double-stranded DNA fragments (G-blocks, Integrated DNA Technologies, IDT). Unless stated, PCR reaction parameters were as follows:

Table 2.1 General PCR reaction composition

PCR component	**Volume per 50µl reaction (µl)**
10x PCR buffer*	5
10mM dNTPs (NEB)	1
10ng/µl Template	1
10µM forward primer	1
10µM reverse primer	1
Phusion polymerase	1
MilliQ water	40

* 10x PCR buffer: 100 mM Tris pH 8.8, 500 mM KCl, 15 mM $MgCl_2$, 1% Triton X-100

All PCR reactions were conducted using a SimpliAmp Thermal Cycler (Applied Biosystems) and the cycling conditions described below unless otherwise stated:

Table 2.2 General PCR cycling conditions.

Step	Temperature (°C)	Duration	Repeat
Denaturation	95	2 min	1x
Denaturation Annealing Extension	95 52 72	30 s 30 s 1 minute/kb	25x
Extension	72	7 min	1x

PCR products were purified via agarose gel electrophoresis using 1% molecular-grade agarose gels supplemented with MidoriGreen (Nippon genetics) in 1x TAE buffer for 30-40 min at 110 V. DNA bands were visualised first with a ChemiDoc Touch gel imaging system (Bio-Rad) and subsequently under UV light. Desired bands were cut out using a scalpel blade and DNA was extracted using the Zymogen DNA Recovery Kit.

Oligonucleotides

Due to large number of oligonucleotides (IDT) used in the generation of the various constructs detailed below, these sequences are not listed but are available on request. Sequences are stored within a Call lab password protected online database and can be readily accessed.

Plasmid vectors

Table 2.3 plasmid vectors

Plasmid name	Antibiotic selection	Description
pTrpLE	Kanamycin	IPTG-inducible expression of peptides with a trpLE fusion tag. Plasmid used within Call lab is based on original pMM-LR6 plasmid.
pLVX-TRE3G	Ampicillin/puromycin	Retroviral vector for doxycycline-inducible expression of protein.
pMSCV-II-IRES-mCherry	Ampicillin	Retroviral expression vector used for expression of CAR constructs in mammalian cells.
pIVT (originally pSP64)	Ampicillin	Used for *in vitro* mRNA production driven by T7-promoter.

Restriction Endonuclease Digest

Restriction endonuclease digests were performed in a final volume of 50µl using 20 units of relevant enzyme (NEB) and 5µl supplied 10x restriction enzyme buffer (NEB) incubated at 37 °C for 1 h. In the case of double restriction digests, a buffer system recommended by the manufacturer's website was used (NEB Double Digest Finder). All vectors were treated with 0.2µl calf intestinal phosphatase (NEB) for the last 20 min of the digest to prevent re-ligation of vectors during the ligation step. Agarose gel electrophoresis was used to purify DNA fragments.

Ligation

Digested and gel purified DNA fragments and recipient plasmid vectors were combined at a molar ratio of 3:1 in a reaction mixture that contained: 1µl Quick Ligase (NEB), 5µl 2x Quick Ligation buffer*, 10µg/ml DNA final concentration, made up to 10µl with milliQ water. Reaction proceeded for 10 minutes at room temperature prior to transformation.

* 2x Quick Ligation buffer: 66 mM Tris-HCl, 10 mM $MgCl_2$, 1 mM dithiothreitol, 1 mM ATP, 7.5% polyethylene glycol (PEG6000), pH 7.6 @ 25°C.

Transformation

9µl of 10µg/ml DNA, either purified plasmid template or ligation reaction mixture, was added to 39µl milliQ water and 12µl KCM chemical transformation buffer*. This mixture was cooled on ice, mixed with 60µl of chemically competent stabl3 *E. coli* (NEB) and incubated on ice for at least 30 minutes. This mixture was then removed and rested at room temperature for 10 minutes prior to plating on agar plates for antibiotic selection.

* KCM buffer: 500 mM KCl, 150 mM $CaCl_2$, 250 mM $MgCl_2$

Cloning of peptide expression constructs for structural studies

DNA sequences of relevant peptides were ordered as double-stranded DNA G-blocks (IDT), codon optimized for expression in *E. coli*, with multiple peptides encoded in a single G-block and separated by HindIII and BamHI restriction digest sites. G-blocks were digested with with BamHI and HindIII and ligated into the trpLE expression vector, several clones were grown and sequenced using sanger sequencing to confirm presence and identity of peptide sequence.

Bacterial expression of peptides for structural studies

proMP containing pTrpLE expression vectors were transformed into KCM-competent BL21-DE3 *E. coli* and grown on LG-agar plates containing kanamycin (50 mg/L). Colonies were picked and added to M9 Minimal Media* starter cultures (equal to 1/10 of total volume) which were grown overnight at 37 °C shaking at 180 rpm. Starter cultures were then added to the desired final volume of M9 media and split 1L per flask. Cultures were grown at 37 °C, shaking at 140 rpm until reaching an optical density at 600 nm (OD_{600}) of 0.6. The incubator with cultures was then cooled to 18 °C while shaking for 1 h and protein expression was induced by addition of IPTG (Sigma-Aldrich) to a final concentration of 0.1mM. Cultures were shaken at 18 °C at 140 rpm o/n and harvested via centrifugation. Cell pellets were either stored at -30 °C or processed immediately as described below.

*M9 minimal media (per 1L): 3 g KH_2PO_4, 1 g NH_4Cl, 7.5 g Na_2HPO_4 (di-hydrate), 0.5 g NaCl, 4 g Glucose, 1 centrum tablet (GSK), 100 µl 1 M $CaCl_2$, 1 ml 2 M $MgSO_4$, 50 µg kanamycin

proMP peptide production

To aid purification, analysis and crystallisation, all designed sequences were modified to include Glu-Pro-Glu at the amino terminus and Arg-Arg-Leu-Cys at the carboxy terminus based on the favourable properties of the glycophorin A TM domain fragment, which crystallises rapidly in many test conditions (Trenker et al., 2015). C-terminal cysteine was included to permit fluorescent labelling, although such labelling was not used in the course of this project. Peptides were produced recombinantly as 9xHis-trpLE fusion proteins in *E. coli*. Cells were lysed in lysis buffer*, sonicated and centrifuged at 20,000 x g to pellet inclusion bodies. Importantly, the C-terminal Cys sulfhydryl group was protected during lysis using 10 mM S-methyl methanethiosulfonate (MMTS, Sigma-Aldrich). Inclusion bodies were then resuspended in guanidine buffer* and mixed for 4 hours to permit solubilization. Supernatant was filtered to remove debris, prior to being added to a Nickel-affinity matrix (Sigma Aldrich) equilibrated with guanidine buffer and mixed overnight. The following day this matrix was poured into a column and then washed with 10 column volumes (CV) urea wash buffer* and eluted with 2 x 1 column volumes of neat trifluoro acetic acid (TFA). TFA/protein mixture was then diluted with water to a final concentration of 80%v/v, mixed with 0.2g of cyanogen bromide per ml of TFA/protein mixture and allowed to react for 3.5 hours in a fume cupboard. Mixture was then dialyzed against water using a 3.5kDa dialysis cassette to remove and neutralise CNBr. The precipitated protein mixture was then lyophilized to form a white powder. Approximately 20mg of lyophilized digest products were dissolved in 1ml neat formic acid and purified using reversed phase high-performance liquid chromatography (RP-HPLC), performed using a Duo-Flow chromatography system equipped with a BioLogic QuadTec UV-Vis detector (Bio-Rad). Using a C8-semiprep column (Agilent technologies) all peptides were purified using a protocol involving a 4-column volume linear gradient from solvent A (80% H_2O, 20% ACN, 0.1% TFA) to solvent B (75% IPA, 25% ACN, 0.1% TFA). Peptide fractions were pooled and small samples of 15ml, 30ml and 45ml were taken for SDS-PAGE analysis. Pooled fractions containing pure peptides were then lyophilized and stored at room temperature until required.

*Bacterial lysis buffer: 200 mM NaCl, 50 mM Tris HCL, pH 8.0, 10mM MMTS

*Urea wash buffer: 8 M urea, 50 mM Tris HCL, 200 mM NaCl, 10mM MMTS

*Guanidine buffer: 6 M guanidine hydrochloride (GuHCl), 1% Triton X-100, 10 mM MMTS

LCP Crystallography

Peptides were dissolved in neat 1,1,1,3,3,3-Hexafluoro-2-propanol (HFIP, Sigma-Aldrich) prior to addition of the fatty acid monoolein. The volume of Monoolein was calculated so as to constitute 60% of the final LCP volume desired. Peptide amount was calculated according to a protein concentration of 40mg/ml of final LCP mixture. Ensuring all peptide and monoolein were dissolved the mixture was then lyophilized overnight. The resultant mixture was then heated at 52°C in a 1.5ml tube to form a viscous liquid at which point it was transferred to coupled 100µl gastight Hamilton syringes (Formulatrix) and combined with 20mM Tris buffered saline* (TBS). TBS volume added was equal to 40% of the final desired LCP volume. With monoolein and Tris buffer loaded in two ends of a dual syringe set-up the mixture was exchanged back and forwards until reaching a desired, transparent appearance. Upon reaching transparency the mixture was dispensed in 100nl drops onto 96-well glass plates (Molecular Dimensions) with 1µl of precipitant solution using a mosquito LCP robot (TTP Labtech) at room temperature. Plates were sealed and stored at 20°C in a Gallery 700 incubator coupled to a Minstrel HTUV imaging system (Rigaku) for monitoring crystal formation.

Crystals were harvested by cutting plastic seals with a hot scalpel (heated using a propane torch). Crystals were then frozen without adding cryo-solution/protection to the drop. A cryo-solution containing 60% glycerol was added to the drop to harvest further crystals. Data were collected at the Australian Synchrotron.
*TBS: NaCl 137mM, KCl 2.7mM, Tris base 20mM

Processing of crystal diffraction data

Data were collected on the MX2 beamline of the Australian Synchrotron at a wavelength of 0.9537 Å and a temperature of 100K. Data were indexed and scaled using XDS and Aimless (CCP4 program suite)(Winn et al., 2011, Kabsch, 2010). Structure factor amplitudes were obtained using cTruncate (CCP4 program suite)(Winn et al., 2011, Otwinowski and Minor, 1997). proMP2.1 and proMP2.2 crystal structures were solved with Phaser(McCoy et al., 2007) by molecular replacement using 5EH6 and 5EH6 mutated to the proMP2.2 sequence

respectively. Iterative rounds of refinement were conducted in PHENIX (Adams et al., 2010) with model building taking place in Coot (Emsley et al., 2010).

Cloning of CAR constructs for mammalian cell expression

Reference CAR construct was generously provided by Dr. Ryan Cross and A/Prof Misty Jenkins from the Walter and Eliza Hall institute. This construct consisted of the CD8α leader sequence (responsible for membrane localisation), FRP5 anti-HER2 scFv, CD8α stalk, CD28 TM/cytosolic tail domain and CD3ζ cytosolic tail; all sequences derived from human source. Stalk cysteine mutations as well as the generation of all CAR constructs with TM mutations (CD28TM mut) or TM insertions replacing the original CD28TM domain were all achieved using overlap PCR, outlined in the figure below (Fig 2.1). CAR fragments were ligated using EcoRI and XhoI restriction sites into the Murine Stem Cell Virus plasmid (pMSCV) containing an IRES-mCherry expression gene (pMIC II) or the pLVX-TRE3G doxycycline inducible expression vector.

A)

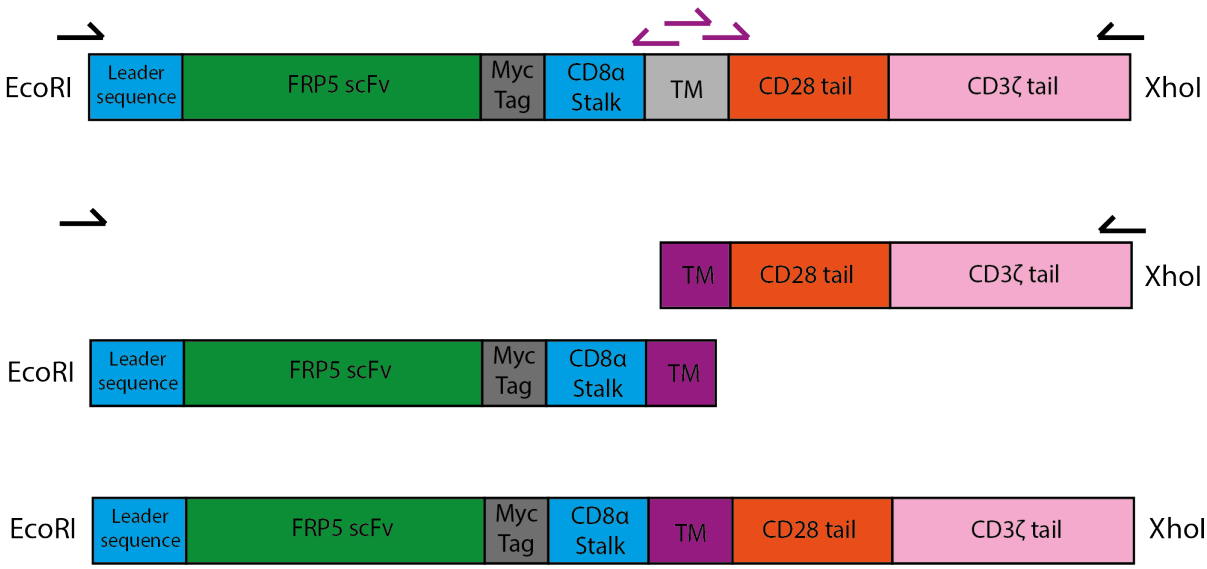

B)

MDFQVQIFSFLLISASVIMSRQVQLQQSGPELKKPGETVKISCKAS
GYPFTNYGMNWVKQAPGQGLKWMGWINTSTGESTFADDFKGRFDFS
LETSANTAYLQINNLKSEDMATYFCARWEVYHGYVPYWGQGTTVTV
SSGGGGSGGGGSGGGGSDIQLTQSHKFLSTSVGDRVSITCKASQDV
YNAVAWYQQKPGQSPKLLIYSASSRYTGVPSRFTGSGSGPDFTFTI
SSVQAEDLAVYFCQQHFRTPFTFGSGTKLEIEQKLISEEDLNGVTV
SSALSNSIMYFSHFVPVFLPAKPTTTPAPRPPTPAPTIASQPLSLR
PEA**C**RPAAGGAVHTRGLDPFWVLVVVGGVLACYSLLVTVAFIIFWV
RSKRSRLLHSDYMNMTPRRPGPTRKHYQPYAPPRDFAAYRSRVKFS
RSADAPAYQQGQNQLYNELNLGRREEYDVLDKRRGRDPEMGGKPRR
KNPQEGLYNELQKDKMAEAYSEIGMKGERRRGKGHDGLYQGLSTAT
KDTYDALHMQALPPR*

Figure 2.1 Cloning strategy and protein sequence of FRP5 construct construction for mammalian expression. *A) Cloning strategy used to generate proCARs from FRP5 Cys Mut CAR. B) Protein sequence of Reference FRP5 CAR, CD8α stalk cysteine is underlined and bold.*

Cell culture

BW5147 and Jurkat E6.1 T cells were both cultured in Roswell Park Memorial Institute (RPMI) media without Glutamine (Lonza) + 10% FBS (Bovogen biological) + 2mM L-glutamine (Gibco) (RPMI+ for short) and maintained at a density less than $1x10^6$ cells/ml. T cells were cultured at 36°C and 5% CO_2. HEK293T cells used for virus production were cultured in Dulbecco's Modified Eagle Medium (DMEM) without Glutamine (Lonza) + 10% FBS (Bovogen biological) + 2mM L-glutamine (Gibco) and cultured at 36°C and 10% CO_2. Primary Mouse T cells were cultured in mouse T cell medium (mTCM) consisting of Roswell Park Memorial Institute (RPMI) 1640 Medium (Gibco) supplemented with foetal bovine serum (10%; Bovogen Biological), L-glutamine (2 mM; Gibco), sodium pyruvate (1 mM; Gibco), non-essential amino acids (1x; Sigma-Aldrich), β-mercaptoethanol (50 µM; Sigma-Aldrich) and recombinant human IL-2 (100 IU/ml; PeproTech). Following removal of magnetic beads, T cells were maintained at $1x10^6$ cell/ml in mTCM.

Virus production

On day 0 HEK 293T cells were plated at $3x10^5$ cells per well in a 6-well plate. On Day 1 (transfection day) cells were inspected and confirmed to be at a density of between 60-70% confluence. Media was changed early in the day and 2 hours later DNA transfection mixture was added dropwise while mixing (mixture outlined below). On day 2 media was replaced with fresh media. On day 3 virus containing media was removed from the 293T cells and filtered using a 0.2µm filter unit and set aside for viral transduction.

Table 2.4 Transfection reaction mixture

Ingredient	Quantity
2X HBS	86µl
Transfer Plasmid (pMSCV II mCherry)[#]	1720ng (43µl)
GAG/Pol Packaging plasmid (psPAX2)[^]	460ng
MLV ecotropic envelope plasmid (mouse cell transduction)[^] or VSVg envelope plasmid (Human cell transduction)[^]	460ng
$CaCl_2$ (0.5M)	43µl

[#] Plasmid generously donated by A/Prof Doug Fairlie

[^] Plasmids generously donated by A/Prof Marco Herold

BW5147 NFκB reporter Cell line

The BW5147 NFκB reporter cell line was previously generated within the Call lab. This cell line was generated via retroviral transduction with a retroviral construct consisting of a gene encoding de-stabilised EGFP (a variant of EGFP with significantly reduced protein half-life) driven by four copies of an NFκB response element. The plasmid containing this NFκB response element was generously donated by Prof John Silke.

BW5147 and Jurkat CAR T cell production

BW5147 mouse cell line or Jurkat E6.1 human T cell line was resuspended to $5.0x10^5$ cells/ml in fresh RPMI+, prior to being mixed with the relevant filtered viral supernatant in a 1:1 volume ratio. Virus/cell mixture was then supplemented with 8μg/ml polybrene (Merck) and mixed thoroughly before progressing to spinfection in a 12-well tissue culture treated plate (2500 rpm, 37℃, 45 mins). The following day media was replaced with fresh media and cells allowed to recover. Surface staining was conducted at day 5 after transduction to confirm successful expression.

Cell surface staining for flow cytometry

Antibodies were diluted to a relevant dilution (see antibody list) in FACS buffer. 50μl of diluted antibody cocktail was added to cell pellets and mixed thoroughly before incubating on ice for 40 minutes. After staining, cells were washed twice in 200μl ice cold FACS buffer then resuspended in 100μl FACS buffer and analysed via flow cytometry.

*FACS buffer: PBS, 0.5% BSA, 2mM EDTA

CAR Immunoprecipitation western blotting

10^7 cells were pelleted and washed twice with ice cold FACS buffer then resuspended in 400μl of 10μg/ml polyclonal anti-IgG (Sigma-Aldrich) and incubated on ice for 40 minutes prior to being washed with ice-cold FACS buffer twice. Cells were then resuspended in 300μl mammalian lysis buffer* and allowed to sit on ice for 30min and subsequently centrifuged at 20000g to clear debris. The presence of iodoacetamide ensured that free cysteine residues were covalently modified to prevent non-specific disulfide formation. Supernatant was then added to 20μl of protein-G agarose (Sigma-Aldrich) and allowed to mix at 4°C overnight. 5% supernatant sample was also in some cases taken at this stage to permit

concurrent whole cell lysate analysis. Beads were then washed twice in mammalian lysis buffer* (minus protease inhibitor) prior to elution with 20μl LDS* and 2 minutes boiling at 95°C. Samples were then removed from beads with a Hamilton syringe and loaded into a non-reducing NuPAGE 4-12% Bis-Tris 10-well gel (Thermofisher), run for 1 hour at 200V. Gel was subsequently transferred to a PVDF membrane (Sigma-Aldrich) at 30V for 2 hours. Membrane was blocked with TBSt* + 5% BSA for 1 hour, then incubated at 4°C overnight with 1:2000 anti-Myc. The membrane was then rinsed in 10ml TBSt twice prior to addition of 1:10000 anti-mouse IgG-HRP for 2 hours. The membrane was rinsed in 5ml TBSt 3 times, 10 minutes per wash. Enhanced chemiluminescent (ECL) reagent (Thermofisher) was mixed and added to the membrane prior to visualization on a ChemiDoc imager (Bio-Rad).

*LDS sample buffer 4X: 106 mM Tris HCl 141 mM Tris Base 2% LDS 10% Glycerol 0.51 mM EDTA 0.22 mM SERVA Blue G250 0.175 mM Phenol Red pH 8.5.
*Mammalian lysis buffer: PBS, 1% IGEPAL CA-630 (Sigma Aldrich), 10mM iodoacetamide, 1X P8340 protease inhibitor.
*TBSt: NaCl 137mM, KCl 2.7mM, Tris base 19mM, Tween-20 0.1% (Sigma-Aldrich)

DAP12-fusion cloning

CAR constructs described above were used as template to generate 5' fragments, whereas a template containing the full-length DAP12 sequence and a CD8α leader sequence was used as template to generate a 3' fragment. Overlap PCR was used to combine these fragments to form the desired DAP12-fusion designs. Full-length fragments were then digested and ligated as described above* into a modified version of the pSP64-Kozak plasmid vector, which included a 3' HA-tag.

A)

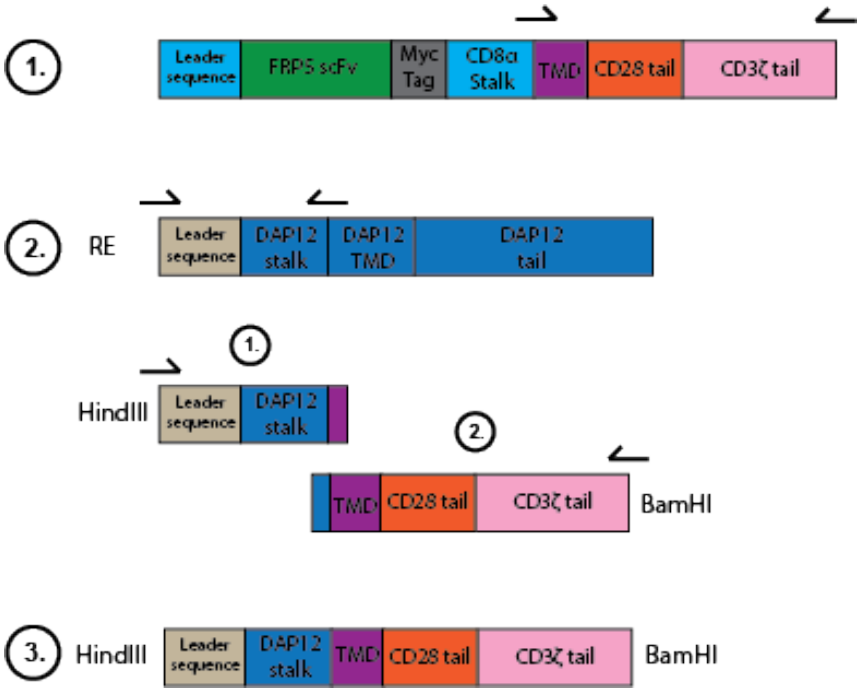

B)

MVPCTLLLLLAAALAPTQTRAQAQSD**C**S**C**STVSPFWLVLILLTFVL

FVFILYWVITWYLIWVRSKRSRLLHSDYMNMTPRRPGPTRKHYQPY

APPRDFAAYRSRVKFSRSADAPAYQQGQNQLYNELNLGRREEYDVL

DKRRGRDPEMGGKPRRKNPQEGLYNELQKDKMAEAYSEIGMKGERR

RGKGHDGLYQGLSTATKDTYDALHMQALPPRGSGYPYDVPDYA*

Figure 2.2 Cloning strategy and protein sequence of DAP12 fusion constructs. *A) cloning strategy used to generate DAP12-Fusion constructs. B) Protein sequence of proMP1 containing DAP12 fusion shown here as example. DAP12 stalk cysteines are underlined and bold.*

In vitro transcription

Messenger RNA (mRNA) was generated synthetically from pIVT DAP12-fusion constructs described above using the RiboMAX® T7 Large-Scale RNA Production kit (Promega) and methyl-G cap analog (Promega). The *in vitro* transcription reactions took place at 37°C for 3.5 hours. mRNAs were then purified using the Qiagen RNeasy® Mini kit (Qiagen) according to manufacturer's protocol.

In Vitro translation dimerization assay

A master mix for all IVT reactions was made according to the table below, assuming a final reaction volume of 25µl/sample. 100ng of mRNA was diluted to 2.5µl with H_2O and was denatured at 65°C for 3 minutes, which was then transferred directly to ice to snap cool. Ice-cold master mix was then added to cold mRNA to give a final volume of 25µl. All reaction tubes were then incubated at 30°C for 15 minutes to allow translation to occur. 2µl of 50mM oxidised glutathione was then added to each tube, mixed and incubated at 30°C for a further hour. Reaction was stopped by addition of 900µl Tris buffered saline (pH 8.0) containing 10 mM Iodoacetamide. All samples were centrifuged at 20000g for 10 minutes at 4°C to pellet ER microsomes. Microsomes were washed twice in 500µl of Tris buffered saline (pH 8.0) containing 10 mM Iodoacetamide then all liquid was removed. Pellets were then resuspended in 20µl of 1X LDS and run on SDS-PAGE using a NuPAGE 12% Bis-Tris gel (Thermofisher) at 200V for 50 minutes, MES buffer. Gel was transferred to PVDF (Sigma-Aldrich) using a wet transfer approach before being air-dried and imaged using a Typhoon FLA 7000 Phosphoimager. The ratio between monomeric and dimeric bands were quantified.

Table 2.5 IVT reaction mixture

Ingredient	**Amount per 25µl reaction**
Nuclease treated rabbit reticulocyte lysate (Promega)	16.5µl
Purified ER microsomes	2µl
^{35}S-labelled cysteine and methionine	2µl
Amino acid mixture minus cysteine and methionine (Promega)	0.5µl
Recombinant Rnasin® ribonuclease inhibitor (Promega)	0.5µl
mRNA (120ng/µl)	2.5µl

Cloning of CAR-GFP fusion constructs for fluorescent correlation microscopy

Overlap PCR was used to generate an eGFP point mutant A206K, a mutation that ablates the weak homo-dimerization inherent to eGFP. A206K was then fused via overlap PCR to the C-terminus of the CD3ζ tail, with the inclusion of a Gly-Ser-Gly flexible linker between the two

sequences. CAR-GFP constructs were ligated into the pMSCV-II-IRES-mCherry retroviral expression vector.

A)

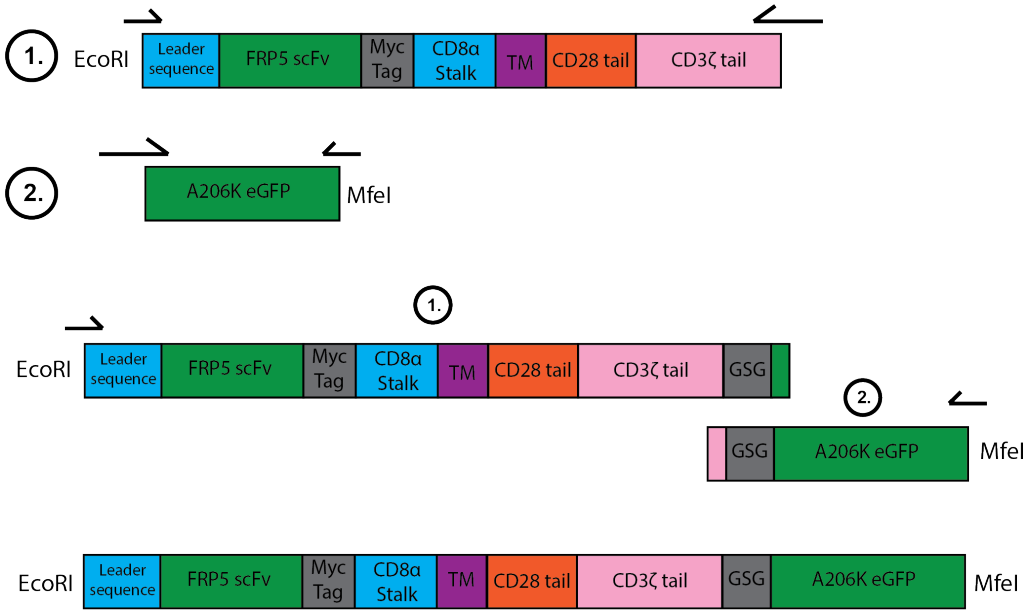

B)

MDFQVQIFSFLLISASVIMSRQVQLQQSGPELKKPGETVKISCKASGYPFTNYGMNWVKQAP
GQGLKWMGWINTSTGESTFADDFKGRFDFSLETSANTAYLQINNLKSEDMATYFCARWEVYH
GYVPYWGQGTTVTVSSGGGGSGGGGSGGGGSDIQLTQSHKFLSTSVGDRVSITCKASQDVYN
AVAWYQQKPGQSPKLLIYSASSRYTGVPSRFTGSGSGPDFTFTISSVQAEDLAVYFCQQHFR
TPFTFGSGTKLEIEQKLISEEDLNGVTVSSALSNSIMYFSHFVPVFLPAKPTTTPAPRPPTP
APTIASQPLSLRPEAARPAAGGAVHTRGLDPFWLVLILLTFVLFVFILYWVITWYLIWVRSK
RSRLLHSDYMNMTPRRPGPTRKHYQPYAPPRDFAAYRSRVKFSRSADAPAYQQGQNQLYNEL
NLGRREEYDVLDKRRGRDPEMGGKPRRKNPQEGLYNELQKDKMAEAYSEIGMKGERRRGKGH
DGLYQGLSTATKDTYDALHMQALPPRQLGSGVSKGEELFTGVVPILVELDGDVNGHKFSVSG
EGEGDATYGKLTLKFICTTGKLPVPWPTLVTTLTYGVQCFSRYPDHMKQHDFFKSAMPEGYV
QERTIFFKDDGNYKTRAEVKFEGDTLVNRIELKGIDFKEDGNILGHKLEYNYNSHNVYIMAD
KQKNGIKVNFKIRHNIEDGSVQLADHYQQNTPIGDGPVLLPDNHYLSTQSKLSK
DPNEKRDHMVLLEFVTAAGITLGMDELYK*

Figure 2.3 Cloning strategy and protein sequence for CAR-GFP fusion constructs. *A) Cloning strategy used to generate GFP-fusion proCARs from relevant CAR constructs described in Figure 2.1. B) Protein sequence of proCAR1 FRP5 A206K EGFP fusion construct shown as example. A206K mutation within EGFP ablates weak propensity for EGFP to homodimerize.*

TIRF microscopy

Relevant BW5147 T cells expressing GFP fusion CAR constructs were resuspended in fresh RPMI+ at a density of $1.0x10^5$ cells/ml and aliquoted onto an 8-well chamber slide (Ibidi) on day 0 to allow them to settle and attach to the tissue-culture treated glass surface. On day 1 samples were placed in the TIRF microscope and allowed to acclimatize in situ at 36°C and 5% CO_2 for 1 hour prior to imaging. Imaging took place using a laser incidence angle of 52° to enable TIRF imaging. Cells were imaged at 2.5% laser power, with 200 frames collected at 500ms intervals. Cells were manually selected for imaging according to observable expression of GFP and stable adherence to the coverslide.

Numbers and brightness (N&B) analysis

Movies were analysed using the simFCS software package. Cells were excluded from analysis if significant photobleaching or cell movement took place over the course of imaging. simFCS was used to determine an average B-value for a 100x100 pixel area at the center of each cell. B-values were tabulated in Excel and according to the equation below 1 was subtracted from each average B-value to calculate the average oligomeric state of the fluorescent protein. These values were then visualized using the software Prism.

$$B = \frac{\sigma^2}{k} = \varepsilon + 1$$

$$\varepsilon = \frac{\sigma^2}{k} - 1$$

B= Brightness

σ = Fluorescence variance

k = Fluorescence intensity

ε = Absolute oligomeric state

BW5147 activation assay

On day 0 relevant adherent HER2+ target tumour cells lines were plated at an appropriate density to ensure 100% confluence the following day. On day 1, target cells were visually inspected to confirm their confluency was between 90-100%. Relevant BW5147-NFκB reporter CAR T cells were counted and resuspended in fresh RPMI+ at a density of $2.5x10^6$ cells/ml. Media was aspirated off target cells and 250µl of BW5147-NFκB CAR T cells were

aliquoted onto the relevant target cell line. For time-course experiments, the 6 hour timepoint was aliquoted first, followed 2 hours later by the 4 hour time point and so on until the 0 hour timepoint, in which all conditions were simultaneously resuspended and removed for antibody staining. Cells were stained with anti-CD69 and then analysed via flow cytometry according to the gating strategy described in figure 4.5.

Mouse CD8+ T cell isolation and culture

Single-cell suspensions of peripheral lymph nodes from 8-10 week old C57B/6 mice were prepared by mechanically dissociating through a 70 mm cell strainer (BD Biosciences) into cold PBS. CD8 T cells were subsequently selected using the EasySep™ mouse CD8α positive Kit II (Stem Cell Technologies) according to manufacturer's instructions. Purity was confirmed as >95% using anti-CD3 and anti-CD8α staining, analysed via flow cytometry (BD LSR II or Cytek Aurora). CD8 T cells were subsequently activated by incubating overnight with Mouse T-Activator CD3/CD28 Dynabeads™ (Gibco) at a bead to cell ratio of 1:1 in mouse T cell medium (mTCM) consisting of Rosewell Park Memorial Institute (RPMI) 1640 Medium (lonza) supplemented with foetal bovine serum (10%; Bovogen Biological), L-glutamine (2 mM; Gibco), sodium pyruvate (1 mM; Gibco), non-essential amino acids (1x; Sigma-Aldrich), β-mercaptoethanol (50 mM; Sigma-Aldrich) and recombinant human IL-2 (100 IU/ml; PeproTech). Following removal of magnetic beads, T cells were maintained at $1x10^6$ cell/ml in mTCM.

Primary CAR T cell transduction

Retrovirus for primary T cells was produced using calcium phosphate transfection of HEK293T cells. Tissue-culture treated 12-well plates were coated with 32 μg/ml retronectin (Takara Bio) for 24 hrs, before plating of $1x10^6$ cells in 1ml viral supernatant and performing a spinfection (2500 rpm, 37℃, 45 mins). Viral supernatant was removed after 16 hr and replaced with mTCM for primary T cells.

Primary CAR T cell chromium release killing assay

Standard ^{51}Cr release assays were conducted to assess CAR T cell cytotoxicity by measuring release of radioactivity into culture supernatants as cells are lysed. Target MC57 mouse

fibrosarcoma cells stably expressing human HER2 (MC57-HER2) were pre-loaded with 100 µCi ^{51}Cr for 1 hour at 37°C, washed three times and then $2x10^4$ tumour cells were co-incubated with CAR T cells at effector-to-target (E:T) ratios ranging from 40:1 to 1.25:1. Supernatants were harvested after 4 hrs of co-incubation, plated onto a 96-well scintillator coated LumaPlate (PerkinElmer) and ^{51}Cr release quantified using a MicroBeta^2 Microplate Counter (PerkinElmer). Target tumour cells incubated in a 5% Triton X-100 solution were used as a maximum release control, while tumour cells incubated in mTCM alone were used as a spontaneous release control. Percent lysis was calculated as: % lysis = ((Experimental release – Spontaneous release) ÷ (Maximum release – Spontaneous release)) 100. Data in Figure 3f and Figure 4d are derived from the 20:1 E:T ratio where killing was maximal for all constructs.

Primary CAR T cell cytokine release assay

To assess cytokine secretion by CAR T cells, cytokine bead arrays on co-culture supernatants were performed. Murine CAR T cells ($1x10^5$ cells) were washed once in PBS and co-incubated with either mTCM alone, a 1:1 bead to cell ratio of Mouse T-Activator CD3/CD28 Dynabeads™ (Gibco) as a positive control, non-target MC57 parental tumour cells ($2x10^4$ cells) as a negative control, or target MC57-HER2 tumour cells ($2x10^4$ cells) in triplicate. After 24 hours, supernatants of co-cultures were collected and used in a LEGENDplex Mouse T Helper Cytokine Panel Version 2 Flexi Kit (Biolegend) for IFN-γ, IL-2 and TNFα, and LEGENDplex Mouse Cytokine Panel 2 Flexi Kit (Biolegend) for GM-CSF according to manufacturer's instructions. All samples were analysed using a LSR II Fortessa or FACSVerse (BD Bioscience) and concentration determined against a standard curve of each analyte using FlowJo™ v10 software.

In vivo MC38 mouse tumour model

On day 0, 5-6 female NSG mice (6-8 weeks of age) were injected subcutaneously with $5x10^5$ MC38 HER2+ tumour cells. On day 1, $1x10^7$ CAR T cells were injected intravenously, supplemented with intraperitoneal IL-2 injection ($5x10^4$ IU) on days 1, 2 and 3 to support T cell engraftment. Tumour size was measured daily using callipers, with mice euthanized at ethical endpoint (defined as tumour with a volume of $1000mm^3$), at which time tumours, spleens and blood samples were taken for processing.

Mouse strains and animal ethics

All animal work was carried out in accordance with the Australian National Health and Medical Research Council guidelines under the approval of the Walter and Eliza Hall Institute Animal Ethics Committee (Ethics number: 2020.030). C57/B6 mice were used as donor mice for all primary CAR-T cell experiments and NOD/SCID/IL2r/J(GM) mice used as recipient mice for all *in vivo* experiments. All mice were supplied from the Walter and Eliza Hall Institute Animal Breeding Facility (Victoria, Australia) and housed in the Walter and Eliza Hall Institute Bioservices Facility (Victoria, Australia).

Co-localization microscopy

$8x10^5$ cells were incubated with anti-Myc primary antibody, diluted in FACS buffer, for 30 min on ice. Cells were washed twice in FACS buffer and further incubated with Alexafluor488 anti-mouse IgG goat secondary antibody in 50µl cold RPMI+ for 10 minutes on ice. 150µl warm RPMI+ was added to each sample and transferred to 37 °C for 10 min to induce crosslinking induced capping. To halt the capping process 500µl ice-cold FACS buffer containing 0.1 % sodium azide was added. Cells were washed twice in ice-cold FACS buffer + 0.1 % sodium azide then stained on ice for 45 minutes with either anti-CD28 APC or anti-CD45 APC diluted in FACS buffer + 0.1 % sodium azide. After washing twice in FACS buffer + 0.1 % sodium azide, cells were fixed with 3% paraformaldehyde, transferred to 8-well chamber slides (Ibidi) and stored at 4°C overnight until imaging.
Analysis was conducted within the Imaris software package as follows. The cluster-picking function was used to detect Alexafluor488 fluorescent CAR clusters. CD28 clusters that co-localised with CAR clusters were then detected and quantified. CAR clusters and co-localised CAR/CD28 clusters were tabulated in Excel and visualised with prism.

Cloning of Yescarta proCAR panel.

Yescarta proCAR constructs were generated using an overlap PCR approach. First, a gene fragment was purchased (g-block® - Integrated DNA technologies) encoding the FMC63 anti-CD19 scFv and CD28 stalk sequence, containing a mutation in the CD28 stalk sequence, converting a stalk cysteine residue to an alanine. This fragment was fused via overlap PCR to

TM and tails fragments from relevant FRP5 CAR constructs. To generate a reference Yescarta CAR with stalk cysteine residues, complementary primers encoding an alanine to Cysteine mutation were used to generate PCR products, subsequently combined via overlap PCR. All fragments were digested with EcoRI/XhoI and ligated into the pMSCV-II-IRES-mCherry retroviral expression vector.

A)

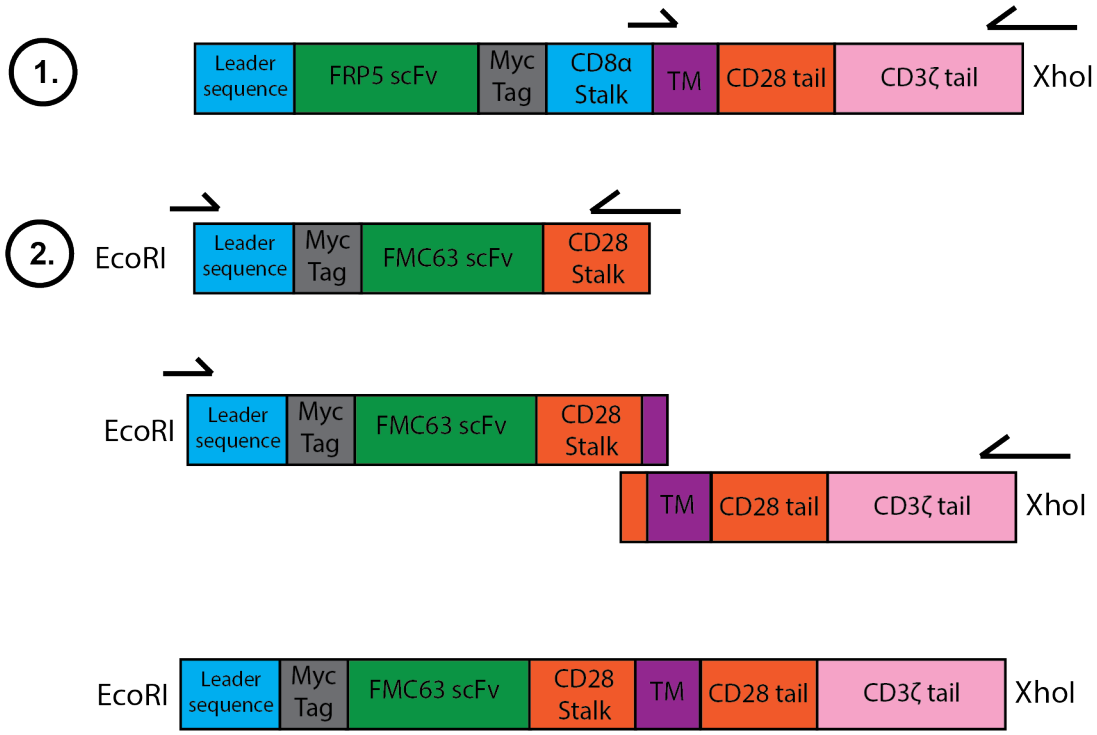

B)

MLLLVTSLLLCELPHPAFLLIPEQKLISEEDLDIQMTQTTSSLSASLGDRVTISCRASQDIS
KYLNWYQQKPDGTVKLLIYHTSRLHSGVPSRFSGSGSGTDYSLTISNLEQEDIATYFCQQGN
TLPYTFGGGTKLEITGSTSGSGKPGSGEGSTKGEVKLQESGPGLVAPSQSLSVTCTVSGVSL
PDYGVSWIRQPPRKGLEWLGVIWGSETTYYNSALKSRLTIIKDNSKSQVFLKMNSLQTDDTA
IYYCAKHYYYGGSYAMDYWGQGTSVTVSSAAAIEVMYPPPYLDNEKSNGTIIHVKGKHL**C**PS
PLFPGPSKPFWVLVVVGGVLA**C**YSLLVTVAFIIFWVRSKRSRLLHSDYMNMTPRRPGPTRKH
YQPYAPPRDFAAYRSRVKFSRSADAPAYQQGQNQLYNELNLGRREEYDVLDKRRGRDPEMGG
KPRRKNPQEGLYNELQKDKMAEAYSEIGMKGERRRGKGHDGLYQGLSTATKDTYDALHMQAL
PPR*

Figure 2.4 Cloning strategy and protein sequence of Yescarta proCAR construct. *A) cloning strategy used to generate proCARs from Yescarta Cys Mut CAR. B) Protein sequence of Reference Yescarta CAR, CD28 stalk cysteines underlined, bold.*

Table 2.6 Antibody list. Flow cytometry (FC), western blot (WB), immunoprecipitation (IP), Immunohistochemistry (IHC).

Antigen specificity	Clone	Conjugation	Supplier	Dilution
Human c-Myc	9B11	AlexaFluor 647	Cell Signalling Technologies	1:100 (FC)
Human c-Myc	9B11	unconjugated	Cell Signalling Technologies	1:100 (IHC)
Mouse IgG	polyclonal	unconjugated	Sigma-Aldrich	10μg/ml (IP)
Mouse CD28	145-2C11	APC	Biolegend	1:200 (IHC)
Mouse CD69	H1.2F3	Pacific Blue	Biolegend	1:200 (FC)
Mouse/human CD3ζ	6B10.2	Horseradish Peroxidase	Santa Cruz Biotechnology	1:1000 (WB)
Mouse CD8α	53-6.7	APC/Cy7	Biolegend	1:400 (FC)
Mouse CD3ε	145-2C11	PE	Biolegend	1:400 (FC)
Mouse IgG	polyclonal	A488	Biolegend	1:200 9IHC)

Chapter 3 Development of a novel *de novo* membrane protein oligomer design pipeline

3.1 Background and rationale.

De novo protein design in recent years has developed from an academic exercise to an increasingly reliable tool capable of solving real world problems (Khoury et al., 2014, Huang et al., 2016). However, most of the work to this point has been carried out on soluble proteins, with the field of membrane protein modelling and design lagging behind. Examples of de novo designed oligomeric membrane proteins to date are scarce, with the only published examples of taking the form of helical hairpin structures (Lu et al., 2018) or ion-transporters (Joh et al., 2014). As these structures were not compatible with expression as type-I transmembrane proteins (due to their inherent requirement for anti-parallel helix packing) they were unsuitable for application in a single-pass transmembrane protein such as a CAR. However, due to recent advancements in the field of membrane protein energetics made by our collaborator Sarel Fleishman and his lab, it appeared feasible that protein sequences tailored for the specific requirements of expression in the context of a CAR could be modelled *de novo* and fit for purpose.

One of the keys to the advancements in membrane protein energetics made by the Fleishman lab has been the use of a deep-sequencing TOXCAT-β-Lactamase assay (dsTβL). This assay works by fusing a desired TM sequence to β-lactamase at its C-terminus, which confers ampicillin resistance only in the context of the bacterial periplasm, hence serving as a marker of successful membrane insertion. At the N-terminus a ToxR domain is fused, which requires dimerization to confer chloramphenicol resistance, serving as a measure of self-association. While the TβL assay is well described (Lis and Blumenthal, 2006, Russ and Engelman, 1999, Langosch et al., 1996), the novel approach taken by the Fleishman lab was to combine TβL analysis with high-throughput deep mutational scanning (Fowler et al., 2014). This approach enabled the rapid generation of thousands of randomized amino acid substitutions within a given TM domain, sequences which could then be characterised by antibiotic survival for their influence on transmembrane domain insertion, stability and self-association (Elazar et al., 2016a).

One of the most significant findings of the data generated by deep-mutational TβL scanning of test TM sequences was that TM domain self-association and membrane stability are coupled far more strongly than was appreciated in previous studies on TM energetics (Senes et al., 2007, Ulmschneider et al., 2005, Schramm et al., 2012). Crucially, the improved understanding of the relationship between TM insertion and self-association was able to inform the constraints imposed upon single-pass transmembrane proteins within protein modelling software. These improved constraints subsequently assisted in the design of a novel modelling approach that proved capable of *ab initio* prediction two thirds of the native homo-oligomeric TM complex structures within the PDB to within a Root Mean Square Deviation (RMSD) of 2.5 Å accuracy (Weinstein et al., 2019). Building on these published findings, the Fleishman lab established a *de novo* protein design pipeline capable of generating thousands of *de novo* designed synthetic TM sequences that are predicted to form homo-oligomeric interfaces in a lipid membrane environment, termed programmed membrane proteins (proMPs). The collaboration between the Call and Fleishman labs aimed to generate and structurally validate a panel of oligomers ranging from monomeric to tetrameric TM sequences that could be used for integration into engineered receptors.

The key features of the pipeline are as follows: from a starting point of poly-valine TM sequences, iterative rounds of symmetrical sequence mutagenesis are undertaken, guided by *in silico* protein modelling approaches in search of low energy oligomeric interfaces. Importantly, mutagenesis was biased to match the sequence of natural TM domains, a feature which proved key in improving the accuracy of the approach. This process generates numerous oligomeric TM models, of which the lowest energy models have their sequence subjected to *ab initio* structure prediction. At this stage, only sequences whose models converge with those generated by this independent *ab initio* structure prediction are progressed. To validate these structures in real cellular membranes, a saturating mutagenesis approach is used in which residues predicted to sit within the oligomeric interface are mutated to every other residue. This panel of mutants is then evaluated using the deep-sequencing TβL system to provide experimental validation of the designed helix interfaces.

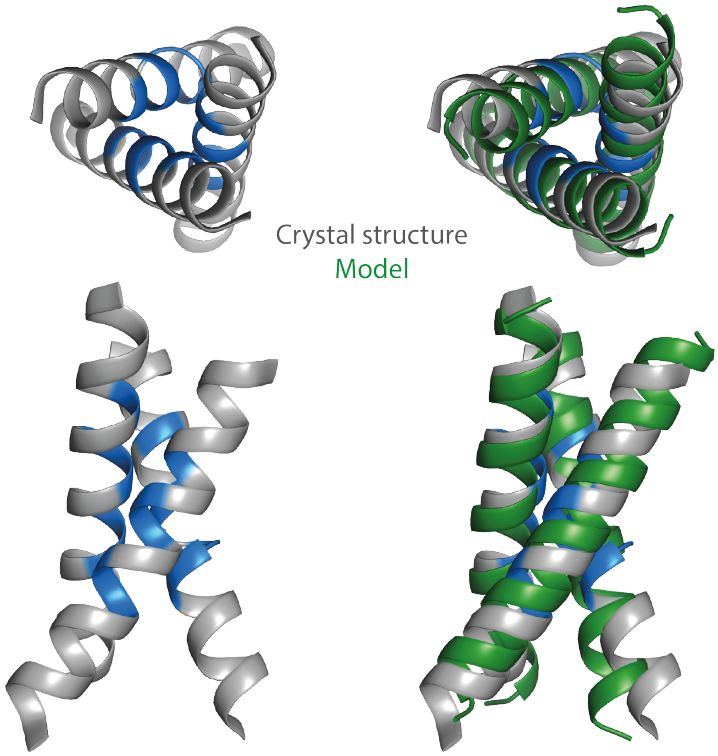

Figure 3.1 Crystal structure of a de novo designed trimeric peptide. *Crystal structure of proMP3.1 (grey) with blue residues indicating small residues involved in the close interchain packing of helices. This crystal structure aligned closely with a sequence model (green), once adjustments were made to the modelling approach within the proMP pipeline (PDB: 6W9Y).*

Using this initial design pipeline, a panel of homodimers was generated and validated for self-association and expression using the dsTβL assay. However, without experimentally determined structures of these sequences it was difficult to confirm the accuracy of the design pipeline. For this reason, a former PhD student within our lab, Dr. Raphael Trenker, undertook structural studies of peptide sequences that came out of an initial screen for homodimers. To this end, candidate TM sequences that were predicted to exhibit low energy dimeric structures were produced and purified from *E. coli.* From SDS-PAGE analysis a number of sequences appeared to be capable of forming SDS-stable dimeric complexes. Surprisingly, several candidates exhibited apparent molecular weights that were more consistent with trimeric or tetrameric complexes. These peptides were progressed to Lipidic

Cubic Phase (LCP) crystallisation screening, which uses a host medium that forms a continuous lipidic bilayer to provide a native-like environment for membrane proteins(Hofer et al., 2010, Landau and Rosenbusch, 1996). By using a membrane environment similar to that of a native membrane bilayer, lateral interactions between peptides are favoured, thus reducing the likelihood of non-native contacts driving crystal growth. A number of designs yielded crystal hits from these screens, with one in particular (referred to herein as proMP3.1) giving excellent X-ray diffraction that yielded a structure at 2.55 Å resolution (PDB: 6W9Y) (Fig 2.1). Interestingly, in this structure the TM peptide was indeed observed to form a trimeric interface correlating with the SDS-stable trimeric complex observed to form in SDS-PAGE analysis of the same peptide. Upon closer inspection, the trimeric interface present in this crystal structure was centred around the same residues predicted to be important for the modelled dimeric interface of the same peptide. This outcome was permitted in the *in silico* pipeline as in this round of design, only structures with C2 (dimeric) symmetry were considered. Additionally, the ToxR domain is not able to differentiate between homo-dimerization and higher oligomeric states. Indeed, when *ab initio* structure prediction of the peptide sequence in the C2, C3 and C4 symmetry (dimer, trimer and tetramer, respectively) was undertaken, the lowest energy C3 symmetric model matched that of the crystal structure to an RMSD of 2.3Å. Incorporating these findings, an additional design round involving modelling in C2, C3 and C4 symmetry was added to the final version of this design pipeline to help ensure future design campaigns could be more effectively targeted to a specific oligomeric state.

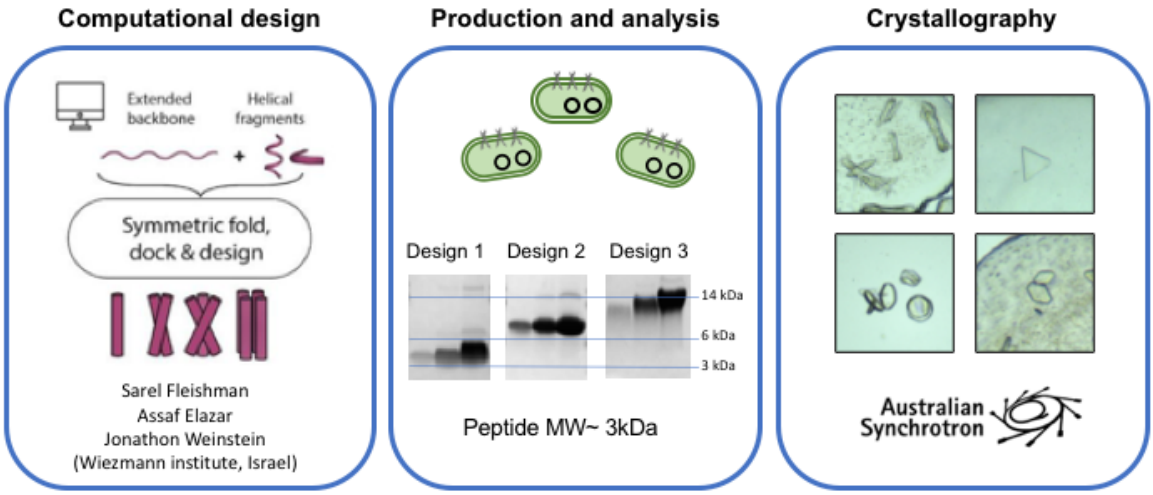

Figure 3.2. Outline of the collaborative proMP design pipeline*. Briefly, computational design of proMP sequences was undertaken by collaborators, where low-energy oligomeric structures were validated in an E. coli TβL-TOXCAT self-association assay. The most strongly associating candidates were expressed and purified in our lab, analysed by SDS-PAGE. Promising candidates were prioritized for crystallization trials.*

My role in proMP design and validation: Using this improved pipeline (Fig 3.2), a new design round was initiated with the aim of generating monomeric, dimeric and trimeric proMP structures. Each of these oligomeric forms was successfully generated and validated for self-association and interface specificity in the dsTβL assay prior to being forwarded to our lab for structural investigation. For the purpose of expediting progression into functional CAR T cell studies, my priority was to identify and structurally validate a dimeric proMP sequence, as a trimeric structure had already been identified. Additionally, there was little need to determine the structure of a monomeric TM sequence as from dsTβL results these sequences appeared completely incapable of self-association. Hence, we chose five sequences from the screen for homodimeric interfaces that scored highest in terms of self-association and expression in the dsTβL assay for further analysis (Fig 3.3). Interestingly, all five proMP dimer interfaces were predicted to contain small residues, such as glycine and alanine, facilitating the close packing of helical backbones. This recapitulated what is observed in natural TM dimers, where small-residue motifs such as the canonical GlyXXXGly glycophorin A motif are prevalent (where X is any hydrophobic amino acid) (Teese and Langosch, 2015). The key variable between the dimeric proMP models was the wide range of crossing angles observed, proMP2.5 in particular possessed an almost perpendicular crossing angle of 86 degrees, far greater than has been observed in the experimentally determined structure of any natural TM dimer to date. The importance of validating these models through experimental structure determination was paramount given the surprising results from our previous design round. To achieve this, I aimed to express and purify a selection of these designed TM domains in order for crystallization trials be undertaken.

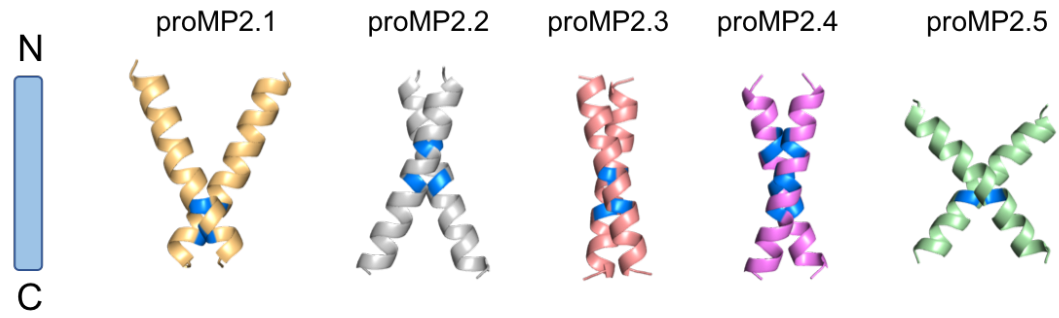

Name	Sequence
proMP2.1	LLILVTIIFILFATVGTVAWLVL
proMP2.2	LTVALILGIFLGTFIAFWVVYLL
proMP2.3	LATLLYFLLIIAVFLAVTFLVWAL
proMP2.4	LLFVTLWAAIIAAWIAIFLATVYS
proMP2.5	VLLIVLLIIFYIFWGLVFTLLFTI

Figure 3.3. De novo designed, dimeric proMP designs. *Five candidate dimeric proMP sequences generated by collaborators for structural investigation. Peptide N- and C-termini indicated to left of structures.*

3.2 Results

Production and purification of two predicted homodimeric TM peptides.

Initially proMP2.1 and proMP2.2 were chosen for structural validation (Fig. 3.3). We hypothesized that their observed differences in C-terminal inter-helical distances would potentially provide an interesting functional comparison in CARs, given that in the case of receptors such as Growth Hormone Receptor (GHR), HER2 and CD3ζ dynamic regulation of TM structure and crossing angle are suggested influence receptor signalling state (Lee et al., 2015, Brooks et al., 2014, Bocharov et al., 2008). Based on previous experience crystallising synthetic peptides within our lab, the TM flanking region of glycophorin A was appended to each of the synthetic TM sequences expressed (Fig 3.4B). These flanking sequences contain multiple charged residues with asymmetric charge distribution: negatively charged acidic residues at the N-terminus (Glu-Pro-Glu) and positively charged basic residues at the C-terminus (Arg-Arg-Leu). These sequences theoretically present an opportunity for contacts between chains located laterally within the LCP bilayer as well as chains between vertically stacked LCP bilayers. These flanking regions had previously been compatible with the

crystallization proMP3.1 and did not appear to interfere with the predicted structure of the proMP3.1 sequence in the absence of these flanking regions. A cysteine residue was also appended to the C-terminal glycophorin A flanking region of proMP2.1 and proMP2.2 (as in all other proMP constructs) to enable covalent modification with fluorescent tags or other moieties that might aid in tracking or crystallisation (Fig 3.4A). However, in the case of both proMP2.1 and proMP2.2 these modifications were not required and therefore the cysteines were covalently protected with the thiol-reactive reagent *S*-methyl methanethiosulfonate to prevent inter-chain disulfide crosslinking. The expression of these peptides was facilitated by the inclusion of an N-terminal TrpLE fusion protein, a sequence that drives protein aggregation into inclusion bodies (Sharma et al., 2013, Miozzari and Yanofsky, 1978). TrpLE fusion proteins expressed in E. coli BL21(DE3) cultures were then solubilised, purified via nickel affinity purification and the desired peptides were liberated via cyanogen bromide (CNBr) hydrolysis of the peptide bond C-terminal to a methionine residue between the TrpLE and proMP sequences.

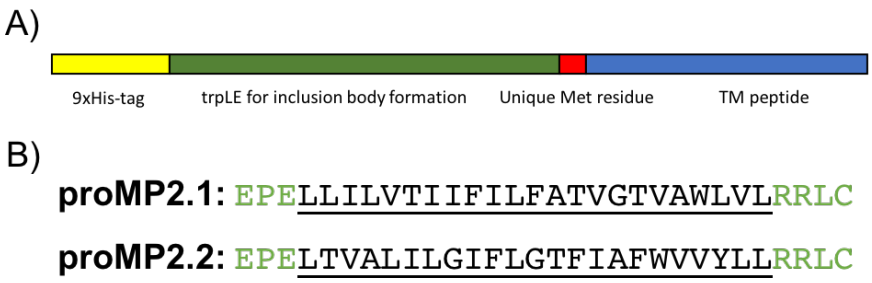

Figure 3.4. proMP expression constructs *A) Schematic diagram of construct design for expression of TM peptides in E. coli. trpLE domain drives protein aggregation into inclusion bodies. 9xHis tag sequence permits Nickel affinity purification. Unique Met residue required for subsequent cleavage of desired peptide. B) Protein sequence of two predicted dimeric TM peptides (Black), glycophorin A TM flanking regions included to aid crystallization (green).*

Both proMP2.1 and proMP2.2 expressed well in *E. coli* and were successfully cleaved using CNBr hydrolysis (Fig 3.5A) and purified by reverse-phase HPLC (Fig 3.5B). Purified peptides were then run on SDS-PAGE to assess protein purity and the presence of higher order complexes (Fig 3.5C). Peptides were run at increasing concentrations to assist in

visualisation given small TM peptides are characterised by poor Coomassie staining. Both proMP2.1 and 2.2 ran at an apparent molecular mass above 6kDa at low protein concentrations, despite actual masses of approximately 3.5kDa, a strong indication of stable dimer formation. With increasing amounts of peptide loaded both proMP2.1 and proMP2.2 exhibited a slight increase in apparent molecular mass of this dimeric band, behaviour that was previously observed in the study the natural glycophorin A homodimer (Trenker et al., 2015). Additionally, there was no evidence of peptide 'laddering', suggested that these sequences exist as a single, stable dimeric species. These results were a strong indication that proMP2.1/proMP2.2 were forming homodimeric structures as predicted, even in the context of the harshly denaturing conditions of boiling in solution with SDS. Hence, both peptides were progressed to crystal screening trials using LCP.

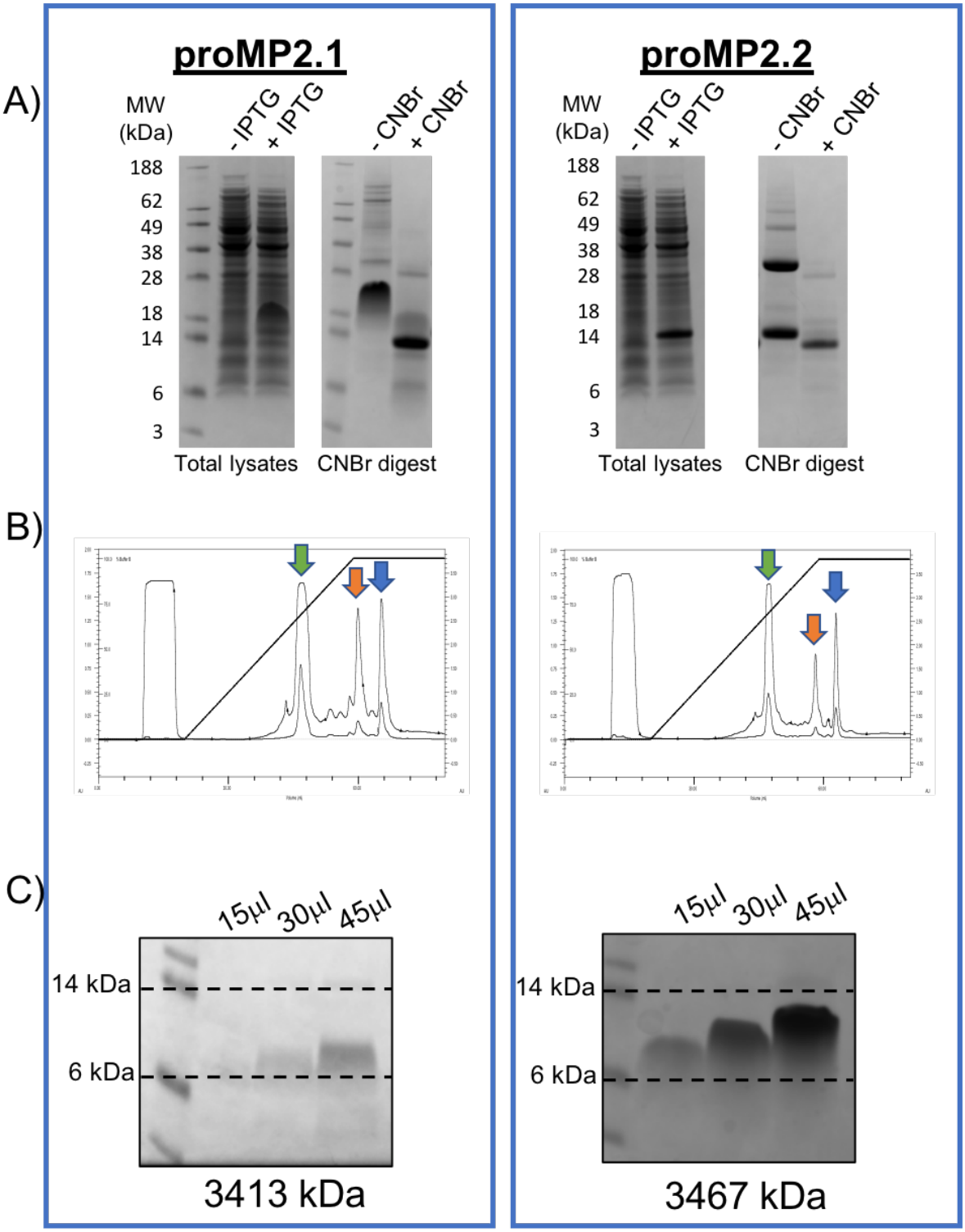

Figure 3.5. Expression and purification of proMP peptides*. proMP2.1 and proMP2.2 were both expressed and purified using an identical process. Peptides were expressed in BL21(DE3) E. coli cells (A), with trpLE fusion protein driving protein accumulation in inclusion bodies. trpLE fusion proteins were extracted from inclusion bodies and isolated via nickel affinity purification. Following acid elution from the nickel affinity matrix, cleavage of the*

trpLE fusion protein was achieved via treatment with cyanogen bromide (CNBr) mediated hydrolysis of a unique methionine at the C-terminus of trpLE (A). Post-cleavage protein mixture was dialyzed against H_2O, precipitated and lyophilized, then dissolved in formic acid for purification via reversed phase-HPLC. B) C8-semiprep column was used, combined with a protocol involving a 4-column volume linear gradient, to purify proMP peptides from uncleaved TrpLE fusion protein and cleaved TrpLE. blue arrow: proMP peptide peak, Orange arrow: TrpLE cleavage product, Green arrow: TrpLE-Peptide fusion. C). Small samples were taken from peptide peak fractions (indicated by arrow in B) at the volumes indicated in C). Samples were lyophilized, dissolved in LDS-buffer and analysed via SDS-PAGE.

Crystallization of two dimeric proMP sequences in Lipidic Cubic Phase (LCP) bilayers

Lipidic cubic phase (LCP) is commonly used in the study of membrane protein structure (Landau and Rosenbusch, 1996). Instrumental in determining the first structures of G-coupled-protein receptors (Cherezov et al., 2007), LCP crystallisation has recently demonstrated significant value in the study of smaller single-pass transmembrane protein assemblies (Trenker et al., 2015, Knoblich et al., 2015, Hofer et al., 2010). The technique is predicated on the ability of lipid/solvent mixtures to form networks of continuous lipidic bilayer when combined at an appropriate ratio. Proteins reconstituted into such lipidic bilayer networks are able to freely diffuse in the bilayer plane, which allows for protein to accumulate at sites of crystal nucleation. Both proMP2.1 and proMP2.2 were reconstituted into such a network, composed of a 3:2 mixture of the lipid monoolein and Tris buffered saline (TBS). Both samples were capable of successfully forming LCP (inferred from the transition of the protein/lipid/solvent mixture from an opaque to transparent appearance) and were subsequently dispensed into crystal screens. Of these two peptides the first to crystallize was proMP2.1, which did so in a number of conditions at day 2 (Fig 3.6A). The same crystal morphology was observed in all conditions and consisted of small bundles of needles that were broken into small shards and frozen for X-ray crystallography.

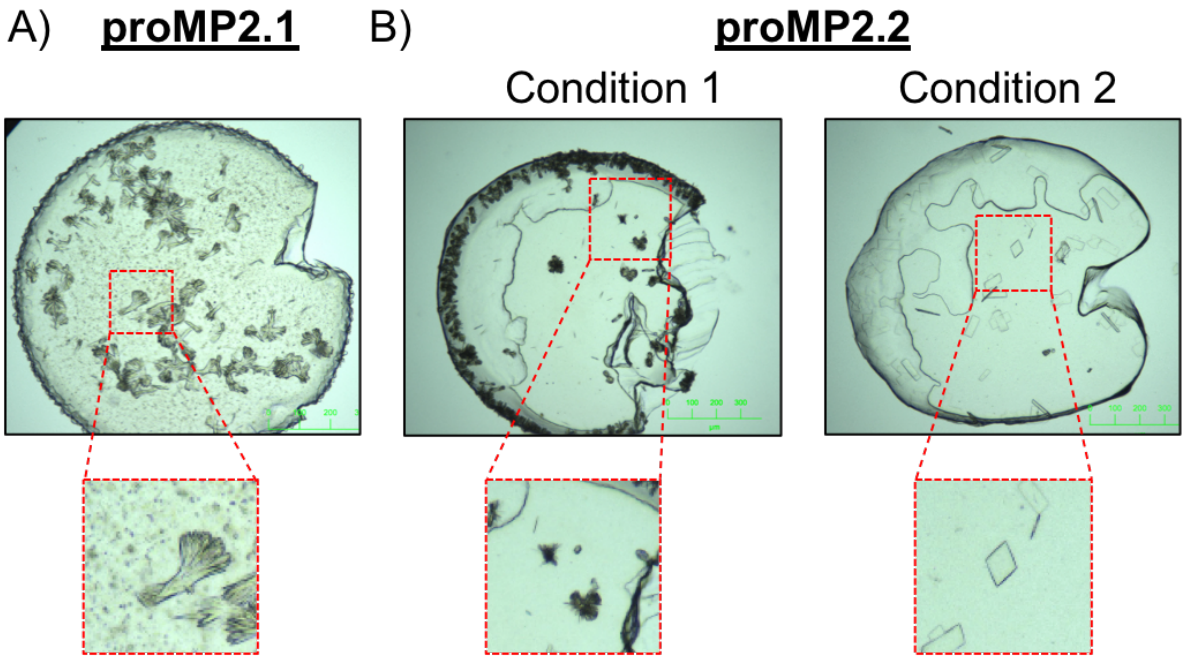

Figure 3.6. Production and crystallization of two predicted dimeric TM peptides. *A) proMP2.1 crystallized in a condition composed of: 0.354M lithium chloride, 34.6% v/v polyethyleneglycol 400, 0.1M sodium HEPES pH 7.6. Crystals from this condition yielded a high-resolution crystal structure. B) proMP2.2 crystallized in two crystal forms. Only condition 2 yielded high resolution crystal diffraction. Condition 1: 4% v/v 2-methyl-2,4-pentanediol, 0.1M lithium nitrate, 0.1M sodium chloride, 0.1M trisodium citrate-citric acid pH 5.6. Condition 2: 8% v/v 2-methyl-2,4-pentanediol, 0.1M ADA pH 6.7, 0.4M potassium nitrate, 0.1M tripotassium citrate.*

Crystal structure of a proMP2.1 in a non-dimeric form

X-ray diffraction data from Crystals in Fig3.2A were collected on the MX2 beamline at the Australian Synchrotron and extended to 1.7 Å resolution. The structure was solved using a single helix from an LCP structure of glycophorin A in a monomeric form (PDB:5EH6, (Trenker et al., 2015)) as a search model for molecular replacement using Phaser. Analysis of crystal packing revealed type 1 crystal packing showing the peptide is embedded in the lipidic bilayer and these layers are stacked within the crystal. However, only one helix was present within the asymmetric unit, and upon closer inspection of the crystal packing the predicted dimeric interface was absent. Instead, helices appeared to associate in two planes, one via anti-parallel dimeric packing and the other via continuous front-to-back packing. While the buried surface area of this anti-parallel dimeric interface was comparable

to that of the predicted, parallel dimeric interface (346 Å^2 vs. 327 Å^2), the minimal interhelical distance observed was almost twice as large (5.9 Å vs. 3.4 Å). Additionally, the contacts observed between parallel helices within the crystal structure were even less significant (buried surface area of 223 Å^2 and interhelical distance 6.3 Å).

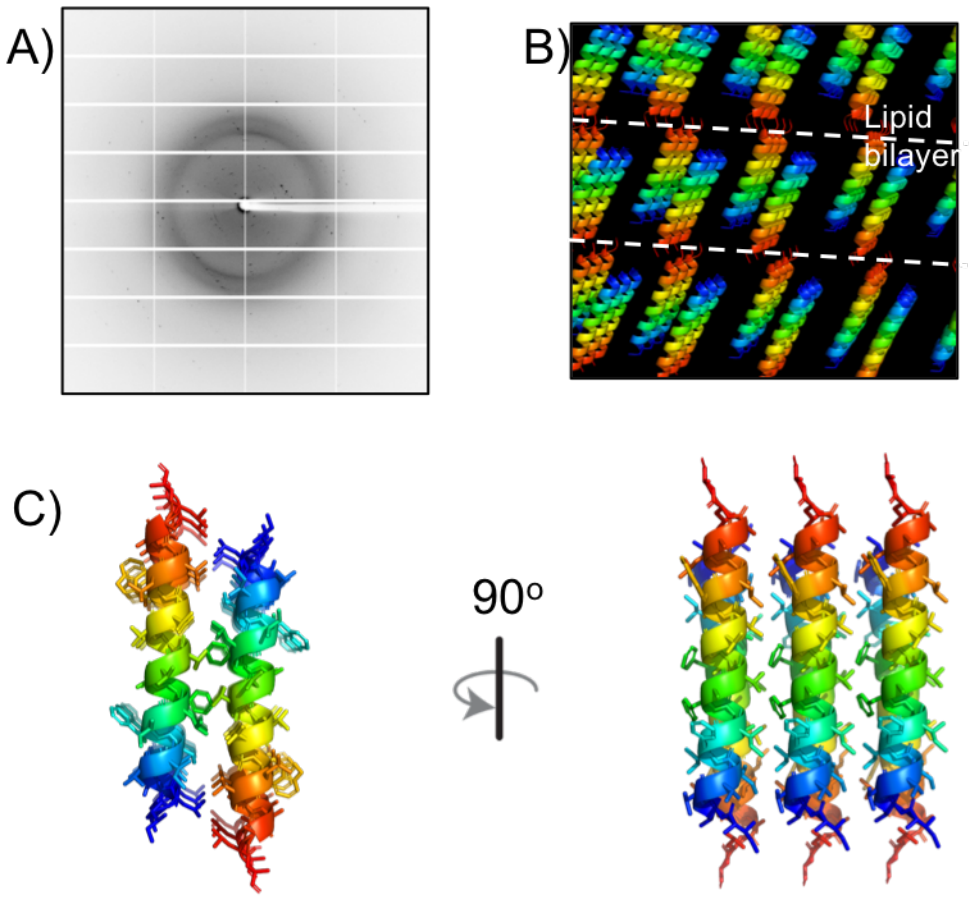

Figure 3.7 Crystal structure of proMP2.1 *A) Diffraction from crystal to 1.7 Å. B) Crystal lattice, N- and C- terminus are colored blue and red respectively. Lipidic bilayer inferred from type-1 packing of peptide helices. C) Cartoon helices with side chains showing complementarity of anti-parallel (left) and parallel interfaces (right) within crystal lattice in 2B.*

Wavelength (Å)	0.9537
Resolution range (Å)	24.98 - 1.74 (1.802 - 1.74)
Space group	C 1 2 1
Unit cell (Å)	59.502 10.124 50.815 90 122.914 90
Total reflections	7266 (646)
Unique reflections	2784 (254)
Multiplicity	2.6 (2.5)
Completeness (%)	96.12 (92.28)
Mean I/sigma(I)	6.25 (1.23)
Wilson B-factor ($Å^2$)	23.09
R-merge	0.07992 (0.5983)
R-meas	0.1 (0.7519)
R-pim	0.0592 (0.4497)
CC1/2	0.995 (0.864)
CC*	0.999 (0.963)
Reflections used in refinement	2773 (251)
Reflections used for R-free	286 (28)
R-work	0.2416 (0.3645)
R-free	0.2512 (0.3454)
CC(work)	0.937 (0.691)
CC(free)	0.906 (0.561)
Number of non-hydrogen atoms	236
Macromolecules	234
Solvent	2
Protein residues	29

Table 3.1 Data collection and refinement statistics **proMP2.1**

A crystal seeding trial was then undertaken with the aim of nucleating different crystal forms in previously unsupportive crystallisation conditions. Micro-crystals were grown in a previously successful condition selected from the initial screen and then seeded into an alternative screen that had previously yielded no crystal hits. This approach yielded many more crystal hits, but each of these resembled the initial crystal form and yielded comparable structures. Given these outcomes, structural studies of proMP2.1 were not pursued further, in favour of focussing efforts on other proMP designs.

Crystal structure of the *de novo* designed homodimeric peptide proMP2.2

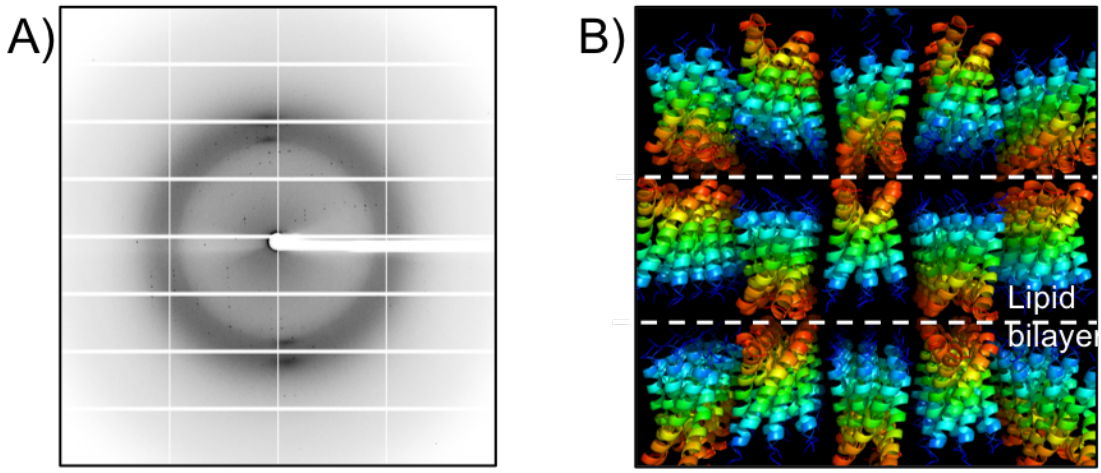

Figure 3.8 X-ray diffraction and crystal packing of proMP2.2 *A) Diffraction from crystal to 2.7Å. B) Crystal lattice, N- and C- terminus are coloured blue and red respectively. Lipidic bilayer inferred from type-1 packing of peptide helices. (PDB: 6W9Z).*

proMP2.2	
Wavelength (Å)	0.9537
Resolution range (Å)	39.74 - 2.7 (2.796 - 2.7)
Space group	P 2 21 21
Unit cell (Å)	44.1 56.205 91.637 90 90 90
Total reflections	28994 (2828)
Unique reflections	6647 (444)
Multiplicity	4.4 (4.4)
Completeness (%)	96.14 (68.62)
Mean I/sigma(I)	13.15 (1.84)
Wilson B-factor (Å^2)	34.89
R-merge	0.06678 (0.8244)
R-meas	0.07598 (0.937)
R-pim	0.0355 (0.4376)
CC1/2	0.999 (0.634)
CC*	1 (0.881)
Reflections used in refinement	6409 (444)
Reflections used for R-free	642 (45)
R-work	0.2165 (0.2248)
R-free	0.2839 (0.2451)
CC(work)	0.917 (0.865)
CC(free)	0.918 (0.721)
Number of non-hydrogen atoms	1479
Macromolecules	1427
Ligands	50
Solvent	2

Table 3.2 Data collection and refinement statistics of proMP2.2

ProMP2.2 was also progressed to LCP crystal screening and within 48 hours two different crystal forms appeared (Fig 3.6B), which were subsequently collected and frozen for X-ray

diffraction analysis. Small needle-like crystals, which appeared in several conditions, did not diffract. By contrast, flat, plate-like crystals which appeared in only a single condition resulted in diffraction to 2.7 Å (Fig 3.8A) with the symmetry of a primitive orthorhombic spacegroup. Once again, a single helix from the crystal structure of a monomeric form of glycophorin A (PDB:5EH6) was used for molecular replacement, yielding a solution in the space group P2-2_1-2_1 (PDB: 6W9Z). Within the asymmetric unit of this crystal there were 6 alpha helices (Fig 3.8B) arranged laterally within discrete layers consistent with stacked lipidic bilayers. Upon closer inspection it was apparent that the hexamer forming the asymmetric unit was actually composed of a trimer of parallel, symmetric dimers (Fig 3.9A).

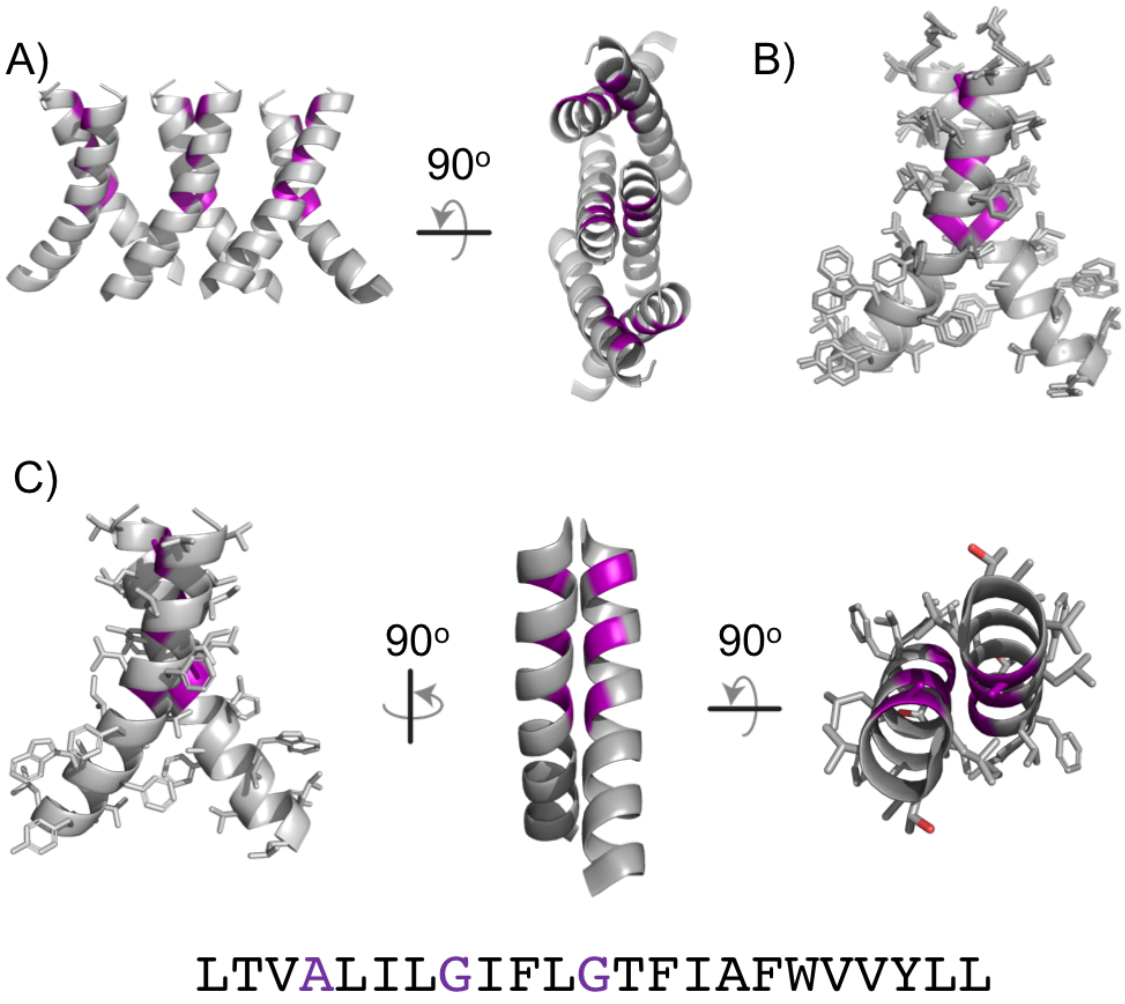

Figure 3.9 Analysis of proMP2.2 asymmetric unit. *A) Representation of the asymmetric unit of proMP2.2 which consisted of 6 helices arranged as a trimeric arrangement of tightly packed dimers. B) Cα backbone alignment of three dimers from the asymmetric unit from A). RMSD of Cα backbone alignments of dimers in asymmetric unit (A) ranged from 0.16Å-0.38Å. C) Close view of middle dimer from A). Purple residues correspond to small residues responsible for allowing close interhelical packing. (PDB: 6W9Z).*

Backbone Cα alignment of each of these three dimers with each other yielded RMSD values between 0.16-0.38 Å (Fig 3.9B), whilst each dimer from this asymmetric unit aligned to the proMP2.2 model with RMSD's between 0.56-0.6 Å (middle dimer alignment shown in Fig3.10A). The dimeric interface was centred around a GXXXG motif resulting in close packing of the peptide backbones and a right-handed crossing angle of 57°C. Flanking this motif on either side within the interface were additional alanine residues, another small

amino acid which appeared to further assist in the close backbone packing within the interface (Fig 3.9C). Alignment of this structure with the structure of glycophorin A yielded an RMSD of 3.47 Å, although the structures aligned very tightly around their shared GxxxG motif (RMSD: 0.48 Å) (Fig 3.10). The close alignment of these GxxxG motifs was further confirmed by the extremely similar interchain distances measured between Cα atoms of the key glycines in the proMP2.2 and GpA interfaces (Fig 3.10C).

By comparison, dimers packed with other dimers within the asymmetric unit did not display close packing of helical backbones but rather associated via nestled hydrophobic sidechains forming small complementary surfaces (Fig 3.9A). Within the crystal these contacts did not propagate past an assembly of three dimers, possibly because extension would cause a twist that cannot be accommodated in the membrane bilayer. Because of this and the weak complementarity, we interpret these interactions between dimers within the asymmetric unit as a result of crystal packing and propose that they are unlikely to contribute significantly to higher-order complex formation in a biological membrane. Overall, these results highlight the improved ability of the proMP design pipeline to accurately encode TM structure when oligomeric state is explicitly accounted for. Furthermore, it underscores the utility of LCP crystallisation in tackling single-pass TM structure determination (Trenker et al., 2016).

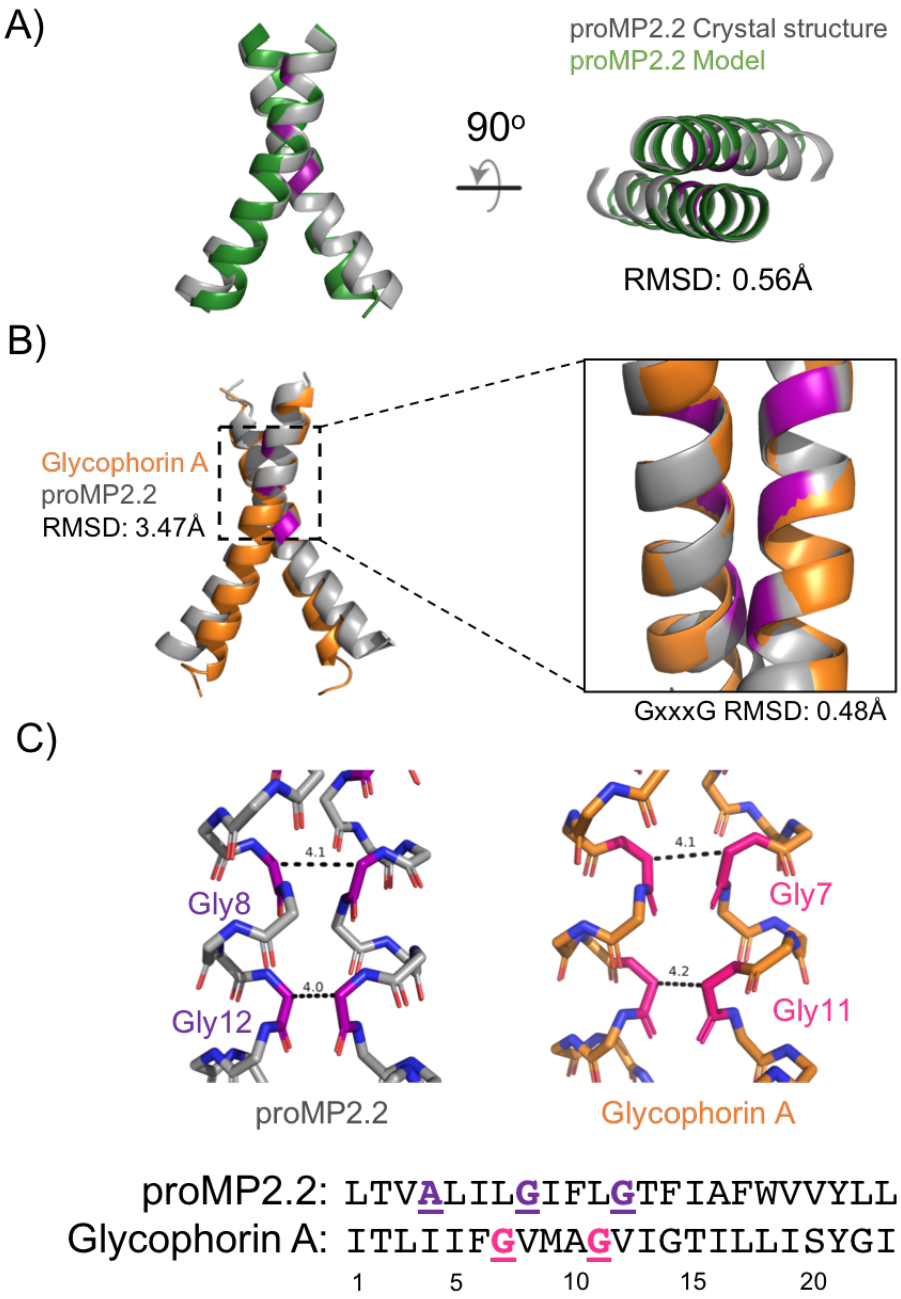

Figure 3.10 De novo and native transmembrane dimers packing around a GxxxG motif. *A) proMP2.2 crystal structure aligned with ab initio modelled structure of proMP2.2 sequence. B) C-α alignments of proMP2.2 crystal structure (PDB: 6W9Z) and Glycophorin A TMD (PDB: 5EH4). RMSD of entire TMD alignment (left) was 3.47Å, RMSD of alignment of GxxxG motif residues (right) only was 0.48. C) Comparison of packing of promP2.2 and Glycophorin A GxxxG motif. Purple and pink residues correspond to glycine residues, with distance between Cα atoms of interface glycine residues depicted in angstroms. Sequence of proMP2.2 and glycophorin A listed below, with proMP2.2 interface small residues coloured purple/underlined and Glycophorin A GxxxG motif residues coloured pink/underlined.*

Design and validation of a monomeric proMP sequence (proMP1)

In addition to the collection of dimeric proMP designs generated, a monomeric sequence (proMP1) was also generated and experimentally validated by collaborators Fleishman and Elazar. This sequence (Fig 3.11A) was modelled and predicted not to form stable higher order complexes of C2, C3 or C4 symmetry. Testing in the dsTβL system confirmed that the sequence was highly expressed in bacterial cells, however displayed very minimal self-association. It displayed a steep and dramatic reduction in self-association compared to the TM sequence of Human Sulfhydryl oxidase 2 (QSOX2), a control TM sequence exhibiting very weak dimeric self-association used as a point of comparison (Fig3.11B).

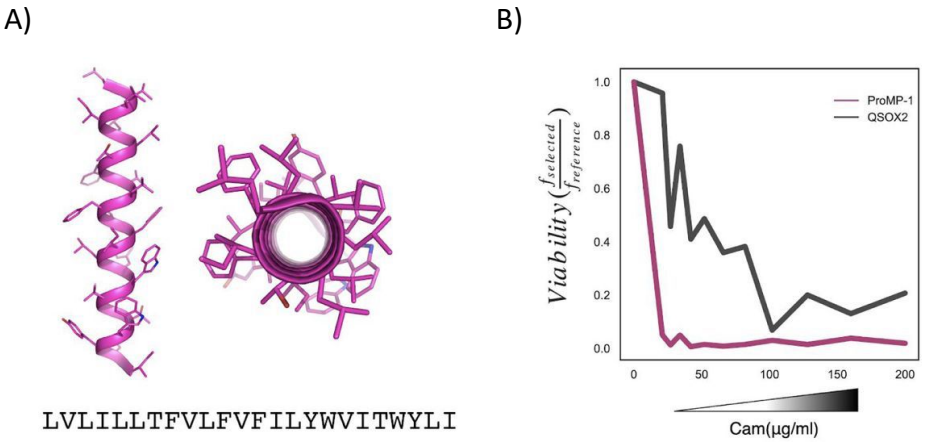

Figure 3.11 Design of a model monomeric proMP sequence. *A) proMP1, a de novo designed monomeric peptide with modelled structure displayed in pink. B) Performance of proMP1 vs. DSOX2 sequences in TOXCAT self-association assay. Y-axis corresponds to the ability of TM sequence to drive dimerization induced bacterial survival in the presence of increasing chloramphenicol concentration (x-axis). Data generated and figure provided by Prof. Sarel Fleishman and Assaf Elazar.*

3.3 Discussion

The ability to probe the relationship between oligomeric state and CAR function was until now complicated by an inability to systematically control receptor oligomeric state without introducing confounding variables that come with repurposing natural protein sequences (Bridgeman et al., 2010). The proMP pipeline described here provided an elegant solution to

this problem, by generating stable TM domains capable of forming any desired oligomeric state. Previous efforts to d*e novo* design TM oligomeric assemblies relied on either collections of hairpin folds (two antiparallel TM domains joined by a loop) inappropriate for inclusion into a type-I receptor (Lu et al., 2018), or modified native proteins (Mravic et al., 2019) inherently limiting the scope of accessible structures due to the small number of experimentally determined natural TM structures. By comparison, the strength of the proMP pipeline is that it is driven by a deep empirical understanding of amino acid behaviour in the context of type-I receptors in a membrane environment (Elazar et al., 2016a, Elazar et al., 2016b, Weinstein et al., 2019). The power of these empirical foundations is highlighted by the very close alignment of the crystal structures and predicted models of proMP3.1 and proMP2.2.

The interfaces of both these structures were characterised by the use of small residues such as glycine and alanine, which permit close inter-helical packing. proMP2.2 was confirmed to pack around a GXXXG motif similar to that originally observed in Glycophorin A (Lemmon et al., 1992, MacKenzie et al., 1997) and since identified to play a role in the dimerization of many other natural TM dimers (Mueller et al., 2014). The GxxxG motif of proMP2.2 enforced a crossing angle of 57°C, a value within the range of values observed of other TM domains dimerising via comparable right-hand crossing angles (Bugge et al., 2016). Interestingly, the trimeric interface of proMP3.1 was also characterized by close inter-helical packing of a small residue motif (GGxxGAxxA), a motif not previously identified in any known trimeric membrane proteins. In both the case of proMP2.2 and proMP3.1 residues other than those core small residues at the interface were observed to play important roles in structural stability. These findings agree with the observation that while small-residue motifs such as GxxxG are frequently found at dimer interfaces, the motif itself is not on its own sufficient for dimerization (Doura et al., 2004).

Furthermore, in the case of proMP2.2 a Blast search query against the NCBI Uniprot human protein database (Altschul et al., 1990) (table 3.3) demonstrated that very few proteins of reasonable similarity exist, with only one protein (5-hydroxytryptamine receptor 1D) possessing both sequence identity over 50% and the putative GxxxG motif of proMP2.2. This supports the prediction that proMP sequences are unlikely to take part in promiscuous

interactions with native, small residue motif containing proteins, as the sequence flanking the GxxxG motif is unlikely to be identical. Additionally, 7 out of 8 of the similar protein sequences identified, including HTR1D, are GPCRs and it is unclear whether the packing of a single-pass transmembrane TM, such as a proMP, with a GPCR would be energetically favourable. Regardless, our experience with proMP3.1 provides evidence that adjustments to the design pipeline can be made that improve the selectivity the sequences generated if required. Further design rounds could feasibly be included to model proMP sequences against native TM sequences suspected of interacting with endogenous proteins, which in turn would permit rational design of mutations to disrupt such interactions.

Entry	Protein names	Identity	Coverage	Sequence
P28221	**5-hydroxytryptamine receptor 1D (HTR1D)** (Homo sapiens)	57.9%	82.6%	ILGIILGAFIICWLPFFVV
Q15391	**P2Y purinoceptor 14** (Homo sapiens)	63.6%	47.8%	FVAIFWIVFLL
A5JUU3	Purinergic receptor P2Y G-protein coupled 14 transcript variant 2 (Homo sapiens)	63.6%	47.8%	FVAIFWIVFLL
Q7RTP6	**[F-actin]-monooxygenase MICAL3** (Homo sapiens)	88.9%	39.1%	LKVALILGI
E9PP85	[F-actin]-monooxygenase MICAL3 (Homo sapiens)	88.9%	39.1%	LKVALILGI
B4DJ91	HCG21531, isoform CRA_b (Homo sapiens)	88.9%	39.1%	LKVALILGI
A0A5F9ZHV5	**F-actin monooxygenase** (Homo sapiens)	88.9%	39.1%	LKVALILGI
Q01629	**Interferon-induced transmembrane protein 2** (Homo sapiens)	87.5%	34.8%	ALILGIFM

Table 3.3 Results from Blast sequence query of proMP2.2.

Interfaces were also observed between symmetrical proMP2.2 dimers within the crystallographic asymmetric unit which, in the context of the proMP2.2 crystal lattice, permitted close packing of 6-helices. These interactions were characterised by loose packing of complementary side-chain surfaces, however there was a lack of close interhelical packing of TM backbones. Interactions between TM backbone atoms, facilitated by close packing of TM helices are integral to TM homodimer structures, particularly in the case of TM sequences lacking polar residues capable of hydrogen bond formation (Bugge et al.,

2016). For this reason, it is unlikely that the interactions observed between proMP2.2 dimers in the asymmetric unit would be capable of driving inter-dimer complex formation in the context of native cellular environments characterised by low protein density relative to a crystallographic system. While this hypothesis is currently speculative, there is no inherent upper limit to the oligomeric state which proMP sequences can be modelled *in silico*. Therefore, the extension of this pipeline to account for pentameric and hexameric complexes could ensure that the designed proMP2.2 homodimeric interface is indeed energetically more favourable than that of any hexamer.

Lessons learned from studies of proMP2.1

proMP2.1 failed to crystallise in it's predicted dimeric form, instead exhibiting a combination of anti-parallel dimeric packing and continuous, front-to-back parallel packing, characterised by weak surface complementarity and a relatively large distance between helical backbones. This finding doesn't necessarily negate the ability of this sequence to form its predicted dimeric structure but suggests, at least in the context of a LCP bilayer, that it has a stronger propensity to crystallise via the alternative observed interfaces. The proMP design process in its current form does not account for anti-parallel interactions, because in a mammalian or bacterial cell context, parallel TM helix orientation in the membrane is encoded by peptide signal sequence. There may be utility for including a modelling step where chains are evaluated in an anti-parallel orientation, to assess the potential for undesirable packing arrangements. Information of this kind could help prioritise oligomeric sequences for structural studies according to their propensity to associate in a non-physiological, anti-parallel orientation. This would serve to increase the efficiency of future crystallisation efforts by focussing on sequences likely to form primarily parallel interfaces in screening conditions. Alternatively, the use of different crystallization techniques may assist in diversifying the crystal forms accessible for a given peptide. For example, crystallisation of highly hydrophobic TM peptides is possible from detergents (Mravic et al., 2019) and this may permit different crystal contacts capable of driving the formation of alternative crystal packing arrangements compatible with proMP dimer interfaces. Additionally, Nuclear magnetic resonance (NMR) represents an alternative technique capable of producing atomic level structures of small TM peptides (Trenker et al., 2016, Call et al., 2006, MacKenzie et al., 1997). However, the significant cost and labour-

intensity of NMR studies limits its utility in screening large numbers of proMP designs, which formed part of the initial rationale for using LCP crystallography.

Continued structural studies of trimeric and tetrameric proMP designs.

In addition to the proMP sequences described above, structural investigations of other proMP sequences have since been continued by others in the lab. Trimeric and tetrameric sequences modelled using the optimised proMP pipeline described above, were generated by Sarel and his team and purified within our lab. Two such sequences successfully yielded crystals, a trimeric design termed proMP3.2 and a tetrameric design termed proMP4.1 (Fig 3.12). Crystals of proMP4.1 have produced low-resolution diffraction (currently at 4-5Å resolution limit) and work is currently ongoing to optimise crystal conditions to improve diffraction resolution (conducted by Julie Ngyuen and Melissa Call).

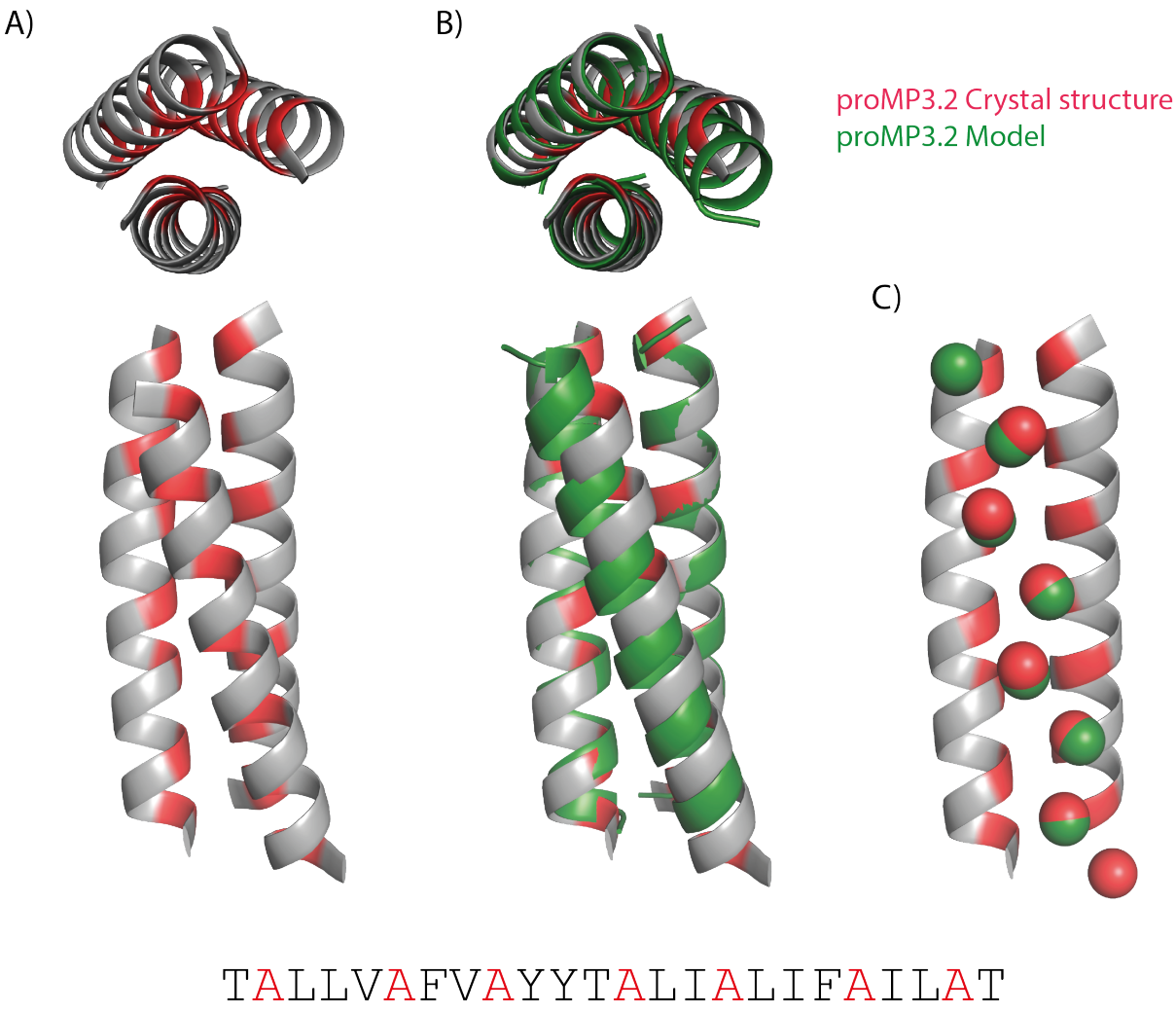

Figure 3.12 Crystal structure of the trimeric peptide proMP3.2. *A) Crystal structure of proMP3.2 solved to a resolution of 3.5 Å. Red colour indicates alanine residues forming key trimeric helical interface. B) Alignment of proMP3.2 crystal structure with modelled structure, with one of the three helices (the helix in the front position in this figure) adopting an anti-parallel orientation. C) Coloured balls depict the close alignment of experimentally determined and modelled Cβ carbons of putative interface alanine residues within the anti-parallel helix. Peptide purification and crystallisation conducted by Julie Ngyuen, Crystal structure determination conducted by Julie Ngyuen and Melissa Call. (PDB: 6WA0).*

By comparison, structure-quality diffraction data were obtained for proMP3.2 (Fig 3.12A), using detergent solubilised protein after the failure to achieve crystallization using LCP crystallography (PDB: 6WA0). Interestingly, the structure derived from this crystal aligned very closely with the design model along two helices but with the third helix in an unexpected anti-parallel orientation (Fig 3.12B, C). This third chain nonetheless used the same predicted interface sequence but in reverse order, akin to a 'structurally palindromic' sequence, which was evident from the close alignment of Cα carbons between model and crystal structures (Fig 3.12C). This finding reaffirmed the need for consideration of helix orientation during proMP modelling to maximise biological relevance of experimental proMP structures, a consideration first highlighted by the non-productive crystallisation of proMP2.1. Alternatively, there may be protein engineering applications in which antiparallel helix arrangements are desirable and as such an improved methodology for adapting the proMP pipeline to accommodate membrane orientation requirements will be of significant utility.

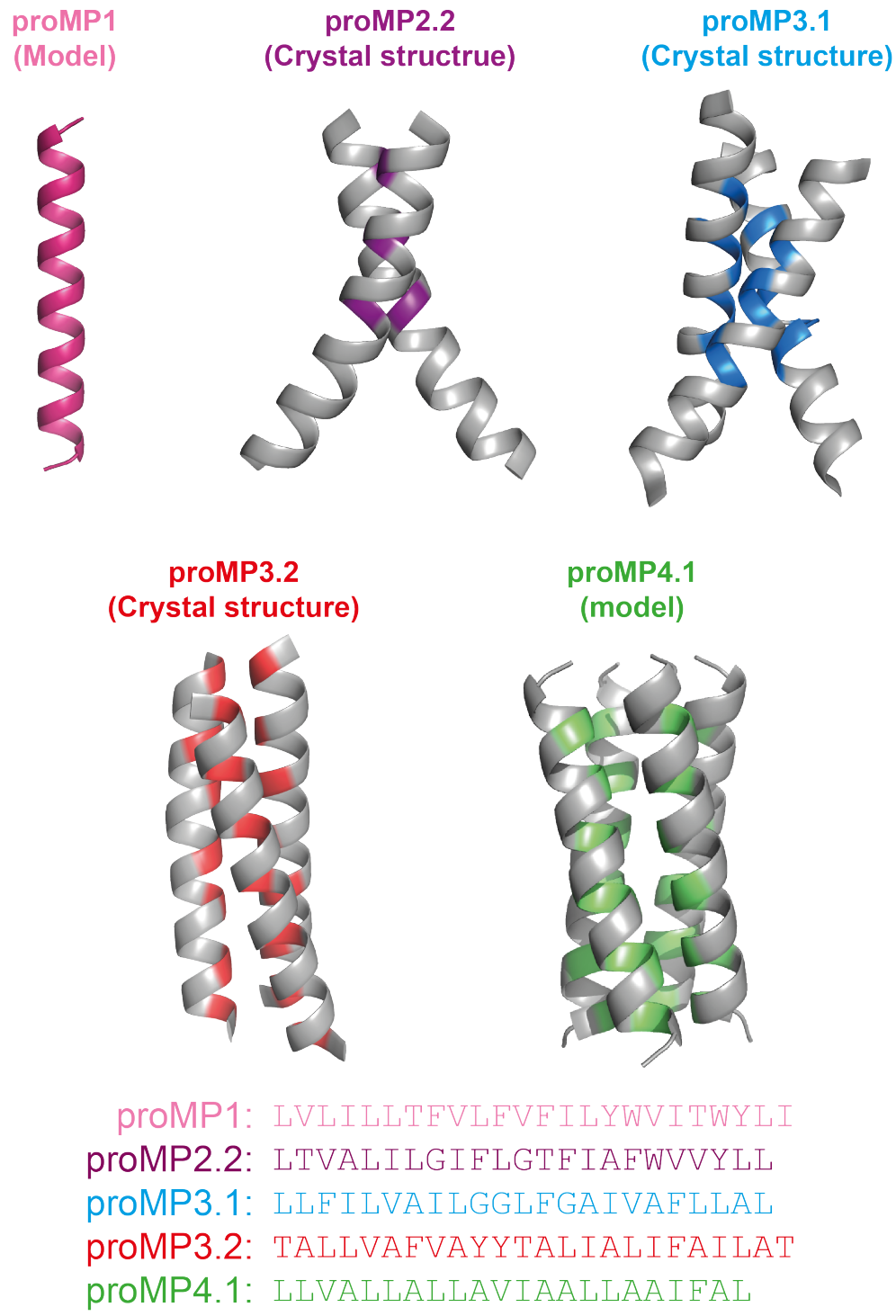

Figure 3.13 Validated proMP designs thus far. *Four proMP sequences have been successfully crystallized resulting in X-ray diffraction. proMP2.2, proMP3.1, proMP3.2 gave crystal structures while proMP4.1 at the time of writing is undergoing crystal optimization to improve the quality of X-ray diffraction. proMP1, a monomeric design, has been modelled, with TOXCAT assays confirming an absence of self-association. Coloured residues in each structure corresponds to small residues responsible for allowing close helix packing.*

These structures presented an appropriate starting point for investigations into the role of oligomeric state in CAR T cell function and therefore proMP1, proMP2.2 and proMP3.1 were selected for inclusion into CAR constructs. These functional studies were initiated with the understanding that continued efforts within the lab to structurally validate additional proMP sequences would provide further opportunities to extend the proCAR approach to higher order oligomers and different packing geometries.

Chapter 4 Generation and validation of novel oligomeric CARs on a HER2-directed background.

4.1 Background and rationale

With confidence in the structures of our dimeric and trimeric TM domains, we carefully considered an appropriate CAR background in which to test the effects of altering receptor oligomeric state. In selecting from the countless variety of published CAR designs, we assessed potential candidates according to two key criteria: clinical relevance, in terms of the antigen specificity and the similarity of CAR constructs to those currently in clinical use; and secondly technical convenience, referring to the availability of optimized CAR DNA sequences in addition to published validation of *in vitro* and *in vivo* experimental systems. Guided by these criteria, we decided a second-generation CAR framework would be most appropriate, a term referring to a CAR consisting of scFv-stalk-TM-costimulatory sequence-CD3ζ tail. The specific 2nd generation construct we selected was composed of an scFv specific for the surface antigen HER2 (the well described FRP5 scFv clone (Harwerth et al., 1992, Orlandi et al., 1989)), a human CD8α hinge, human CD28 TM and costimulatory domains and the human CD3ζ stimulatory tail. This construct, referred to below as the FRP5 CAR, demonstrated several important technical advantages over other CARs (summarized in the following sections), while also presenting an opportunity to improve treatments for HER2^{+} solid tumours with notoriously poor prognoses.

HER2: a clinically relevant CAR T cell target.

HER2 is a surface receptor belonging to the epidermal growth factor receptor family, which works with other members of this receptor family to oppose apoptosis and enhance cell proliferation (Moasser, 2007). The dysregulation of HER2 signalling, via overexpression or constitutive activity due to gain of function mutations, is well described as a key oncogenic driver in a variety of cancer settings (Moasser, 2007, Iqbal and Iqbal, 2014). Crucially, HER2 expression is almost universally associated with poor prognosis across numerous cancer settings (Yoon et al., 2012, Liu et al., 2010, Nakamura et al., 2005, Camilleri-Broet et al., 2004, Slamon et al., 1987) and has therefore been the subject of intense research and pharmaceutical targeting. This intense research culminated in the development of the monoclonal antibody trastuzumab (Herceptin), currently approved for the treatment for

HER2+ breast and gastric cancer (Cardoso et al., 2020, Bang et al., 2010). Trastuzumab is believed to rely on a dual mechanism of action: firstly by binding HER2 (Fig 4.1) and blocking oncogenic signalling; and secondly, through the ability of the therapeutic antibody Fc domains to bind various host immune cells and initiate antibody-dependent cell-mediated cytotoxicity (ADCC) (Baselga et al., 2001). While trastuzumab is a highly successful frontline treatment against breast cancer, in the context of other HER2^{+} tumour settings such as lung and bladder cancer it has proved far less effective (Langer et al., 2004, Hussain et al., 2007).

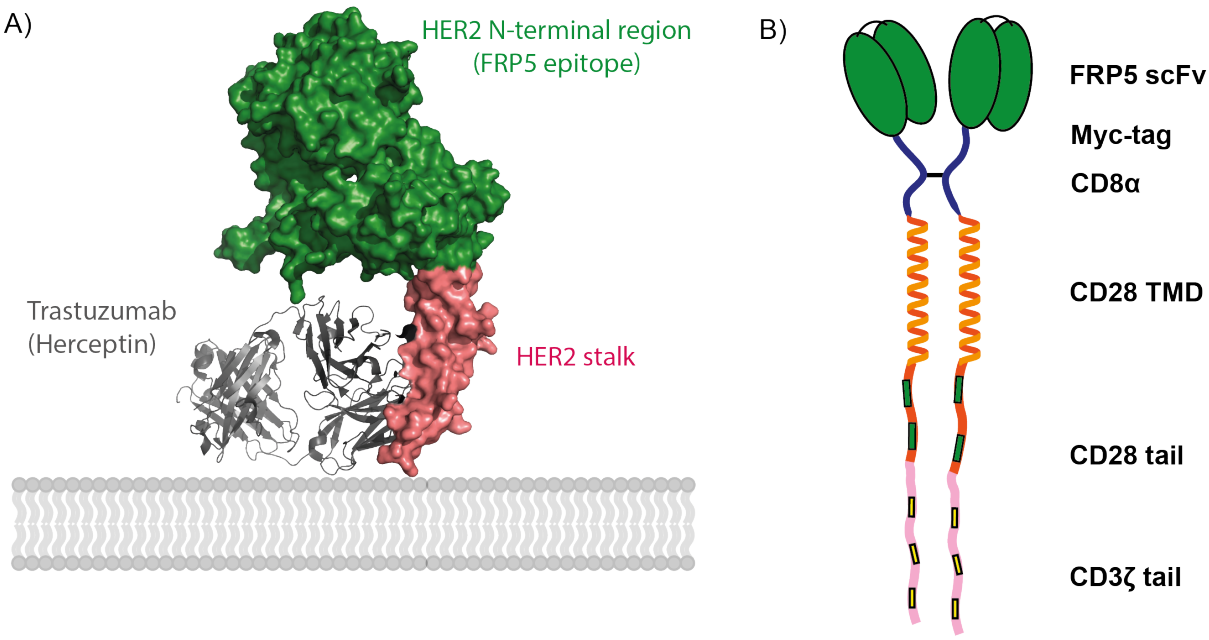

Figure 4.1 HER2 – A clinically significant therapeutic target. A) *Crystal structure of HER2 bound to the therapeutic anti-body Trastuzumab (grey) (PDB:1N8Z). Trastuzumab binds HER2 stalk region (pink), in contrast the therapeutic FRP5 scFV clone binds an uncharacterised epitope within the HER2 N-terminal region (green). B) Depiction of the domain architecture of the FRP5 CAR, with the native proteins from which CAR domains were derived listed alongside.*

Given the broad clinical relevance of HER2 expression it was one of the earliest antigens targeted by 1st generation CAR designs (Stancovski et al., 1993). The advent of improved 2nd generation CAR designs has since resulted in several HER2-directed CAR therapy trials targeting HER2+ cancers such as glioblastoma, gastric cancer and sarcoma (Liu et al., 2017). However, one of the key complexities in the development of HER2 targeted CAR T therapies is that HER2 is expressed widely through-out the body by a multitude of different tissues at

steady state. This presents the possibility of on-target, off-tumour toxicity, in which cytotoxicity is directed towards healthy cells expressing low levels of HER2 (relative to those of HER2 overexpressing tumours). For this reason, the ability to carefully control CAR T cell potency is especially crucial in ensuring both the efficacy and safety of treatment. This was dramatically highlighted in an early dose escalation trial in which a patient treated with anti-HER2 CAR T cells for metastatic $HER2^+$ colon cancer experienced severe toxicity due to recognition of $HER2^+$ lung epithelial cells, unfortunately resulting in death (Morgan et al., 2010). Accordingly, more recent phase I and II clinical trials have carefully optimized reduced T cell numbers to improve treatment safety. However, while isolated instances of long-lasting remission have been observed (Hegde et al., 2020), the bulk of HER2 directed CAR T cell dose escalation studies have resulted in ineffective, albeit largely toxicity-free therapies.

For this reason, novel CAR engineering approaches targeting HER2 have been pursued in recent years, with the aim of optimizing CAR potency to maximize treatment efficacy while minimizing on-target, off-tumour toxicity. An elegant example of this was published by Liu et al (2015), in which a panel of scFvs with diverse affinities for HER2 were used to control the potency of a CAR composed of the CD8α stalk/TM, 4-1BB costimulatory domain and CD3ζ tail. Using an *in vivo* mouse model, they observed that CARs containing an scFv of intermediate affinity to HER2 induced potent killing of tumour cells expressing high levels of HER2 but did not respond to those expressing low levels of HER2 within the same mouse. By comparison, CARs containing a high affinity scFv killed both high and low HER2 expressing cells in the same mouse model. This provides clear evidence that off-tumour toxicity can be effectively balanced with anti-tumour efficacy through deliberate manipulation of CAR potency. Additionally, this presents a clear opportunity to use novel HER2 CAR 'tools', such as altered affinity scFvs, in combination with our *de novo* designed TM structures to expand the potency landscape of our approach (Fig 4.2).

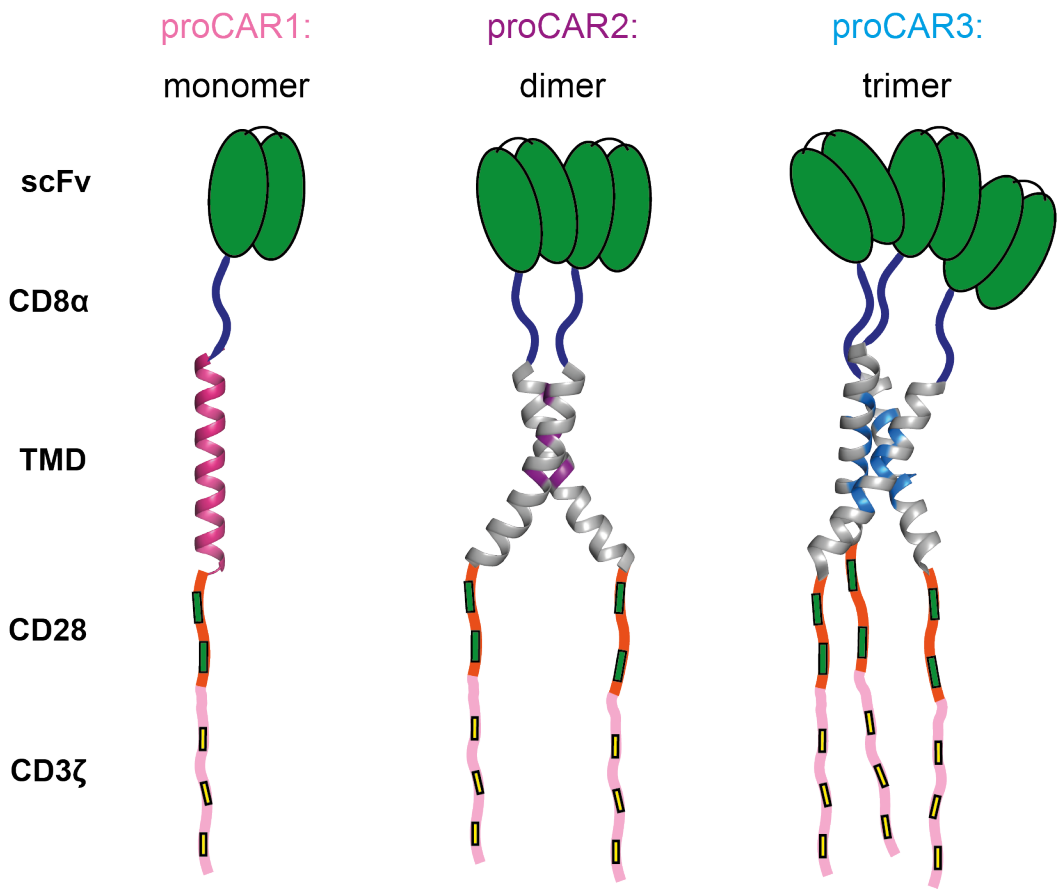

Figure 4.2 The proCAR platform. *Insertion of oligomeric proMP sequences into the FRP5 CAR construct is intended to dictate receptor oligomeric state. CARs containing proMP sequences are referred to herein as proCARs (programmed CARs). Numerical suffic indicates intended oligomeric state of proCAR.*

FRP5 CAR experimental system

Importantly, each of the previously described studies utilised a subtly different combination of CAR domains; therefore, the CAR sequence used in our study required careful consideration. We selected a CAR sequence composed of the FRP5 anti-HER2 scFv clone in combination with a CD8α stalk, CD28 TM/costimulatory tail and CD3ζ tail, (herein termed the FRP5 CAR), as it presented several important technical advantages. The construct was the subject of extensive and well-documented optimization at the Peter MacCallum Cancer Centre (adjacent to WEHI in Melbourne), including the establishment of several experimental systems and target cell lines previously shown to be suitable for interrogation of FRP5 CAR T cell function *in vitro* and *in vivo*. Robust surface expression of this CAR has been achieved in primary mouse T cells and these CAR T cells have demonstrated potent

killing of human and mouse derived HER2$^+$ target cells *in vitro* (Haynes et al., 2002). Furthermore, these primary FRP5 CAR T cells exhibit potent anti-tumour activity against both human and mouse derived HER2$^+$ tumour cells in mouse models of lung, colon, and breast cancer (Haynes et al., 2003, Moeller et al., 2005, Haynes et al., 2002). These studies provided us with confidence that the FRP5 CAR design presented a validated experimental pathway from fundamental *in vitro* optimization through to pre-clinical *in vivo* mouse studies.

Another important characteristic of this CAR construct is that its architecture aligns closely with constructs used in a number of phase I and II clinical trials internationally. A majority of HER2 targeted CAR T cell clinical trials, (reviewed in Liu, 2017) utilize the same FRP5 anti-HER2 scFv clone linked via a CD28 TM to the CD28/CD3ζ tail. These studies have demonstrated that safety is attainable when T cell doses are carefully managed. The potential of the FRP5 CAR T cells was highlighted by recent isolated incidence of curative treatment of a patient with metastatic rhabdomyosarcoma (Hegde et al., 2020); however, the lack of obvious clinical benefit in the treatment of HER2$^+$ glioblastoma (Ahmed et al., 2017) highlights the urgent need for improvements to this therapy. Importantly, the similarity of these constructs to our chosen CAR backbone maximizes the clinical relevance of our study and paves the way for rapid inclusion of synthetic oligomeric TMs into these clinically relevant CARs.

Experimental Aims

The aim of my work presented in this chapter, in the context of the broader work of our collaborative team, was to evaluate the expression and function of FRP5 proCARs containing monomeric, dimeric and trimeric proMP TM sequences. Through the use of immortalised T cell lines these confirmatory experiments were deemed crucial to deciding which proCAR designs were suitable to be progressed into more expensive and labour-intensive primary CAR T cell experiments.

4.2 Results

Design of receptor constructs

While recent studies have underscored the functional influence of CAR stalk/TM sequence, scant evidence exists as to the molecular features of these domains responsible for their functional contributions. This is underscored by the fact that transmembrane domains commonly found in almost all current-generation CAR constructs are included as a legacy of historical stalk and/or costimulatory tail insertions (CD8α TM came with the stalk; CD28 TM came with the costimulatory domain). Therefore, we relied on careful consideration of protein biochemistry first principles when generating the sequence modifications necessary for generation of our proCAR panel.

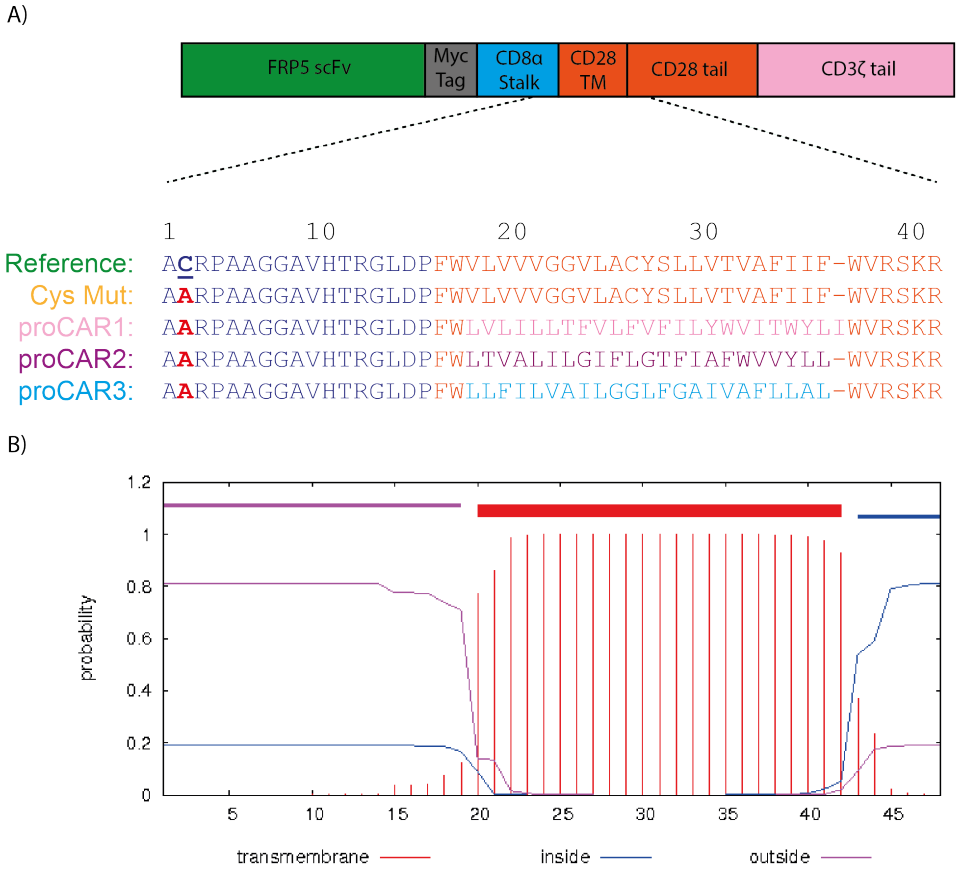

Figure 4.3 Design of the FRP5 proCAR panel. *Domain architecture depicting components of the FRP5 CAR, with insertion site of proMP sequences displayed inset. The mutation of a cysteine residue (bold/underlined) within CD8α stalk sequence to alanine is depicted in red font. B) Analysis of CAR stalk and TM domain using the TMHMM transmembrane domain prediction server (located at - http://www.cbs.dtu.dk/services/TMHMM/) to characterise position of TM domain and guide selection of proMP insertion site.*

Generation of a base CAR construct for proMP insertion

Within the CD8α–derived stalk sequence of the FRP5 CAR we identified a cysteine residue known to facilitate covalent trapping of receptor dimers in the context of the native CD8α protein (Fig 4.3A). We reasoned that it would be preferential to mutate this cysteine to minimise the number of influences upon CAR oligomeric state. Therefore, this cysteine in the reference FRP5 CAR construct was mutated to an alanine and termed the cysteine mutant (Cys Mut). This Cys Mut construct was then compared to the reference CAR for its ability to express to the cell surface. Reference and Cys Mut receptor were cloned into the pLVX-TRE3G doxycycline-induced retroviral expression vector and transduced into the mouse BW5147 T cell thymoma line. These cells are deficient in the expression of several key T cell surface receptors such as CD4, CD8, CD3ζ and TCRαβ, whilst they do express other key T cell regulatory proteins such as CD28 and CD45 (White et al., 2020). Hence, this cell line was considered a simplified system in which basic biochemical characteristics of the proCAR panel could be interrogated and optimised prior to progressing into more physiologically relevant primary T cells with a full complement of T cell surface receptors. CAR expression was controlled by supplementation or removal of doxycycline from cell culture medium, allowing receptor surface trafficking to and downregulation from the surface, respectively, to be quantified. Expression level was comparable between reference and Cys Mut constructs according to surface staining and flow cytometry analysis, as was the rate of receptor trafficking to and from the cell surface (Fig 4.4A). Additionally, western blot analysis confirmed that mutation of the CD8α stalk cysteine was sufficient to prevent the formation of higher order covalent CAR species (Fig 4.4B). Given its robust comparable expression to Reference and its inability to form covalent higher order oligomers, Cys Mut became the base construct into which proMP sequences were inserted.

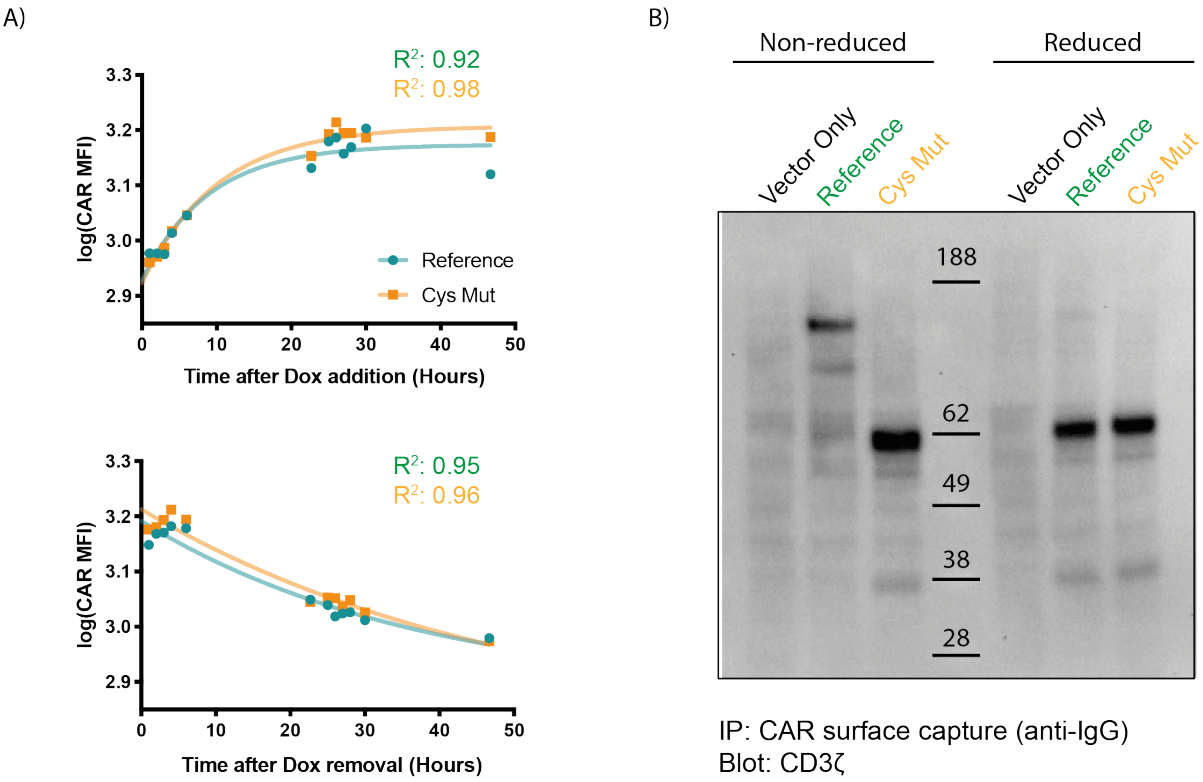

Figure 4.4 Characterisation of FRP5 CAR stalk cysteine mutant. (A) *FRP5 reference or stalk cysteine mutant (Cys Mut) CARs were expressed using a doxycycline (Dox) inducible retroviral expression vector in BW5147 cells. Top – surface expression measured after treatment with dox. Bottom – Surface expression following removal of cells from dox-containing media. Surface expression measured by anti-myc saining and flow cytometry. Plots are representative of N=2 independent experiments. B) The same cell lines described in A) were treated with dox for 48 hours, then stained with a polyclonal anti-IgG capable of binding the FRP5 scFv. Antibody bound CAR complexes were immunoprecipitated following cell lysis and analysed by SDS-PAGE and western blotting. 2x10^7 cells used as input, split in half between reduced and non-reduced samples. Theoretical molecular weight (MW) of FRP5 CAR is ~57kDa. N=1 independent experiment.*

Construction and expression testing of FRP5 proCARs

The FRP5 CAR TM domain and flanking regions were analysed via the TMHMM transmembrane helix predictor (Fig 4.3B) and it was decided that the most appropriate TM insertion was between two tryptophan residues at either end of the CD28 TM domain (Fig 4.3A). Aromatic residues are frequently found at the aqueous-membrane interface and play an important role in anchoring the protein in the membrane by forming cation-pi

interactions with lipid head groups (Petersen et al., 2005). Hence, we reasoned that preserving these tryptophan residues would promote membrane stability and expression regardless of the TM sequence inserted. This 23-residue portion of the receptor was therefore replaced by the sequences of proMP1, proMP2.2, proMP3.1 to generate the proCAR1, proCAR2 and proCAR3 constructs, respectively, with the number suffix referring to the target oligomeric state (Fig 4.3A). These proCAR constructs were cloned into the pMSCV-IRES-mCherry retroviral expression and transduced alongside reference and Cys Mut constructs into a variant of the BW5147 T cell line expressing a GFP reporter containing NFkB-responsive promoter elements. This permitted easy measurement of T cell downstream signalling via flow cytometry analysis in subsequent experiments. Cell surface staining using an anti-Myc antibody was analysed via flow cytometry, confirming the successful expression of proCAR1, 2 and 3 (Fig 4.5B-D). Although proCARs generally exhibited lower levels of surface expression compared to both Reference and Cys Mut CARs, these differences were not statistically significant. CAR expression was also evaluated using the human Jurkat T cell line. Confirming expression in human T cells was particularly important given the ultimate aim of translating promising findings in mouse models into a clinical human T cell setting. Surface staining and flow cytometry confirmed the expression of proCAR designs at levels comparable to Reference and Cys Mut CARs (Fig 4.5E). Subtle differences in relative proCAR expression in Jurkat T cells compared to BW5147 T cells were observed, such as a reduction in proCAR2 expression, compared to enhanced proCAR1 and proCAR3 expression relative to both reference and Cys mut.

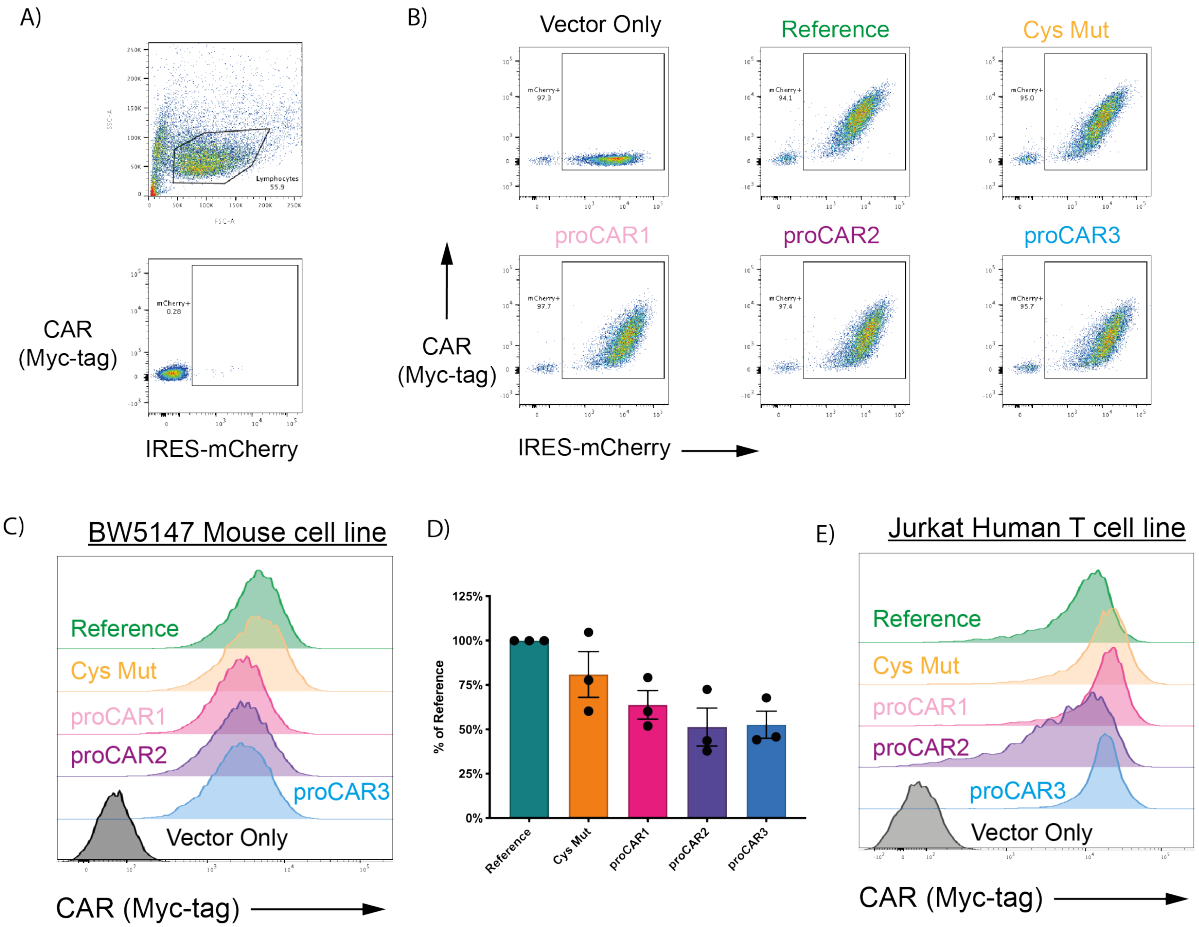

Figure 4.5. Surface expression of FRP5 proCAR panel in mouse and human cell lines. *At day 10 after retroviral transduction cells were stained with anti-Myc antibody and analysed via flow cytometry. A) The gating strategy used to select live cells (top) and mCherry positive cells indicating successful transduction of the pMSCV-IRES-mCherry vector (bottom). B) Representative example of successful expression of proCAR panel in BW5147 mouse T cell line with C) corresponding histogram overlay of CAR staining with anti-Myc. D) Quantification of CAR surface expression via Myc staining and flowcytometry. Calculated as % of Reference CAR, mean +/- SEM, N=3 experiments. E) Histogram overlay of CAR expression in the human Jurkat E6.1 T cell line. CARs were expressed using a variant of pMSCV expression vector lacking IRES-mCherry, hence Myc histogram overlay derives solely from live cell gate. Representative of N=2 independent experiments.*

An immunoprecipitation (IP)-western blot analysis was then undertaken using the BW5147 CAR T cell lines described above to confirm that the CARs expressed to the cell surface were the correct size and that the stalk cysteine mutation was successfully ablating covalent dimerization. A surface capture approach was used, where cells were pre-coated with anti-

IgG antibody capable of binding the CAR scFv domain, allowing antibody-bound receptors to be immunoprecipitated and analysed via non-reducing SDS-PAGE and western blot. From these data it was evident that the mutation of the CD8α stalk cysteine to alanine in Cys Mut and proCAR constructs resulted in the complete loss of covalent higher order species, running at the expected monomeric molecular mass of approximately 55kDa (Fig 4.6B). This result was expected, as SDS-PAGE will be particularly disruptive to the extracellular domains of full length proCAR constructs and this is likely to impact any TM domain interactions that were seen when isolated proMPs were assessed by SDS-PAGE. It was also observed that all CAR designs ran as doublets, whereas proCAR designs exhibited an additional doublet running at a molecular weight slightly lower than that expected of a proCAR monomer (Fig 4.6B). We hypothesized that this lower weight band might be the result of a protein cleavage event close to either the N- or C- terminus of the receptor, given the small difference in molecular weight observed. Blotting with an antibody targeting an epitope at the N-terminus of the CD3ζ sequence in the CAR tail (Fig 4.6C), also yielded the same lower molecular weight bands. The equivalence of results yielded by extra- and intra-cellular epitope blotting provided confidence that cleavage was not taking place within the proMP sequence itself; however, I could not exclude the possibility of cleavage events closer to the C-terminus of the CD3ζ tail or at the scFv N-terminus. proCAR2 demonstrated the lowest proportion of this lower molecular weight doublet, suggesting that this phenomenon was TM sequence specific.

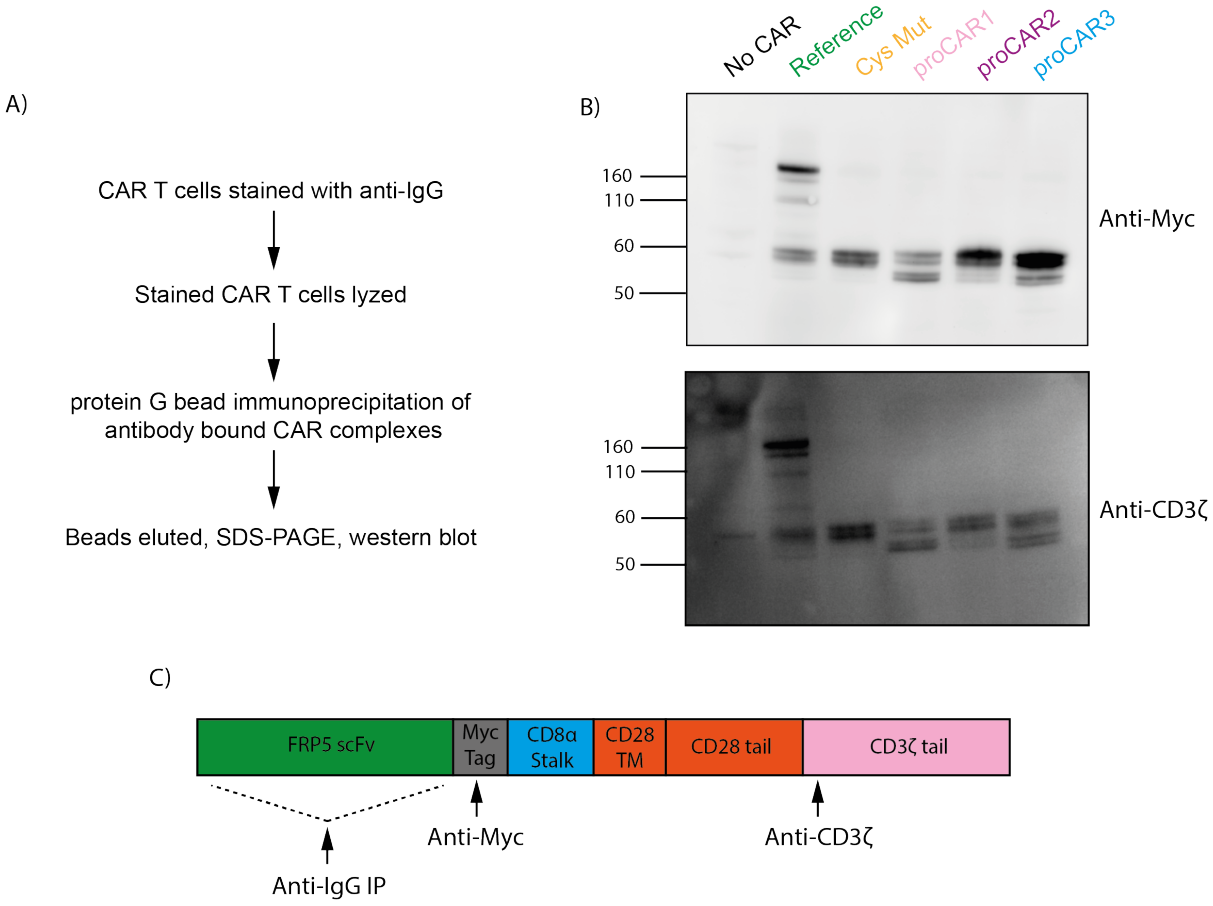

Figure 4.6 FRP5 proCAR protein analysis. *A) Flowchart depicting surface capture IP approach used for analysis of surface expressed fraction of cellular FRP5 CAR. Polyclonal anti-IgG binds constant region of scFv domains. B) Western blot analysis of FRP5 proCAR panel following surface capture IP and SDS-PAGE. 10^7 cells used as input per construct. Representative of N=2 independent experiments. C) FRP5 domain architecture with position of relevant antibody binding epitopes. Theoretical MW of FRP5 CARs = 57kDa.*

Determination of proCAR oligomeric state using biochemical methods

Given the successful expression of the proCAR monomer, dimer and trimer panel we sought to confirm that the TM sequences within the proCAR designs were driving formation of their predicted oligomeric species. While the entirety of the data generated from molecular modelling, bacterial self-association TOXCAT assays and crystal structures gave us confidence in the strength of the oligomeric TM interfaces, I also wished to confirm these findings in the context of a mammalian membrane environment. The determination of receptor oligomeric state in mammalian membranes is a notoriously difficult technical

challenge, and therefore ultimately two orthogonal experimental approaches were required for us to provide confidence in the oligomeric state of the proCAR panel.

One of the first experimental approaches undertaken utilized an *in vitro* translation (IVT) expression system designed to trap higher order protein species, an approach previously used within our lab to interrogate oligomerization of the DAP12 transmembrane immune receptor (Knoblich et al., 2015). Briefly, radio-labelled protein is translated in reticulocyte lysate and in the presence of mammalian endoplasmic reticulum membranes (Fig 4.7A). Incorporated protein is then oxidized in order to promote disulfide crosslinking of oligomeric, cysteine-containing proteins. To enable crosslinking of CAR oligomers scFv and stalk regions were replaced with the stalk region of the immune receptor DAP12, which possesses 2 cysteine residues. In previous studies conducted by our lab, it was demonstrated that this stalk sequence was capable of forming inter-chain disulfide bonds that resulted in the covalent trapping of dimeric, trimeric and tetrameric species of DAP12 (Fig 4.7B) (Knoblich et al., 2015). Constructs were therefore generated to encode DAP12 stalk-variable TMD-CD28 costimulatory tail-CD3ζ tail and termed 'DAP12 fusions' (Fig 4.7C), with the aim of covalently trapping specific any oligomeric species formed. In addition to generating DAP12 fusions of the proCAR panel and FRP5 reference construct (possessing the CD28 TM domain) several control constructs were designed (Fig 4.7D). A DAP12 fusion possessing the TM domain composed of 23 valine residues (poly-valine, PolyVal) was included as a monomeric control, as valine residues are energetically favourable within lipid bilayers but the featureless all-valine helices are not expected to take part in inter-chain interactions (Hessa et al., 2005). The TM domain of the red blood cell surface glycoprotein glycophorin A (GpA) was also included as a dimeric control due to its well described propensity to drive homo-dimerization (MacKenzie et al., 1997, Doura and Fleming, 2004). Each of these domains are well-studied within the receptor biology field and therefore constituted appropriate benchmarks against which to compare the capacity of our proMP sequences to adopt their respective oligomeric species.

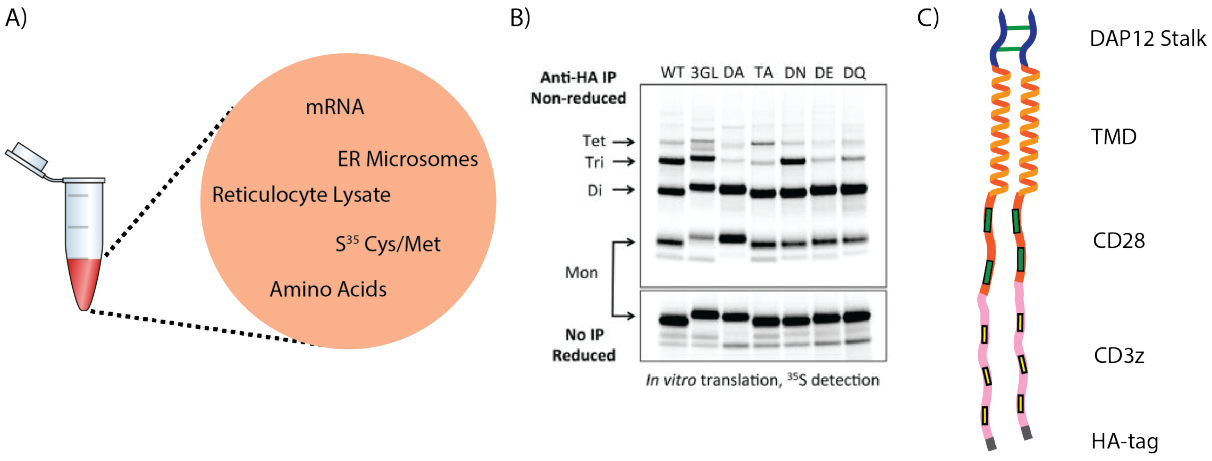

D)

```
                1         10         20         30
Reference:      QAQSDCSCSTVSPFWVLVVVGGVLACYSLLVTVAFIIF-WVRSKR
proCAR1:        QAQSDCSCSTVSPFWLVLILLTFVLFVFILYWVITWYLIWVRSKR
Poly-Valine:    QAQSDCSCSTVSPFWVVVVVVVVVVVVVVVVVVVVVVVV-WVRSKR
proCAR2:        QAQSDCSCSTVSPFWLTVALILGIFLGTFIAFWVVYLL-WVRSKR
Glycophorin A:  QAQSDCSCSTVSPFWITLIIFGVIAGVIGTILLISYGI-WVRSKR
proCAR3:        QAQSDCSCSTVSPFWLLFILVAILGGLFGAIVAFLLAL-WVRSKR
```

Figure 4.7. Analysis of receptor oligomeric state in mammalian membrane using In vitro translation (IVT). *A) Depiction of IVT reaction components. ER microsomes are derived from mammalian plasma-cell lines. B) Previously published data depicting the ability of IVT approach to covalently trap and visualise higher order oligomeric receptor species. Data adapted from Knoblich et. al., (2015). C) Domain architecture and D) sequence alignment of DAP12 fusion constructs used in Figure 4.8.*

While theoretically this assay was capable of trapping and visualizing oligomeric species of a higher order than dimers, we encountered technical challenges that prevented confident quantification of trimeric species. DAP12 samples demonstrated a notable reduction in its ability to trimerize compared to previously published work (Fig 4.7B). Additionally, higher molecular weight bands observed in figure 4.8A appeared to be slightly too large to account for the expected 72kDa and 96kDa bands expected of a trimeric and tetrameric DAP12-fusion complex respectively, and these bands were also faintly visible in the lane corresponding to DAP12. Hence, given we couldn't be absolutely confident in the identity of these bands we decided this assay was not appropriate for robust quantification of the presence of trimeric species.

By comparison, unambiguous bands of an appropriate molecular weight corresponding to monomeric and dimeric species (Fig 4.8A) were present and I therefore undertook quantitative measurement of the dimer:monomer (D:M) ratio (Fig 4.8B). As expected, the predicted monomeric poly-Valine and proCAR1 DAP12 fusions exhibited the lowest D:M ratio, indicating that these TM domains demonstrated the weakest propensity to self-associate. However, this ratio was not zero, which indicated a small degree of dimerization, possibly attributable to stochastic interactions trapped by irreversible disulfide formation. By comparison the GpA TM domain demonstrated approximately double the degree of dimerization, aligning with the extensive literature reports of its ability to homo-dimerize. Impressively, the proMP2.2 DAP12-fusion demonstrated enhanced propensity to homodimerize compared to GpA, re-affirming the ability of our optimized TM design pipeline to generate structures capable of surpassing native TM domain affinity. It was also observed that the CD28 TM domain exhibited a propensity to dimerise similar to that of GpA (albeit with a high degree of variation), in support of the recent identification of a conserved CD28 TM homo-dimerization motif (Leddon et al., 2020). These findings demonstrated the reliability of the proMP1 and proMP2.2 sequences in forming their expected oligomeric states in a mammalian membrane, extending upon data generated by our collaborators in bacterial TOXCAT system. However, given we were unable to confidently quantitate the formation of trimeric complexes, alternative approaches were considered to provide insight into the oligomeric state of proMP3. Furthermore, in the interest of physiological relevance it was desirable to further validate the oligomeric state of proMP1 and proMP2.2 in the context of full-length receptors and in live cell membrane.

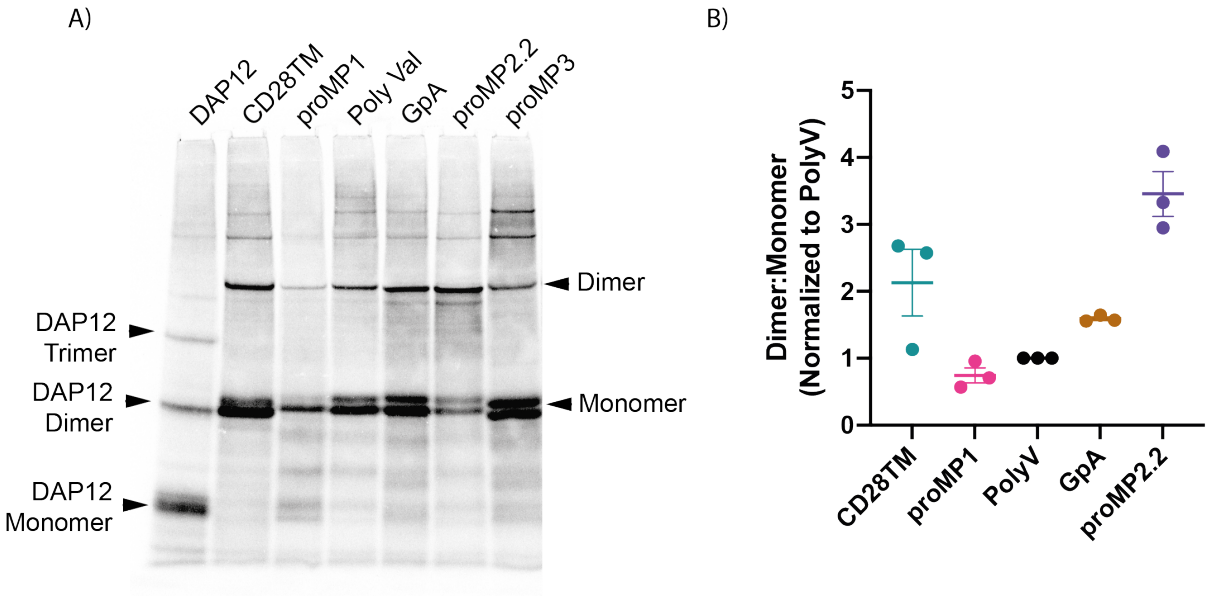

Figure 4.8 Interrogating proMP oligomerisation using IVT. *Constructs detailed in figure 4.7 were expressed using an IVT system. Protein translated into mammalian ER membranes was oxidised to enable interchain cysteine disulfide crosslinking. Reactions were dissolved in LDS containing buffer and run via SDS-PAGE. A) Representative data depicting DAP12 fusion constructs produced using IVT. Full-length native human DAP12 receptor was included as a control to confirm assay reliability. B) Quantification of ratio between monomers and dimers for each of the TM domains listed. N=3, error bars = mean +/- SEM.*

Quantitative fluorescence imaging– determining receptor oligomeric state in live cells

Several microscopy approaches have been utilized to measure the oligomeric state of receptors expressed in mammalian cells and these offered an opportunity to validate the oligomeric state of our proCAR panel expressed in T cells. A relatively simple approach known as number and brightness (N&B) analysis is particularly well suited to answering our question (Nolan et al., 2018). This approach relies on the assumption that increases in oligomeric state of fluorescently labelled protein species correspond with increased variation in the measured fluorescence intensity of a given pixel over time (summarized in figure 4.9). In simple terms: the diffusion of a trimeric fluorescent protein in and out of a pixel will result in an increase and decrease in the measured fluorescence intensity of that pixel by a factor of 3. By comparison, a monomeric protein will give rise to a relative increase and decrease in the fluorescence intensity by a factor of 1 as it diffuses in and out of a pixel. This relationship is summarised by the formula: Brightness (B) = fluorescence

variance/fluorescence intensity. A key consideration of this technique is that it does not determine absolute oligomeric state, but rather relies on the comparison of B-values benchmarked against a known monomeric standard. One of the key benefits of this approach was that theoretically brightness could be calculated regardless of the fluorescence intensity of a target cell line, therefore enabling the analysis of cell lines expressing physiologically relevant surface expression levels.

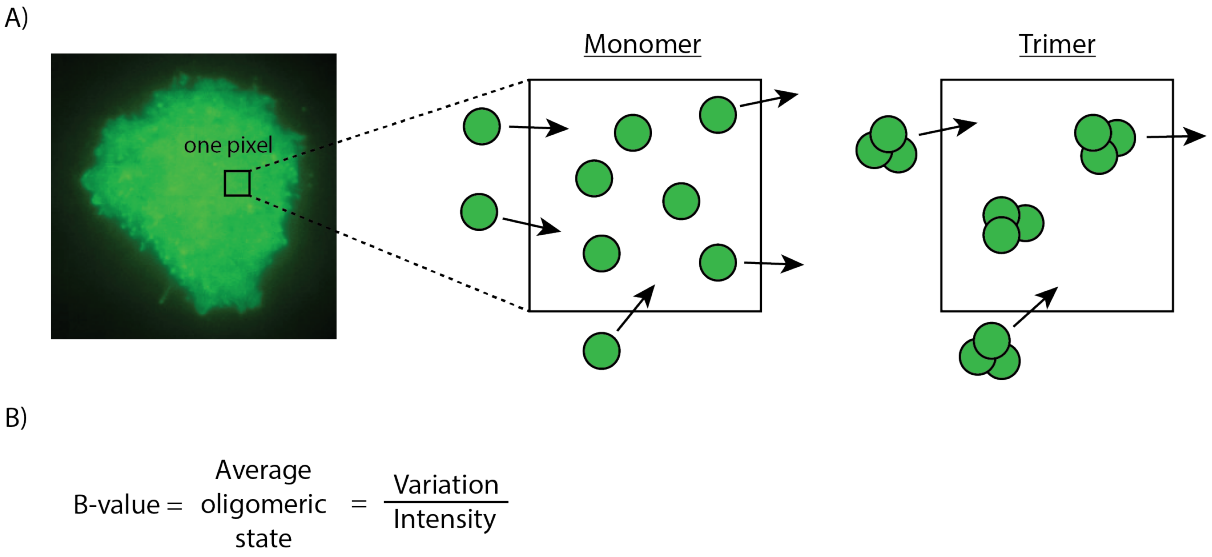

Figure 4.9. Measuring protein oligomeric state using quantitative fluorescence microscopy. *A) Diagram depicting the theoretical basis of number and brightness (N&B) analysis, a form of quantitative fluorescence microscopy. Briefly, N&B analysis correlates the relationship between fluorescence intensity and variance on a pixel-by-pixel basis. Increases in receptor oligomeric state of a fluorescently tagged protein results in increases in fluorescence variance. Eg. as a trimeric protein diffuses in or out of a pixel the corresponding fluorescence intensity of that pixel increases of decreases by 3 relative units. By comparison, the diffusion of a monomeric receptor in or out of a pixel will result in an increase or decrease in fluorescence intensity of that pixel by a relative unit of 1. B) This characteristic is quantified by calculating fluorescence variance over time as a ratio of fluorescence intensity, on a pixel-by-pixel basis. This calculation gives rise to a relative, aggregate measure of protein oligomeric state.*

The proCAR designs were re-cloned to include a monomeric eGFP variant fusion c-terminal to the CD3ζ tail (Fig 4.10A) and retrovirally transduced into the BW5147 cell line for

analysis. These receptors were successfully expressed and demonstrated comparable levels of surface expression (Fig 4.10B). Given the ability to of N&B to make relative comparisons of oligomeric state the proCAR panel was imaged and analysed, with the aim of estimating the oligomeric state relative to proCAR1. Cell lines were imaged using TIRF microscopy, an approach which excites fluorophores a short distance away from the coverslip, enabling specific visualization of proteins at the plasma membrane. Cells were cultured in tissue-culture treated chamber slides (Ibidi) which permitted live cell imaging. Short videos of individual cells were captured and subsequently analysed using the simFCS N&B analysis tool, with B-values normalised to represent average oligomeric state on a per-cell basis, relative to proCAR1. In an idealised scenario a B-value of 1, 2 and 3 would be expected for proCAR1, 2 and 3, respectively. Experimental data confirmed that the expected positive correlation between intended oligomeric state of proCARs 1-3 and B-value was observed (Fig 4.10C). Both proCAR2 and proCAR3 exhibited lower B-values than expected of an idealised scenario (1.3 and 2.8 vs. 2 and 3 respectively). It was not possible to differentiate between a lesser propensity of proCAR2,3 to form their target oligomers or a slight propensity for proCAR1 to form higher order oligomers, both of which would yield the results observed. These data, in combination with the results of prior IVT-dimerization experiments, gave us confidence that the expected positive correlation between desired and experimentally determined oligomeric states of proCARs1-3. Further experiments using orthogonal experimental approaches would be useful in confirming absolute measurements of the distribution of oligomeric species between the proCAR designs (discussed in chapter 4 discussion below), however the data generated are generally consistent with predicted proMP oligomeric state. For this reason, I deemed it appropriate to progress this panel of proCAR designs forwards for functional testing.

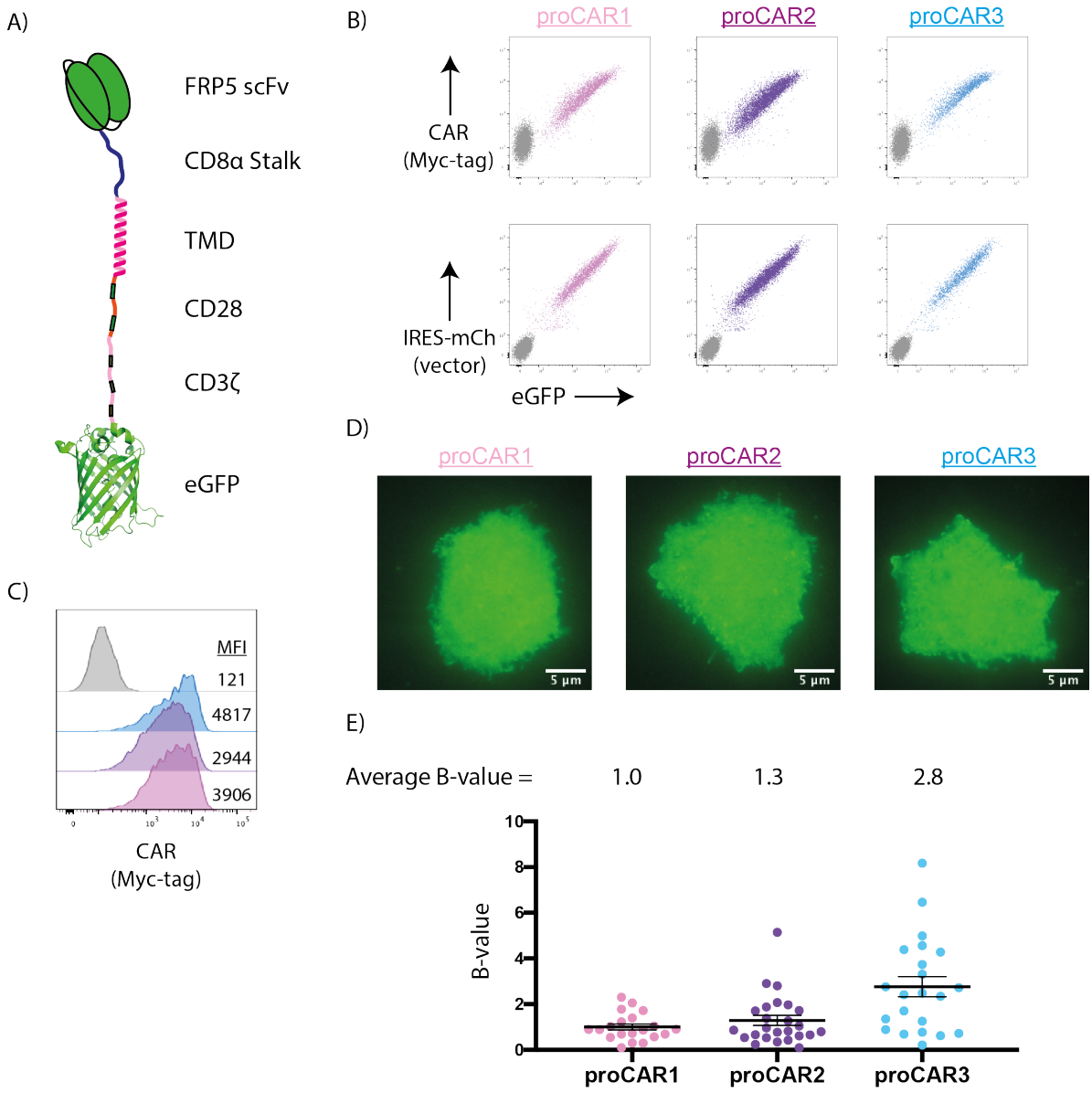

Figure 4.10 Investigating proCAR oligomeric state using numbers and brightness analysis. *A) Domain architecture of CAR-GFP fusion construct. B) Expression of proCAR-GFP fusion CARs in the BW5147 cell line. CAR expression determined using anti-Myc surface staining, correlated with eGFP expression and pMSCV IRES-mCherry. With Myc staining presented as histograms in C). D) representative images of BW5147 proCAR-GFP fusion T cells imaged using TIRF microscopy. E) B-values measured from at least 20 cells for each cell line. Error bars = mean +/- SEM.*

Preliminary assessment of proCAR signalling ability *in vitro*

To assess the ability of the proCAR panel to initiate signalling in response to antigen I designed a co-culture assay, making use of the aforementioned NFkB GFP-reporter element

present within the BW5147 cell line. These cells could be incubated on target cells expressing HER2 and GFP tracked to report on NFκB and stained for CD69, an early activation marker of T cells (Fig 4.11).

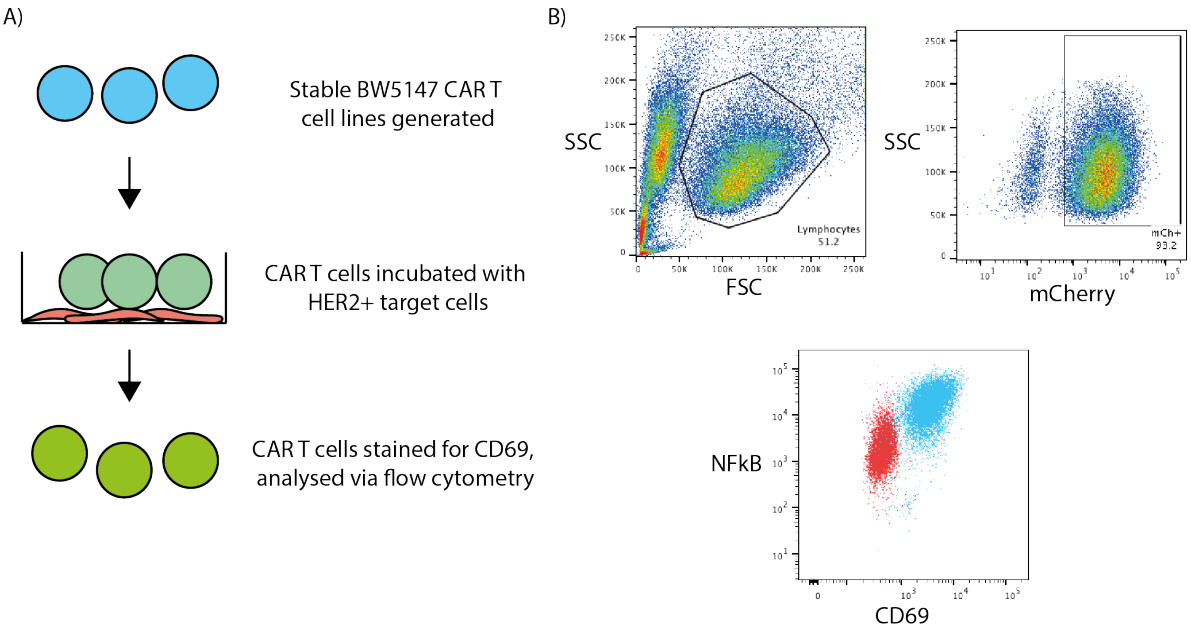

Figure 4.11. Quantifying T cell signalling using a BW5147 T cell reporter assay. *A) flowchart detailing the use of a BW5147 cell line expressing an GFP NFkB transcription factor reporter cell line. B) Flow cytometry gating strategy used to gate for live, mCherry+ cells and subsequently quantify expression of the activation marker CD69 and the expression of GFP, corresponding to activation of NFkB. Representative example presented is BW5147 Reference FRP5 CAR T cells co-cultured for 6 hours with HER2+ SKBR3 target cells (blue) or in the absence of target cells (red).*

Initially reference, Cys Mut and proCAR-expressing cells were compared for their signalling in response to co-culture with the SKBR3 human breast cancer cell line, which expresses high levels of HER2 (See figure 4.13A), and all receptors exhibited comparable kinetics and magnitude of both NFkB activation and CD69 expression (Fig 4.12). Additionally, the absence of NFkB activation and CD69 expression on cells at a steady state (0hr timepoint, cells analysed without exposure to target cell lines) demonstrated that signalling was antigen-dependent and the "No CAR" control demonstrated that signalling was strictly CAR-dependent. Given these results demonstrated that the proCAR designs were signalling

competent, we decided to assess the potency of the proCAR panel in response to tumour cell lines expressing low and intermediate HER2 surface expression.

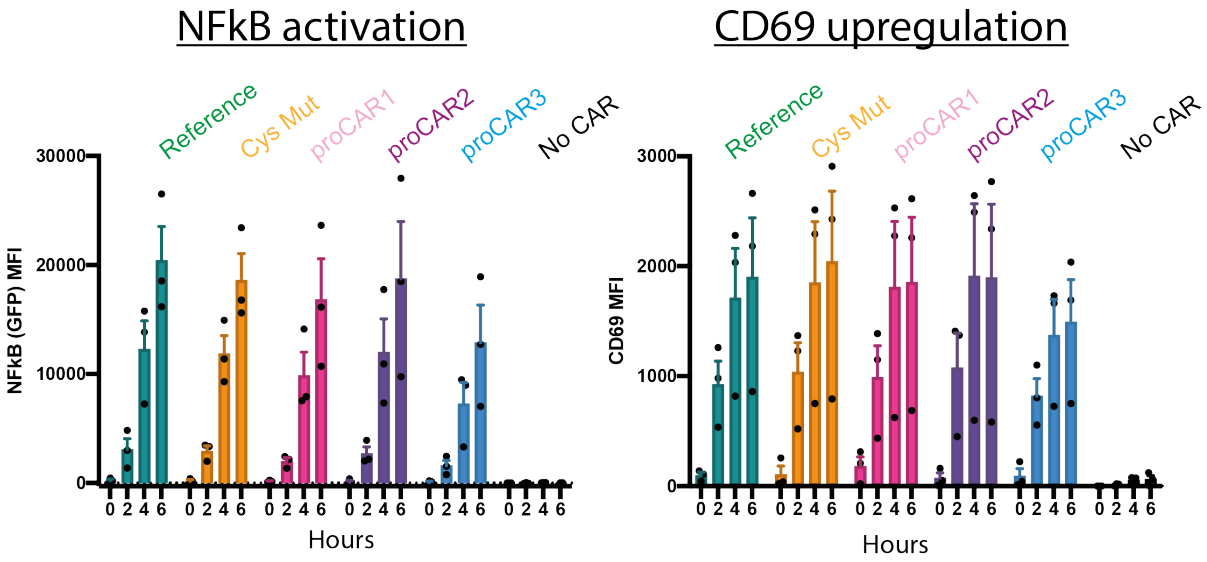

Figure 4.12. **Analysis of proCAR signalling capacity *in vitro***. *BW5147 T cells were transduced with CAR constructs, once CAR expression stabilised CAR T cells were co-cultured with HER2+ target cell lines for up to 6 hours. At completion CD69 surface expression and NFkB activation was measured via flow cytometry using the approach detailed in figure 4.10. NFkB activation and CD69 upregulation in response to SKBR3 target cells. N=3, mean +/- SEM.*

The cell lines selected (listed in figure 4.13) exhibited HER2 surface expression levels ranging from 2-fold to 20-fold lower than the SKBR3 cell line. We hypothesized that at lower ligand expression levels, differences in ligand sensitivity between proCAR designs may become apparent. Four additional cell lines were acquired which demonstrated a range of different HER2 expression levels: the human breast cancer MCF7 and MDA-MB-231 human cell lines as well a MC57 mouse fibrosarcoma cell line ectopically expressing human HER2 (MC57-HER2) and parental MC57 cells with no expression of human HER2. Each of these cell lines expressed lower levels of HER2 compared to the SKBR3 cell line.

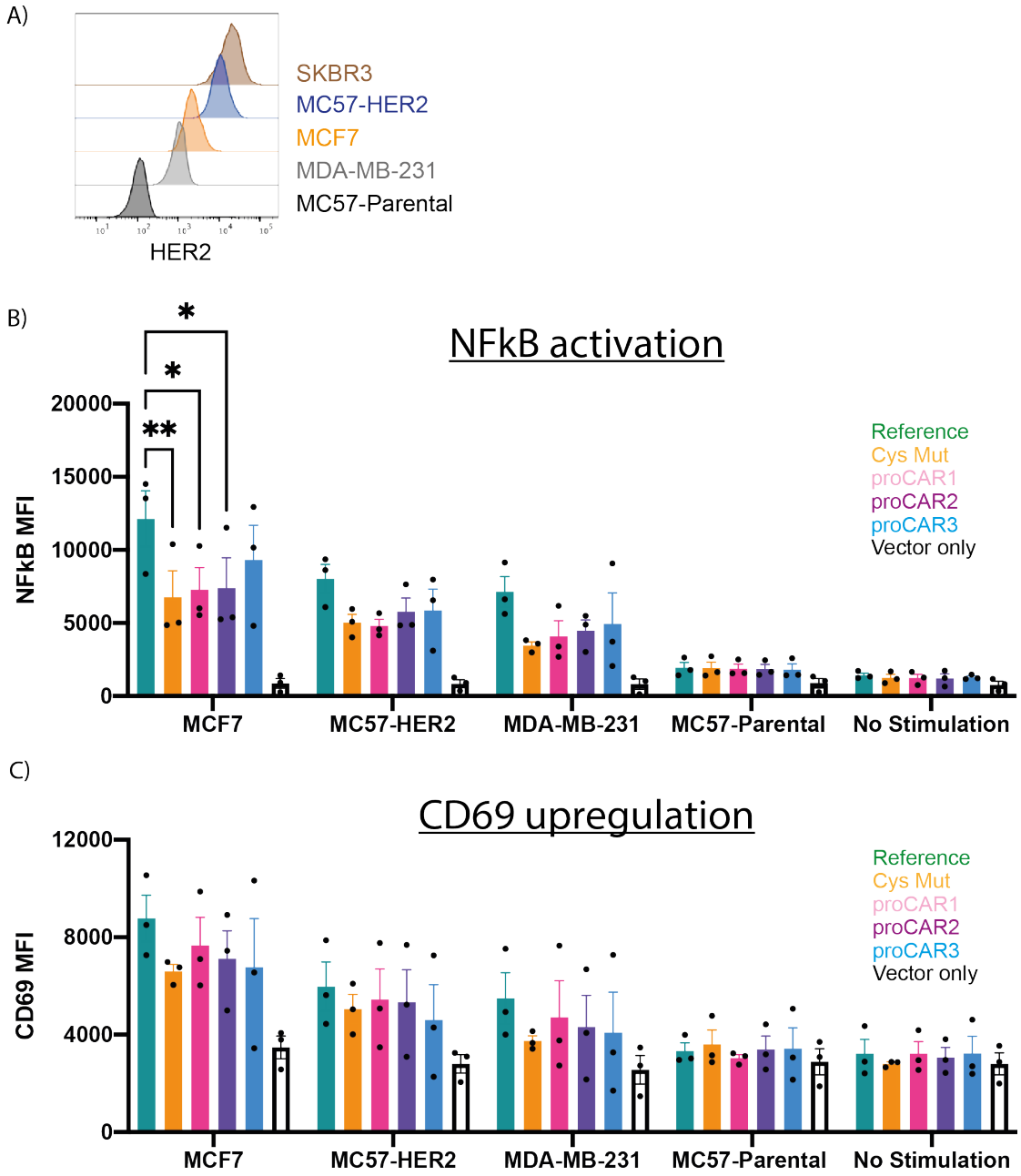

Figure 4.13 FRP5 proCAR response to cell lines with varied HER2 expression. *BW5147 CAR T cells were co-cultured with target cell lines with a range of HER2 expression levels for 6 hours to assess T cell signalling capacity. A) Flow cytometry analysis of target cell lines stained for HER2. B) NFκB activation and C) CD69 stimulation following 6-hour co-culture with relevant target cell line. Mean +/- SEM, * = p<0.05, **=p<0.001, one-way ANOVA.*

I observed that the magnitude of signalling response did not directly correlate with HER2 expression levels in all cases (Fig 4.13 B, C), MCF7 cells for example gave rise to the greatest magnitude in NFκB and CD69 signalling despite expressing lower levels of HER2 than MC57-

HER2 cells. The cell line expressing the lowest level of HER2, the MDA-MB-231 cell line, did however give rise to the lowest degree of T cell activation as expected. I observed a trend across all target cell lines tested that Cys Mut and proCAR T cells demonstrated a comparable reduction in the magnitude of NFκB activation and CD69 upregulation to low and intermediate HER2 expressing target cells. However, this difference only reached statistical significance in response to the MCF7 target cell line. Additionally, the lack of T cell activation in response to the MC57-parental cell line, which doesn't not express human HER2, again confirmed the antigen specificity of these CAR T cells.

These data indicated that all proCAR designs were capable of initiating T cell signalling and activation in response to target cell lines expressing a wide range of ligand expression levels and with similar kinetics and magnitude compared to Reference and/or Cys Mut controls in most cases. These findings justified progression into primary mouse T cell functional assays, which allowed the measurement of biologically relevant T cell functions such as target cell cytotoxicity and cytokine release, functions that tumour cell lines (such as the bW5147 cell line) are unable to recapitulate.

proCAR constructs maintain robust tumour cell killing while attenuating cytokine release

Reference, Cys Mut and proCAR constructs were expressed in mouse primary CD8+ T cells and demonstrated comparable surface expression levels as had been observed in mouse and human tumour T cell lines previously. Primary CD8 CAR T cells were activated and expanded for use in two alternative *in vitro* functional assays. One of these assays was a cytotoxicity assay, in which primary CAR T cells were co-cultured for 4 hours with target cells and assessed for their ability to kill (Fig 4.14A). Killing was quantified by loading target cells with radioactive chromium prior to co-incubation with CAR T cells, with cytotoxicity quantified as the amount of chromium liberated into cell culture medium at a 4-hour timepoint. By comparison, a cytokine release assay involved co-culture with target cells for 24 hours, at which point media is collected and analysed via cytokine detection cytometric bead array (CBA) assay (Fig 4.15A). For both assays MC57-parental and MC57-HER2 cells were used, allowing quantification of both ligand independent and dependent functionality, respectively. It should be noted that all primary T cell experiments discussed under this sub-

heading were conducted by Dr. Ashleigh Davey using the CAR constructs I designed and produced.

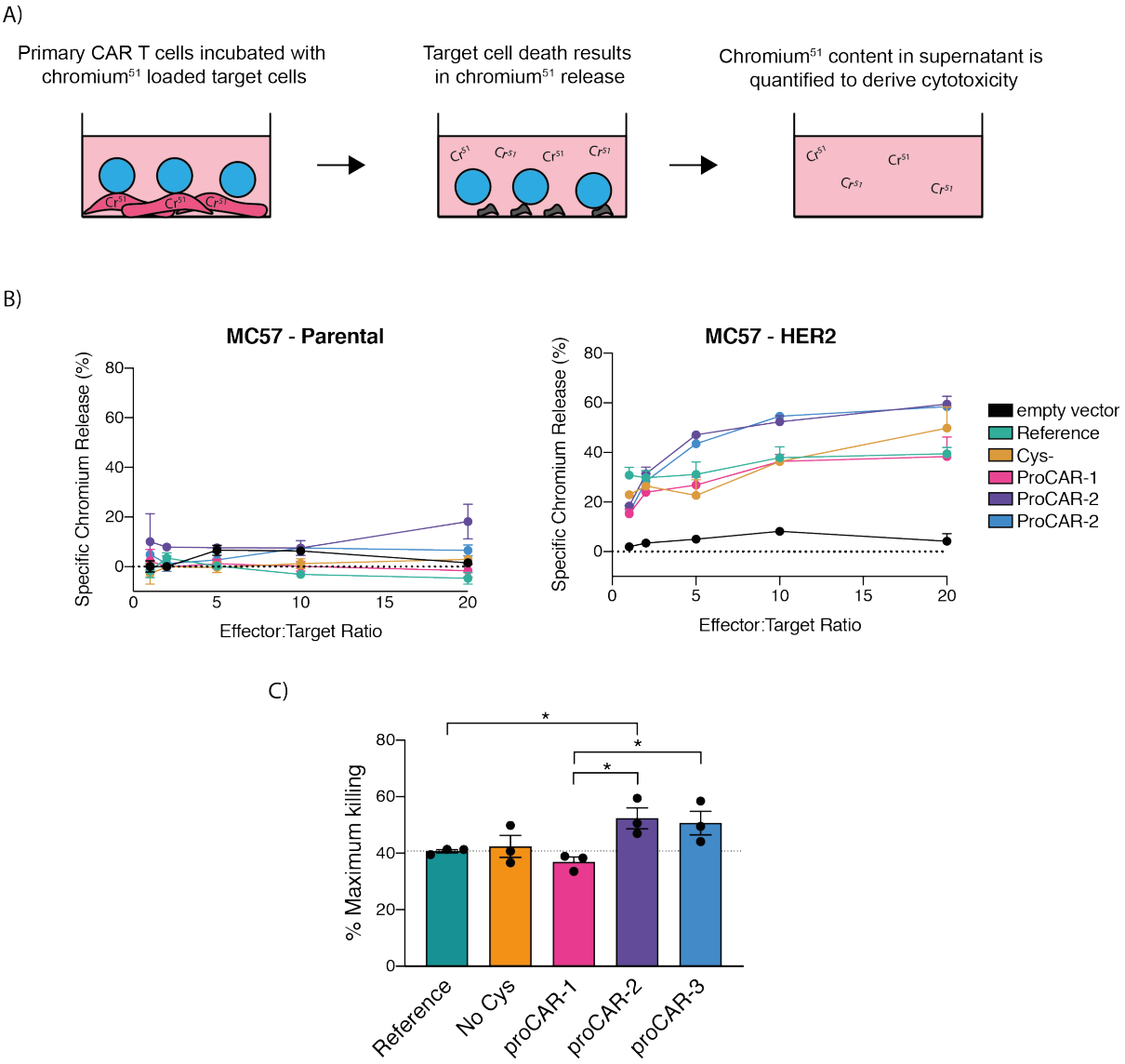

Figure 4.14. FRP5 proCARs can enhance primary T cell cytotoxicity. *A) Cytotoxicity assay involved target cells incubated with radioactive ^{51}Chromium co-cultured for 4 hours with primary CAR T cells. Target cell killing by CAR T cells results in liberation of ^{51}Chromium into cell media. Quantification of ^{51}Chromium in cell media is interpreted as proportionate to target cell killing. B) Representative examples of chromium cell killing experiment. Increasing ratio of T cell to target cells (depicted on x-axis) results in an increase in proportion of target cells killed. HER2 negative MC57 parental cells shown on left, HER2 positive MC57 cells on right. C) Maximum cell killing extracted from the 20:1 E:T ratio, compiled from 3 independent experiments, error bars = +/- SEM, * = p<0.05, one-way ANOVA. Experiments conducted by Dr. Ashleigh Davey.*

Reference, Cys Mut and proCAR1 all demonstrated comparable killing ability, while proCAR2 and proCAR3 exhibited a 25-30% improvement upon the cytotoxicity (Fig 4.14). A statistically significant difference between Reference and proCAR2 was of particular note, given both receptors are expected to exist as dimeric complexes at the cell surface. CAR T cells demonstrated negligible killing of MC57-parental target cells (Fig 4.14B), whereas T cells transduced with empty vector were unable to kill MC57-HER2 targets (Fig 4.14B), again demonstrating CAR- and antigen-specificity of all receptor designs. Additionally, cytokine release assays demonstrated these same cells exhibited strongly attenuated release of IL-2, IFNγ, TNFα and GM-CSF in response to MC57-HER2 targets (Fig 4.15B). By comparison, anti-CD3/anti-CD28 stimulation yielded comparable levels of cytokine release across all constructs, highlighting that the attenuated cytokine release was intrinsic to proCAR stimulation. Furthermore, subtle differences in proCAR surface expression amongst different constructs and individual preparations were not correlated significantly with T cell cytokine secretion (Fig 4.15C).

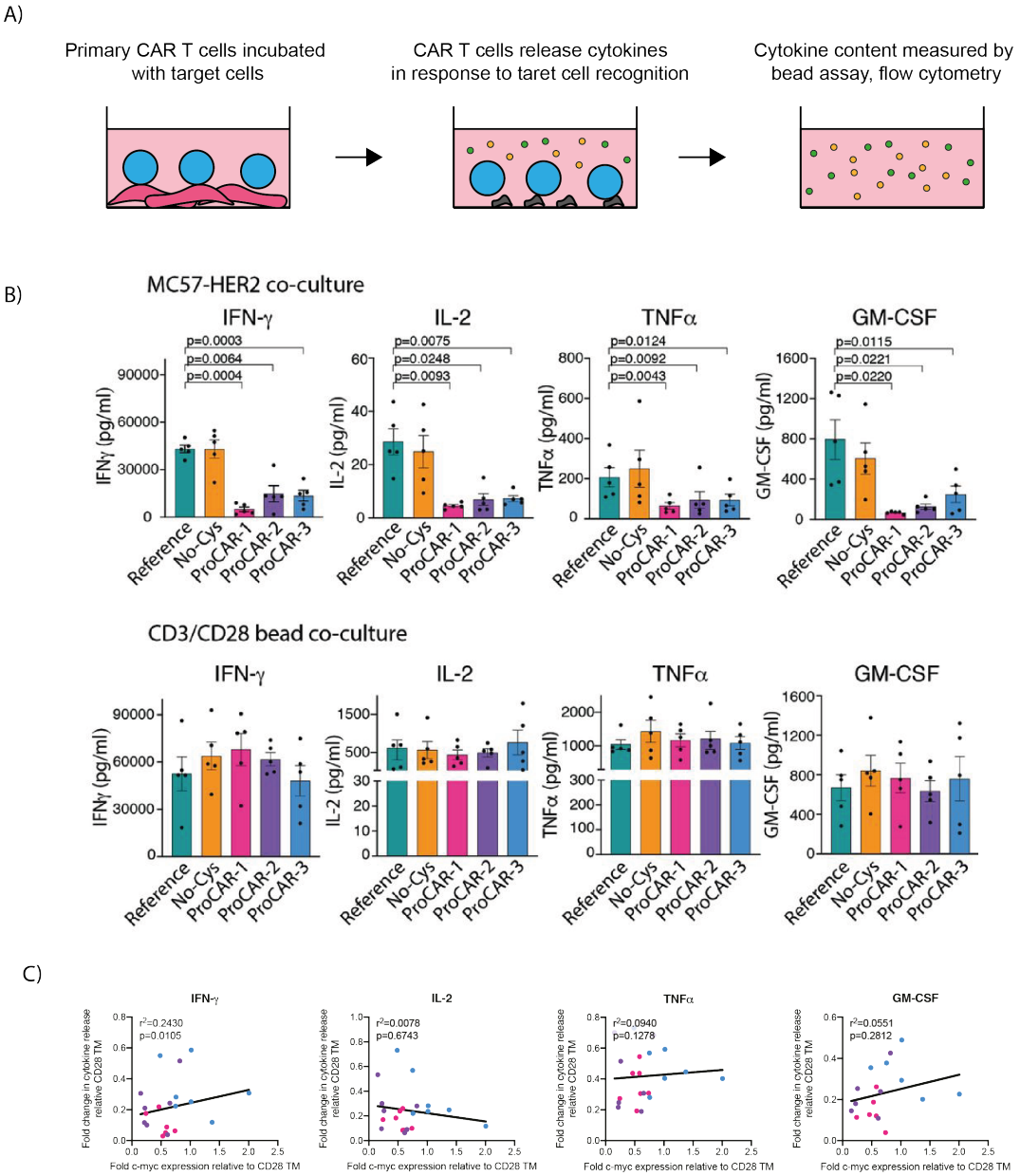

Figure 4.15 FRP5 proCARs attenuate primary T cell cytokine release. *A) Depiction of CBA cytokine release assay conducted over 24 hours. B) FRP5 CAR cytokine release in response to either HER2+ target cell co-culture or TCR stimulation via CD3/CD28 crosslinking. N=5, mean +/- SEM. P-values listed, one-way ANOVA. C) Correlation plots of proCAR cytokine secretion and surface expression, both calculated relative to Reference CAR. N=7 independent experiments. Experiments conducted by Ashleigh Davey with assistance from Nicholas Chandler.*

In vivo anti-tumour activity of proCAR T cells positively correlates with oligomeric state

To test the anti-tumour efficacy of proCAR T cells *in vivo*, a tumour mouse model previously optimised by other research groups in the assessment of FRP5 CAR anti-tumour efficacy (Slaney et al., 2017, von Scheidt et al., 2019) was established in our lab. This model involved subcutaneous injection of human, $HER2^+$ MC38 colon adenocarcinoma tumour cells in Non-obese diabetic, Severe Combined Immune deficient, IL-2Rγ chain deficient mice (NOD-SCID-Gamma, NSG). NSG mice are immunodeficient, lacking B and T cell compartments, which enables human tumour cell lines such as MC38 to avoid rejection by the mouse host immune system. The establishment of this mouse model and all *in vivo* assays described below were conducted primarily by Dr. Ashleigh Davey, while I provided assistance in the harvesting and processing of tumours at ethical endpoint.

proCAR1,2,3 and FRP5 reference CAR T cells and vector-only T cells were produced using an identical protocol to that used for the production of CAR T cells for *in vitro* activity assays in Fig 4.14 and Fig 4.15. These T cells were stained and analysed via flow cytometry to confirm CAR expression prior to administration (Fig 4.16A). On day 1, $1x10^7$ proCAR1,2,3 and FRP5 reference CAR T cells and vector-only T cells were injected intra-venously into NSG mice (5-6 mice per group, female, 6-8 weeks of age) bearing MC38 tumours (grafted one day prior to T cell administration). Tumour size was then measured daily using callipers (Fig 4.16B), with mice being euthanized at ethical endpoint (defined as tumour with a volume of $1000mm^3$), at which time tumours, spleens and blood were taken for processing. Immune profiling and cytokine release was intended to be conducted on spleen, blood and tumour samples, however due to technical difficulties these measurements were unsuccessful and are being evaluated in subsequent experiments underway at the time of writing. All experiments were conducted with approval from and under regulations imposed by the WEHI Institutional Animal Ethics Committee.

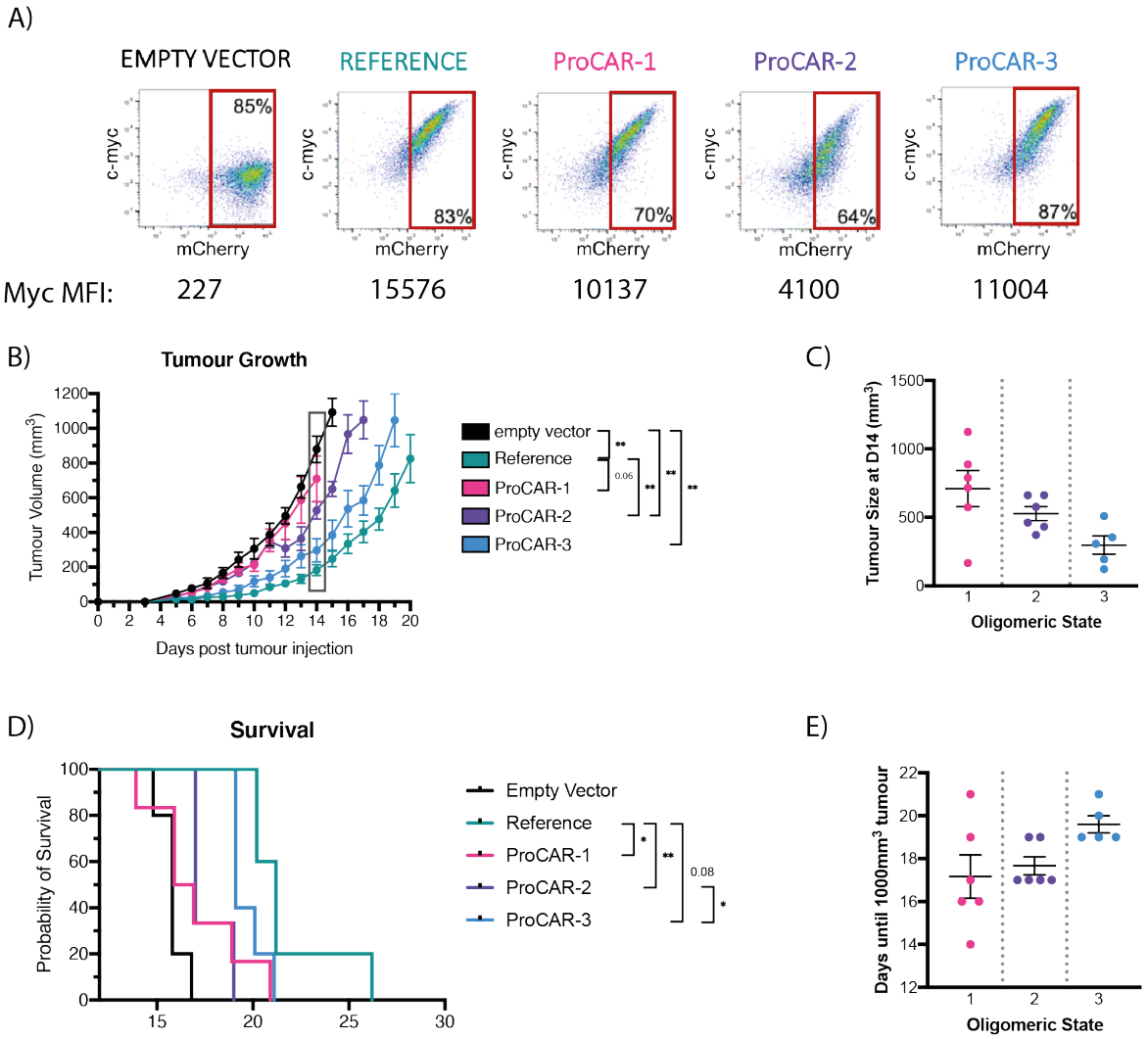

Figure 4.16 proCAR oligomeric state correlates with anti-tumour efficacy in a mouse solid tumour model. *A) primary mouse CAR T cells were generated and assessed for transduction efficiency (pMSCV-IRES-mCherry) and CAR expression level (Myc). NSG mice (minimum of 5 per group) were administered with 5x10^5 MC38 HER2+ tumour cells on day 0. On day 1 1x107 CAR T cells were administered intravenously with administration of 5x10^4 international units (IU) of IL-2 administered intraperitoneally on days 1, 2 and 3. B) Tumour volume was measured daily with calipers and mice were euthanized at ethical endpoint, defined as tumour volume of 1000mm^3. P-values calculated using a two-way Anova test. D) Kaplan-Meier plot showing mouse survival over entire course of experiment. P-values calculated using a log-rank (Mantel-Cox) test. C) and E) represent correlation between proCAR oligomeric state and C) tumour size at day 14 (the latest day where all mice were alive) or E) days until 1000 mm^3 tumour.*

Reference CAR T cells were comparatively most effective at tumour control, resulting in significantly greater survival compared to all proCAR designs (Fig 4.16D). Compared to one another, proCAR groups did not display significant differences in survival (Fig 4.16D), however proCAR3 did offer a subtle delay in the morbidity compared to proCARs 1 and 2. When tumour size was compared at day 14 Reference CAR T cell Reference group once again outperformed all proCAR designs (Fig 4.16B), however a negative correlation was observed between proCAR oligomeric state and average tumour volume (Fig 4.16C)). Upon close inspection, a trending positive correlation between proCAR oligomeric state and mouse survival was also observed (Fig 4.16E).

Expression of a tetrameric proCAR

The observation that oligomeric state positively correlated with tumour control *in vivo*, but that proCAR3 demonstrated anti-tumour activity inferior to FRP5 reference CAR T cells, provided a compelling rationale for the design of a tetrameric proCAR-4. As described in chapter 3 continuous efforts were made during the course of my project, by others in the lab, to crystallise additional proMP designs, including a tetrameric sequence (proMP4.1). At the time of writing proMP4.1 was successfully crystallised, however was yet to yield the high-resolution X-ray diffraction required for reliable structure determination. Efforts are underway to optimize these crystals (work conducted by Julie Nguyen and Dr. Melissa Call), however in lieu of an experimentally determined crystal structure, I proceeded to clone the proMP4.1 sequence into the FRP5 CAR, presuming the accuracy of its modelled structure (Fig 4.17B). I then expressed proCAR4 in the BW5147 cells line, in which surface staining indicated that proCAR4 was successfully expressed at a comparable level to reference CAR (Fig 4.17C). Given the lack of correlation observed between NFκB signalling and CD69 expression with primary cell outputs in previous experiments, proCAR4 was progressed directly to primary T cell analysis, conducted by Ashleigh Davey. proCAR4 expressed robustly in primary CD8+ mouse T cells, comparable to the reference FRP5 CAR. At the time of writing these constructs are undergoing assessment CAR T cell cytotoxicity and cytokine release, with the aim of promptly assessing proCAR4 efficacy in the previously described MC38 $HER2^{+}$ mouse tumour model.

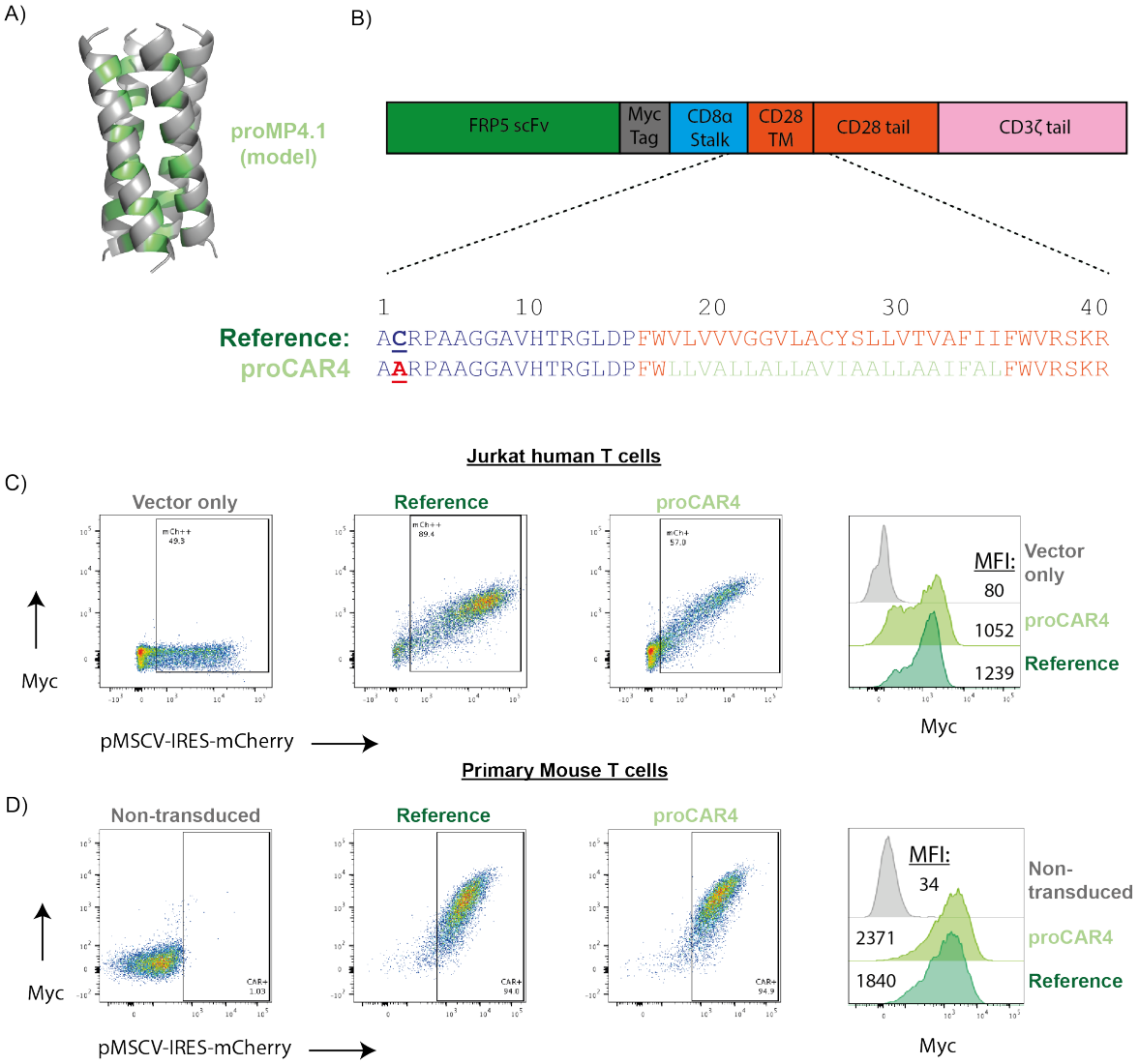

Figure 4.17 Rational design of a tetrameric FRP5 proCAR. *A) Sequence alignment of reference FRP5 CAR alongside the tetrameric proCAR4, generated by inserting sequence of proMP4.1 peptide into FRP5 Cys Mut construct. C) Flow cytometry analysis of surface proCAR surface expression in the Jurkat human T cell line relative to reference CAR. N=1. D) Flow cytometry analysis of proCAR expression in primary mouse CD8+ T cells, Non-transduced cells were CAR negative, CD8+ T cells. N=1 (Conducted by Ashleigh Davey).*

4.3 Discussion

proMP sequences facilitate robust CAR cell surface expression

The data presented above highlight that the replacement by proMP sequences of the native CD28 TM sequence facilitates robust CAR surface expression. Surface staining indicated that

in both mouse and human cells, proCAR designs expressed at comparable levels to Reference. These observations confirm the reliability of the proMP design pipeline to produce TM sequences that support robust expression in the context of a mammalian membrane. The ability to achieve robust cell surface expression is particularly significant given the growing appreciation that CAR expression levels influence CAR sensitivity to ligand (Walker et al., 2017). While subtle differences in expression between proCARs and Cys Mut/Reference CAR were observed, these differences did not correlate with functional output. For example, although proCAR1 expression was generally greater than that of either proCAR2 or proCAR3 and comparable to that of Cys Mut (Fig 4.5), it consistently performed worst in terms of both cell killing and cytokine release compared to all other CARs (Fig 4.14, 4.15). Analysis of surface expression variation between experiments also failed to correlate positively with cytokine release (Fig 4.15), further supporting the conclusion that our observed phenotype was not significantly influenced by differential CAR surface expression.

One potentially confounding difference between proCARs and the Reference FRP5 CAR was the presence of additional, low molecular weight bands in western blot of CAR complexes immunoprecipitated from the cell surface. These bands were detected with antibodies targeting epitopes of both the extra- and intracellular portions of the CAR (Fig 4.6C), which confirmed that these bands were not due to a cleavage event within the proMP sequence itself. This finding was particularly encouraging, as it confirmed that synthetic proMP sequences were resistant to cleavage by transmembrane domain cleaving enzymes such as γ-secretase (Wolfe, 2019). Given the relatively small reduction in apparent molecular weight of the proCAR specific products it is possible that other cleavage events proximal to the N- or C-termini of the FRP5 could give rise to these bands. However, subsequent experiments (discussed in chapter 5) using a different CAR construct did not yield the same products despite identical TM and tail sequences, suggesting that these bands derive from the contrasting scFv and stalk sequences. Differential glycosylation of the CD8α and CD28 stalks may explain this difference: the CD8α stalk region in the context of its full-length protein contains a high abundance of serine and threonine residues known to be the subject of high levels of O-linked glycosylation (Moody et al., 2001, Merry et al., 2003). It is therefore possible that differences in protein trafficking between the CAR containing native CD28 and proMP TM sequences may give rise to differences in the efficiency of stalk glycosylation.

This would suggest that Reference and Cys Mut CARs exist in a fully glycosylated form, whereas proCAR designs can exist in either fully or partially glycosylated forms.

Interestingly, the prevalence of lower molecular weight bands is sequence-specific, given that proCAR2 exhibits very minimal evidence of these products. Whether differences in either glycosylation or N-terminal cleavage are a result of sequence specific features or are a result of differences in oligomeric state remains to be determined, and the evaluation of alternative proMP sequences with the same oligomeric state would go some way to resolving this. Additionally, mass spectrometric analysis of proCARs may be useful by conclusively determining the proCAR protein species present at the cell surface and identifying the presence of any specific modifications.

Subtle differences in the expression of proCARs relative to Reference CAR in the BW5147 and Jurkat T cell lines were also observed, for example a noticeable shift in the proCAR2 expression profile via anti-Myc labelling (Fig 4.5). To further verify these differences, comparisons are required in which identical CAR retrovirus is used in parallel on both cell lines, in addition to further replicates to enable robust quantification. Inter-species proCAR surface expression variation could theoretically arise from proMPs interactions with endogenous proteins expressed differentially between species, resulting in impaired stability or trafficking to the membrane. It appears unlikely that such interactions would result from symmetrical interactions with proteins containing similar small-residue dimerization motifs, as evidenced by the lack of suitable candidates presented in table 3.3; however, it is possible that cryptic or asymmetric interfaces with endogenous proteins could occur. Identification of such endogenous interacting proteins would require proCAR immunoprecipitation combined with mass spectrometry in human versus mouse primary T cells in search of differentially enriched proteins. However, reduced surface expression levels of proCARs compared to Reference CAR did not correlate with T cell functionality (Fig 4.15C), suggesting that reduced surface expression of the magnitude observed in the proCAR system is not problematic. While it appears unlikely that reduced proCAR expression would result in dramatically different functionality in human T cells, the strength of the proMP design pipeline is that alternative proMPs of the same oligomeric state can be

readily generated and empirically validated for robust surface expression (as was demonstrated with the design of proCAR4).

Characterization of proCAR oligomeric state

Various experimental approaches are capable of offering insight into the oligomeric state of surface receptors, each with their own unique combination of strengths and limitations. The combination of IVT crosslinking and quantitative fluorescence microscopy approaches I undertook were chosen due to their relative technical simplicity and provided valuable preliminary evidence of the ability of proMP sequences to control CAR oligomeric state.

IVT crosslinking experiments clearly demonstrated the pattern expected of proMP sequences when compared with canonical monomeric and dimeric TM sequences. proMP1 exhibited comparable self-association to a poly-Valine TM, while proMP2.2 exhibited a significantly higher degree of self-association compared to glycophorin A. These results indicate that in regard to predicting monomeric and dimeric TM self-association the dsTβL TOXCAT assay is a reliable predictor of self-association in the context of mammalian membranes. Additionally, these findings highlight the significant differences in self-association observed between TM domains sharing a common dimerization motif. The differential features between proMP2.2 and GpA are therefore worthy of closer inspection in the future. Interestingly, while an alanine residue 4 residues N-terminal to the GxxxG of proMP2.2 appeared to permit close helical packing, the introduction of a Leucine to alanine mutation in the same location in GpA did not result in an increase in dimerization *in vitro* (Langosch et al., 1996). This once again highlights that the determinants of GxxxG motif dimerization are complex and likely to be influenced by several factors.

I also observed that within my IVT system the TM sequence of CD28 demonstrated a propensity to self-associate, compared to monomeric polyVal and proMP1 constructs, although this difference did not reach statistical significance. This observation does however align with recent observations that motifs within the CD28 TM domain are responsible for driving homo-dimerization (Leddon et al., 2020). While IVT crosslinking experiments have previously been effective in covalently trapping trimeric and tetrameric complexes, it was unfortunate that such measurements could not be reliably made in this case. One

explanation for these high-weight bands could be the covalent linkage of DAP12-fusion constructs with endogenous proteins within the ER microsomes used within the IVT system for protein translation. Although only DAP12-fusion protein is expected to be visible in autoradiograms (as only protein translated in the presence of radio-labelled S^{35} Cys/Met will generate signal), covalent linkage of DAP12 stalk sequences with endogenous proteins within the ER could give rise to the apparent high-molecular weight bands observed. This hypothesis could be tested using an alternative source of ER microsome, with the intention of avoiding undesirable covalent interactions with endogenous proteins.

Numbers and brightness (N&B) analysis of proCAR-GFP fusion constructs in live cells agreed with those made within the IVT crosslinking system, also identifying a positive correlation between predicted and experimentally determined oligomeric structures was observed. Crucially, N&B analysis provided the strongest insight into the behaviour of proCAR3, indicating a propensity to form higher-order oligomers compared to proCAR-1 and -2. Crucially, neither experimental system was suggestive of the existence of higher order hexameric assemblies of proCAR2, confirming earlier speculation that weak contacts between dimers of the proMP2.2 asymmetric unit were unlikely to be relevant outside of the context of high protein concentration crystallographic system. An important consideration in these experiments was that N&B analysis is inherently limited to making *relative* comparisons of oligomeric state. At the time of writing a membrane-tethered monomeric GFP standard has been expressed, with the intention of acting as a strictly monomeric reference against which proCAR-GFP constructs can be compared. The inclusion of such a control will enable a more objective quantitation of proCAR oligomeric state and provide insight into the relatively small difference between B-values observed of proCAR1 vs. proCAR2. Given the striking difference in self-association of proMP1 and proMP2.2 in TOXCAT and IVT crosslinking experiments it appears likely that in the context of a full-length CAR, self-association is likely to be at least partially influenced by extra- and/or intracellular receptor components. For example, the interchange of scFv VH and VL domains (known as domain swapping) is observed in the context of other scFv engineering applications (Zhang et al., 2015) and could foreseeably contribute to CAR self-association. Such an explanation seems more likely than contributions from the CD8□ stalk, given the lack of evidence of CD8□ stalk self-association and the observation that the CD8□ TM domain is largely

responsible for homodimerization of native CD8α proteins (Hennecke and Cosson, 1993). In addition to the optimization of monomeric standards for more robust N&B analysis, alternative high-resolution microscopy approaches are in planning at the time of writing. Recent advances in single-molecule imaging used to quantitate surface receptor oligomeric state present an exciting opportunity to quantify *absolute* receptor oligomeric state, as well as providing insight into the distribution of oligomeric species (Karathanasis et al., 2020).

How do proMPs exert differential effects on *in vitro* CAR T cell killing and cytokine release?

This work, enabled by a novel protein design approach, constitutes the first systematic investigation of the influence of oligomeric state on CAR function. Comparison of monomeric, dimeric, and trimeric proCAR T cells in primary mouse cells was suggestive of a positive correlation between receptor oligomeric state and target cell killing. proCAR2/3 demonstrated enhanced cytotoxicity compared to proCAR1 when expressed in primary mouse T cells, despite displaying equivalent signalling capacity in immortalized BW5147 mouse T cells. These findings align with the observation that an increased number of CD3ζ ITAMs per CAR resulted in enhanced CAR T cell ligand sensitivity (Majzner et al., 2020). The observation that proCAR2 and proCAR3 exhibit indistinguishable *in vitro* cytotoxicity in response to the $HER2^{high}$ MC57-HER2 target cell line may indicate that CAR cytotoxicity is saturated at these levels of antigen. Majzner et al. (2020) demonstrated previously that CAR constructs exhibiting indistinguishable cytotoxicity at high levels of antigen subsequently demonstrate vastly different cytotoxicity in the context of antigen low target cell line. It will therefore be valuable to evaluate proCAR4 activity in the context of target cells expressing lower levels of HER2. BW5147 proCARs demonstrated sub-maximal signalling, comparable to reference CARs, in response to target cells expressing lower levels of HER2, suggesting that these cell lines may provide the desired antigen limiting setting required.

It is also possible that the relationship between CAR oligomeric state and signalling output is non-linear and hence differences in function between different oligomeric states may vary. For example, ZAP-70, a key downstream kinase responsible for binding phosphorylated ITAMs within the CD3ζ tail is known to show a strong preference for dimeric CD3ζ tails (Hatada et al., 1995, James, 2018). Dimerization is consequently required for ZAP-70 trans-autophosphorylation, an important prerequisite for ZAP-70 to initiate downstream

signalling cascades. Hence, it may be expected that the difference between monomeric and dimeric CARs may be a result of a combination of both increased ITAM multiplication and increased ability to facilitate ZAP-70 dimerization. It follows that increases in oligomeric state beyond dimerization may not result in enhanced ZAP-70 dimerization and trans-autophosphorylation but may still result in an increase in receptor potency. Such hypotheses could be tested via quantitative analysis of ZAP-70 phosphorylation status and would provide a valuable insight into early CAR observations of the superiority of dimeric versus monomeric CAR architectures (Fitzer-Attas et al., 1998, Bridgeman et al., 2010).

It was also notable that proCAR2 demonstrated enhanced cytotoxicity when compared to Reference CARs, even though each of these constructs was expressed as a dimer. One explanation for this observation may relate to the relative differences in the dimeric structures adopted by the CD28TM domain vs. that of proCAR2. While no crystal structure is currently available of the native CD28 TM domain, a reasonable prediction could be taken from the structure of the CD3ζ TM domain, which shares the same YxxxxT dimerization motif. The CD3ζ TM dimer when compared to that of proMP2.2 is noticeably upright, demonstrating a dramatically different crossing angle. Given that alterations of the CD28TM domain dimer structure are suggested to influence receptor signalling (Leddon et al., 2020, Sanchez-Lockhart et al., 2011) it is possible that the structure adopted by proMP2.2 may influence the downstream signalling capacity of the CD28 signalling tail in a manner that enhances cytotoxicity. Teasing apart these hypotheses will require a greater understanding of the functional role of TM structure in the native CD28 receptor, as well as a greater understanding of the influence of proximal CAR signalling events to T cell effector function.

Intriguingly, a significant reduction in release of IL-2, TNFα, IFNγ and GM-CSF was observed of all proCAR designs, regardless of oligomeric state, compared to Reference and Cys Mut CAR T cells. This suggested that the CD28TM domain was responsible for driving CAR T cell cytokine release, an observation that aligns with previous studies which demonstrated the CD28 stalk and TM domains together resulted in elevated cytokine release compared to CAR utilising CD8α stalk/TM domains (Majzner et al., 2020, Alabanza et al., 2017). These studies did not investigate the individual contributions of stalk vs. TM domains and therefore our findings constitute the first evidence that the CD28TM domain is independently capable of

driving this enhanced cytokine release phenotype. In addition to this reduction in cytokine release compared to Reference CAR, subtle differences between the cytokine release of proCARs were also observed. In the case of each IL-2, TNFα and IFNγ release, proCAR2 and proCAR3 demonstrated marginally greater cytokine release than proCAR1, while GM-CSF release appeared to correlate positively with oligomeric state in the case of all three proCARs. These differences were small and did not reach statistical significance, however this trend warrants careful scrutiny as tetrameric proCAR4 designs are progressed to *in vitro* primary T cell evaluation.

Does *in vitro* proCAR phenotype translate *in vivo*?

We observed a promising indication that proCAR oligomeric state correlates positively with tumour control in a preliminary mouse tumour model. In spite of indistinguishable *in vitro* cytotoxicity between proCAR2 and proCAR3, proCAR3 demonstrated a noticeable improvement in tumour control at day 14 compared to proCAR2, with proCAR1 performing worse than all other receptors tested. This supports the hypothesis that oligomeric state directly influences CAR T cell efficacy, though what specific pathways are responsible for this effect is not yet clear. *In vivo* performance is influenced by many T cell parameters, including but not limited to cytotoxicity, cytokine release, proliferative capacity, survival and T cell memory phenotype. It was therefore not surprising that while *in vitro* cytotoxicity measurements had indicated an enhanced killing ability of proCAR2 and proCAR3 relative to Reference CAR, in the context of an *in vivo* tumour model reference FRP5 CAR T cells demonstrated significantly greater survival benefit and tumour control. These findings correlate with earlier findings that reference FRP5 CARs greatly outperformed first-generation FRP5 CARs (FRP5-CD3ζTM/tail) in terms of cytokine release and a tumour control (Haynes et al., 2002). Subsequent studies demonstrated that mutation of the canonical PYAP and YMNM sequence motifs within the CD28 tail (responsible primarily for Lck and Grb2 recruitment respectively (Boomer and Green, 2010)) resulted in attenuation of cytokine release as well as attenuated tumour control (Moeller et al., 2004). These findings suggest there may be a non-redundant requirement for both CD28TM and tail sequences to drive maximum cytokine release. To address this hypothesis, efforts were made within the *in vivo* experiment described in this thesis (Fig 4.16) to measure CAR T cell cytokine release from blood samples taken at day 7 post-treatment and at ethical endpoint, however no

signal was observed for the cytokines measured within these samples for any CAR T cells. Efforts are currently underway to repeat a modified version of this *in vivo* experiment, with the aim of measuring in-tumour cytokine release shortly following the administration of CAR T cells to NSG mice bearing pre-established MC38 HER2^{+} tumours.

It may also be informative to assess the efficacy of FRP5 proCAR designs in the context of alternative mouse tumour models. The MC38 HER2^{+} model selected for this experiment is particularly aggressive, highlighted by the fact that in other HER2^{+} tumour models FRP5 CARs are capable of curative monotherapy (Wang et al., 2010). This study also demonstrated long-term persistence of FRP5 Reference CAR T cells beyond day 50, presenting an opportunity to compare long-term persistence of proCAR T cells *in vivo* (Wang et al., 2010). Given the correlation observed between CAR T cell persistence and positive patient outcomes these types of long-term tumour models will be crucial in evaluating the clinical potential of our proCAR approach.

Unravelling and extending proCAR functionality

Given the observation that proCAR3 outperformed other proCARs but failed to match Reference FRP5 CAR T cell efficacy, the *in vitro* and *in vivo* validation of the tetrameric proMP4 design is a high priority. Given proCAR2 and proCAR3 demonstrated indistinguishable cytotoxicity within the previously described chromium release cell killing assays we would not expect proCAR4 to provide any additional benefit. Experiments currently in planning at the time of writing will instead utilise a live microscopy cell killing assay, which allows visualization of target cell death following co-incubation with CAR T cells over the course of 24-72 hours in an IncuCyte imager. Transition to this experimental system may permit the disentanglement of proCAR cytotoxicity *in vitro*, as previous studies using similar approaches demonstrated an ability to differentiate subtle variations in killing capacity by making repeated measurements of the same well at low ratios of T cell to target cell density (Majzner et al., 2020).

Suitable pentameric TM designs are also currently being considered in the event that proCAR4 is able to improve upon the activity of proCAR3. Pentameric designs have previously not been attempted using the proMP pipeline, although there are no theoretical

limits to such designs. However, a recent published study on several highly-stable variants of the pentameric transmembrane segments of the protein phospholamban (Mravic et al., 2019) present an intriguing opportunity to further extend the proCAR approach. In the event that pentameric proMP sequences can be designed, phospholamban will also provide an interesting comparison of sequences generated using two very different membrane protein design approaches.

CHAPTER 5 Interrogating the mechanism of the CD28 TM domain contribution to CAR-T cell cytokine release

5.1 Background and rationale

Our interest in unravelling the mechanism linking CD28TM sequence to cytokine release was rooted in the pressing clinical need to find means of controlling CAR cytokine release to reduce the high incidence of toxicity plaguing current generations of CAR therapies. Over 50% of patients treated with CAR T cells directed against B cell malignancies experience severe toxicity in the form of neurotoxicity or Cytokine Release Syndrome (CRS) (Neelapu et al., 2018). These toxicities are associated initially with fever, malaise and delirium, however in severe cases these symptoms can progress to cause multi-organ failure and even death if not rapidly treated. CRS and neurotoxicity are dose-limiting and are triggered by excessive release of inflammatory cytokines, such as IFNγ, TNFα and GM-CSF by CARs, which in turn drives other immune cells to release excessive quantities of additional inflammatory cytokines. Macrophages in particular contribute significantly to the progression of CRS, via the release of high levels of IFNγ and the pro-inflammatory cytokine IL6. These toxicities are currently managed through the administration of IL-6 blocking antibodies and steroid treatments; however, these interventions significantly impact the cost (Zhu et al., 2020) and efficacy of CAR therapies (Neelapu et al., 2018). Hence, there is significant interest in re-engineering CAR designs to reduce CAR T cell cytokine release without sacrificing overall efficacy. Two recent papers independently identified that reductions in cytokine release could be achieved via modifications to the TM/stalk regions of 2nd generation CARs (Brudno et al., 2020, Ying et al., 2019). Brudno et al (2020) compared receptors possessing either CD28 or CD8α stalk/TM domains, in contrast to Ying et al (2019) who compared the impact of small extensions to the CD8α stalk and TM sequences commonly found in 2nd generation CARs. Both modifications resulted in reduced expression of TNFα, IL-2 and IFNγ, whilst remarkably Ying et al (2019) demonstrated lower-than-expected incidence of neurotoxicity and CRS amongst patients in a small phase-I clinical trial for the treatment of Refractory B cell lymphoma (Ying et al., 2019).

Importantly, further studies have since detailed to complex relationship between CAR cytotoxicity and cytokine release, suggesting that TM/Hinge modifications can in some cases

result in simultaneous reductions in cytokine release and cytotoxicity (Majzner et al., 2020). Therefore, it is vital that the molecular mechanisms underpinning these observations and the independent contributions of TM vs. hinge domains are elucidated in finer detail. Our findings indicated that the replacement of the CD28 TM domain with any of our proMPs corresponded with a profound reduction in cytokine release, and that some of them achieved this without an associated reduction in target cell killing. This was highly suggestive of a sequence-specific role for the CD28TM domain and we therefore set out to establish which structural features may be capable of influencing CAR function.

A conserved homo-dimerization motif in the CD28TM domain

Transmembrane domain interactions play an essential role in single pass transmembrane domain receptor assembly and function. Highly conserved TM motifs dictate the architecture of multi-subunit receptor assemblies of immune receptors such as the TCR/CD3, DAP10/NKG2D and CD19/CD81 complexes (Berry and Call, 2017). Furthermore, in several type-I receptors dynamic regulation of TM structures is proposed to contribute to transducing ligand binding events across the cellular membrane and initiating intracellular signalling (Lee et al., 2015, Brooks et al., 2014, Bocharov et al., 2008, Susa et al., 2021). A comprehensive understanding of the relationship between CD28 structure and function is still lacking, however several recent advances have outlined a series of functionally relevant structural features.

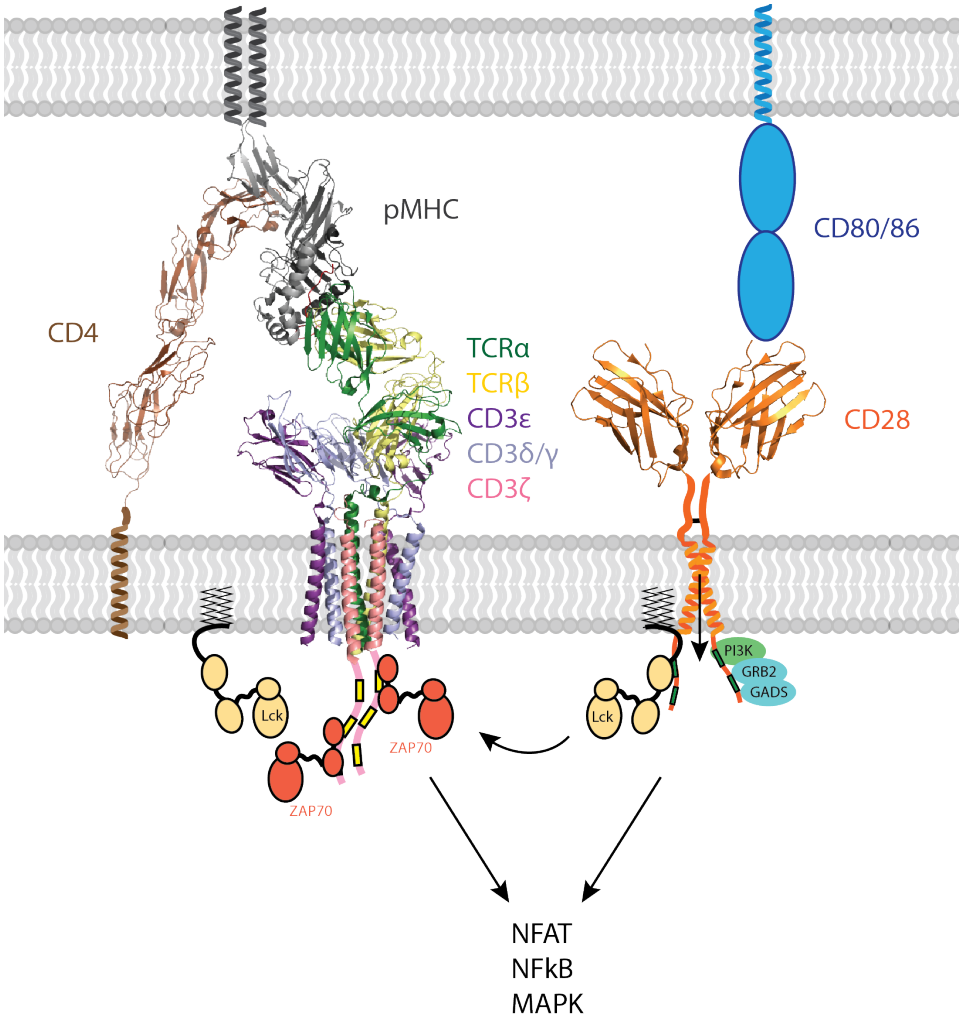

Figure 5.1 CD28 co-stimulation of T cell signalling. *T cell receptor (TCR) signalling is initiated by binding of TCR$\alpha\beta$ to stimulatory peptide antigen presented by proteins of the Major histo-compatibility complex (pMHC). This interaction is enhanced by CD4/CD8 coreceptor binding to pMHC. Binding of CD28 to its cognate antigen CD80/86 facilitates recruitment to pMHC activated TCR complexes. CD28 provides crucial costimulatory support to TCR signalling via activation of canonical T cell signalling pathways and recruitment of the membrane localised activating kinase Lck. CD4/pMHC/TCR$\alpha\beta$ (PDB ID: 3TOE), TCR (PDB ID: 6XJR) (TCR$\alpha\beta$ from PDB ID: 3TOE aligned against TCR$\alpha\beta$ chains in 6XJR using pymol, 3TOE TCR$\alpha\beta$ chains not shown), CD28 (PDB ID: 1YJD).*

CD28 is a costimulatory receptor expressed constitutively on T cells and consists of a single extracellular ligand binding domain connected via a short extracellular stalk region to a transmembrane domain and cytosolic tail (Fig 5.1). It exists as a homodimer at the cell surface, covalently stabilised by a single disulfide crosslink between stalk regions. It is

responsible for amplifying TCR signalling upon binding of the ligands CD80 and CD86, both found on the surface of professional antigen presenting cells such as dendritic cells. Upon ligand binding, signalling motifs within the CD28 cytoplasmic tails are phosphorylated by the membrane associated kinase Lck (Holdorf et al., 1999), resulting in the recruitment and activation of signalling molecules such as PI3K (Pages et al., 1994, Harada et al., 2003), Grb2 (Raab et al., 1995) and GADS (Watanabe et al., 2006), integral members of canonical TCR signalling pathways. This serves to lower the threshold for activation of T cells responding to stimulatory pMHC ligands while simultaneously promoting cell survival and proliferation. Crucially, CD28 co-stimulation also enhances the production of several cytokines such as IL-2, TNFα, IFNγ and GM-CSF (Thompson et al., 1989). Due to the pivotal role of CD28 signalling in T cell function, the structural determinants of CD28 activation have been the subject of intense interest for several decades. However, only in recent years has a complete picture of the mechanism of CD28 signalling begun to take shape and understanding the relationship between CD28 structure and function is crucial to understanding the influence of CD28 sequences on CAR function.

Relevant to the FRP5 CAR, a recent study by Leddon et al. (2020) has detailed the importance of homodimeric interactions between CD28 transmembrane domains, facilitated by a highly conserved dimerization Yx_4T motif (a tyrosine and threonine separated by 4 other amino acids) (Fig 5.C). While an experimental structure of the CD28 TM domain has not been determined, a similarly located Yx_4T motif is found in the CD3ζ TM homodimer for which an NMR structure is available (Call et al., 2006), suggesting that the CD28 TM domains may form a similar dimeric interface (Fig 5.2A, B). The mutation of this Yx_4T motif to Lx_4L in primary mouse T cells resulted in a dramatic reduction in surface expression and T cell developmental defects in mice, suggesting an important role in receptor surface stability in addition to its role in dimerization (Leddon et al., 2020).

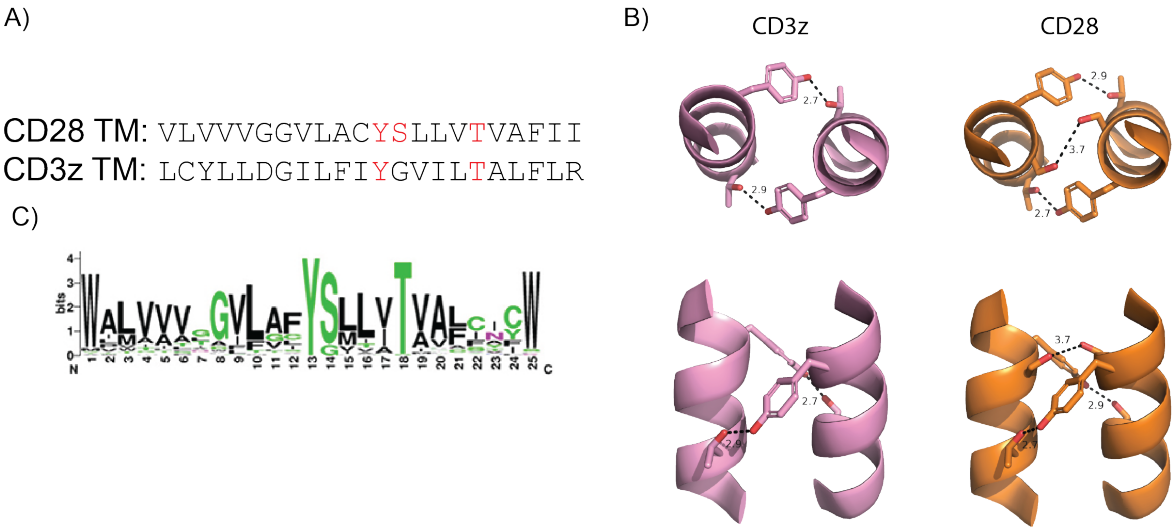

Figure 5.2 A conserved YxxxxT motif shared among immune receptors. *A) Alignment of CD28 and* CD3ζ *TM domains with YxxxxT motif shown in red. Additional serine residue within CD28 YxxxxT motif highlighted in red. B) NMR structure of the* CD3ζ *YxxxxT dimerization motif interface, with hydrogen bonds labelled with distance between hydroxyl oxygen atoms (PDB: 2HAC). CD28 sequence (right) was modelled onto* CD3ζ *homodimer. Homologous Tyrosine to threonine predicted hydrogen bonds labelled, in addition to distance between oxygen atoms of CD28-sequence specific serine residue within YxxxxT motif. C) Web logo depicting sequence conservation of CD28 TM sequence. Web logo adapted from leddon et al (2020), constructed from 51 species. Black font: hydrophobic, green font: polar, red font:acidic.*

Influence of CD28 sequences on CAR T cell functionality

We hypothesized that CD28 TM domains in the context of CAR constructs may mediate recruitment of endogenous CD28 via this highly conserved Yx_4T dimerization motif and thereby enhance CD28 signalling (Fig 5.3). The corollary of this hypothesis is that the replacement of the CD28 with our panel of proMP designs would result in a decrease in CD28 recruitment, and therefore a decrease in CD28 signalling and CD28-mediated cytokine release. This hypothesis is founded on the observations that the inclusion of CD28stalk and/or TM/tail sequences into first generation CARs (scFv-CD3ζTM/tail) resulted in dramatic enhancement of T cell proliferation and cytokine release *in vitro* (Finney et al., 1998, Maher et al., 2002, Vallina and Hawkins, 1996). Hence, our hypothesis was that this phenotype results at least in part from TM interactions between CAR and endogenous CD28TM

domains. To investigate this hypothesis, we made targeted mutations to the CD28 TM dimerization motif within our reference FRP5 CAR (termed CD28TM mut). This construct was assessed for its target cell killing and cytokine production capacity in comparison to the reference FPR5 CAR. Additionally, this construct alongside the proCAR panel, was assessed via biochemical and fluorescence microscopy techniques for their ability to directly co-associate with endogenous CD28 at the cell surface.

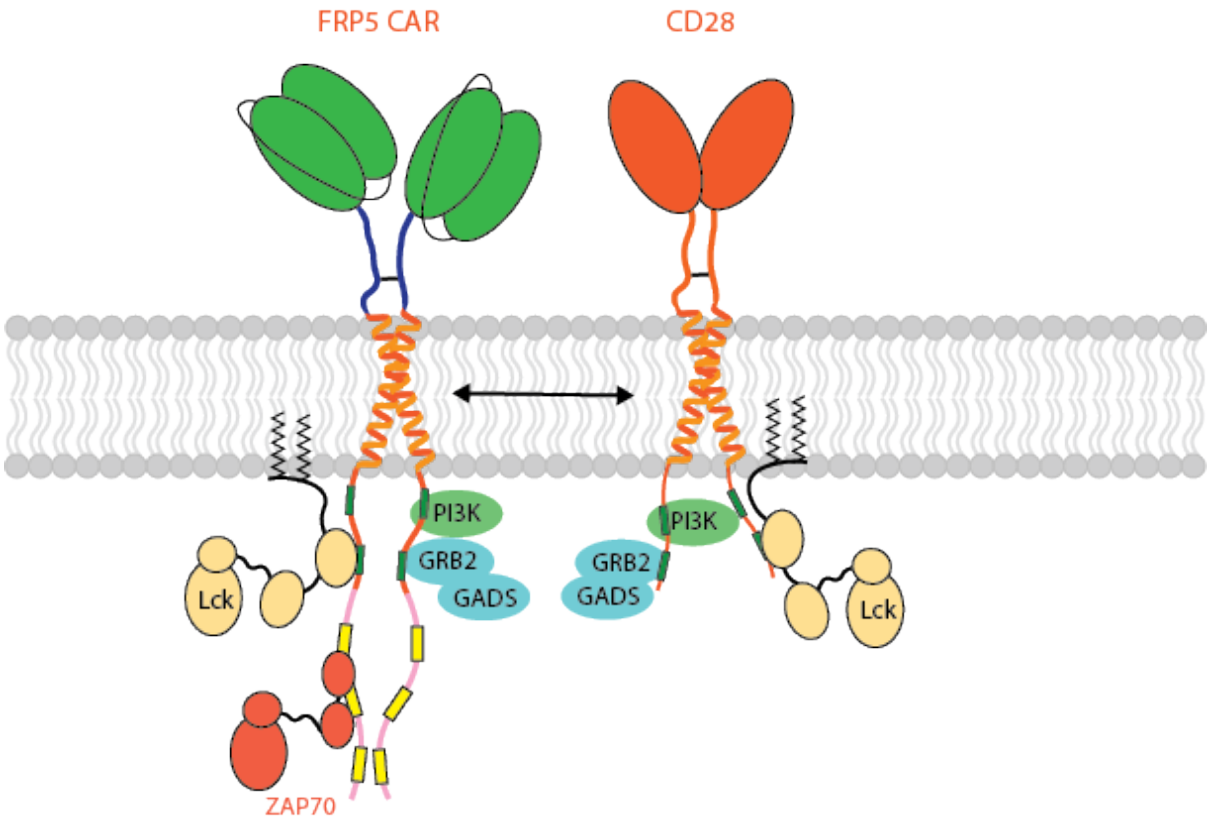

Figure 5.3. A functional role for Heterotypic CAR-CD28 interactions. *We hypothesise that CD28 is recruited to the FRP5 CAR via heteromeric CD28 TM interactions. Increased recruitment of CD28 would consequently result in an increased accumulation of CD28 associated signalling molecules such as PI3K, GRB2, GADS and Lck, corresponding with increased CD28 co-stimulation.*

5.2 Results

Design of CD28 TM mutations and mouse T cell line validation

In a recent paper by Leddon et al. leucine mutations were introduced to the tyrosine and threonine of the conserved Yx_4T motif in mouse CD28 and observed to ablate dimerization.

In addition to these two polar residues the human CD28 sequence (found within the FRP5 CAR) contains a serine residue in between the tyrosine and the threonine (YSx_3T). As shown in Figure 5.2 when the CD28 TM sequence is modelled on the structure of the CD3ζζ homodimer, aligned according to the position of the conserved Yx_4T motif, the position of this serine indicated it was likely capable of forming hydrogen bonds with the opposing serine residue and thereby providing an additional stabilising contact. For this reason, we decided to mutate this serine in addition to the canonical interface tyrosine and threonine residues (Fig 5.4A). In contrast to the mutations described in Leddon et al (2020) we made conservative amino acid substitutions, converting the human YSx_3T motif to FAx_3V, thus removing hydroxyl groups capable of forming interchain hydrogen bonds whilst otherwise preserving the chemical structure as much as possible. The FRP5 CAR construct encoding this FAx_3V motif was termed the CD28TM Mutant (CD28TM Mut) and was compared alongside the reference FRP5 CAR to determine its comparative expression and function. BW5147 mouse T cells were transduced with Reference or CD28TM mutant CAR constructs, both of which expressed robustly to the cell surface (Fig 5.4B). Western blot analysis of the CD28TM mut CAR revealed that in spite of the mutations made it was still capable of forming a comparable degree of covalent dimer to Reference FRP5 CAR at the cell surface (Fig 5.5). These T cells were then co-incubated with the SKBR3 HER2+ target cell line and demonstrated comparable CD69 upregulation and NFκB activation (Fig 5.4B). This experiment was only conducted once in favour of progressing to primary cell assays, given that we had previously observed that CD69/NFκB were poor predictors of primary cell functionality, but they indicated that the receptor remained functional.

A)

Reference (CD28 TMD): ...VLVVVGGVLACYSLLVTVAFII...

CD28TM mut: ...VLVVVGGVLACFALLVVVAFII...

B)

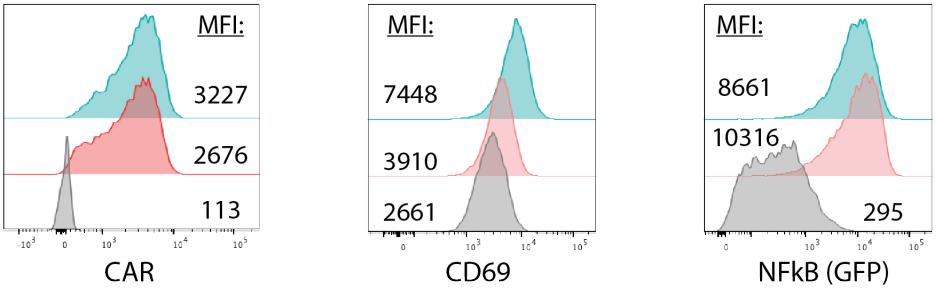

Figure 5.4. Validation of expression and signaling capacity of an FRP5 CD28TM mutant *A) Sequence alignment of native human CD28 TM sequence from Reference FRP5 CAR and the CD28TM mut construct with mutations to polar residues involved in CD28 TM dimerization motif. B) Histograms showing CAR expression in BW5147 T cell line as measured by surface Myc staining; CD69 upregulation and NFκB activation in response to 6-hour co-culture with SKBR3 target cells. N=1.*

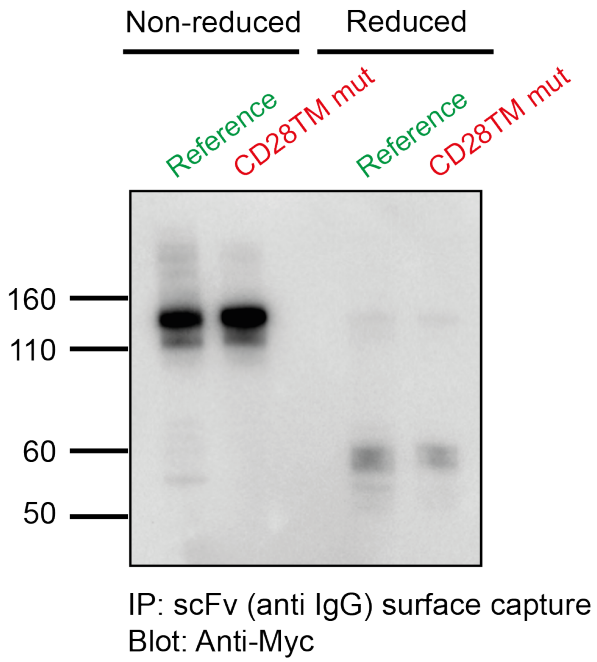

Figure 5.5. CD28TM mutant forms covalent homodimers. *Surface capture IP, SDS-PAGE western blot analysis of reference vs. CD28TM mut expressed in BW5147 cells. 5x10^6 cells/lane. Predicted MW of both CAR sequences is ~57kDa. SDS-solubilised samples split prior to SDS-PAGE, treated with +/- 10mM DTT to generate reduced and non-reduced samples. N=1.*

Primary Cell functionality

Reference and CD28TM mut constructs were expressed in primary mouse T cells, with CD28TM mut exhibiting somewhat lower surface expression (Fig 5.6 A), in line with observations that mutation of the YxxxT motif disrupts surface expression of CD28 in primary T cells (Leddon et al., 2020). These cells were progressed to *in vitro* killing and cytokine release assays using the same MC57-HER2/MC57-Parental cell lines used previously to interrogate proCAR functionality.

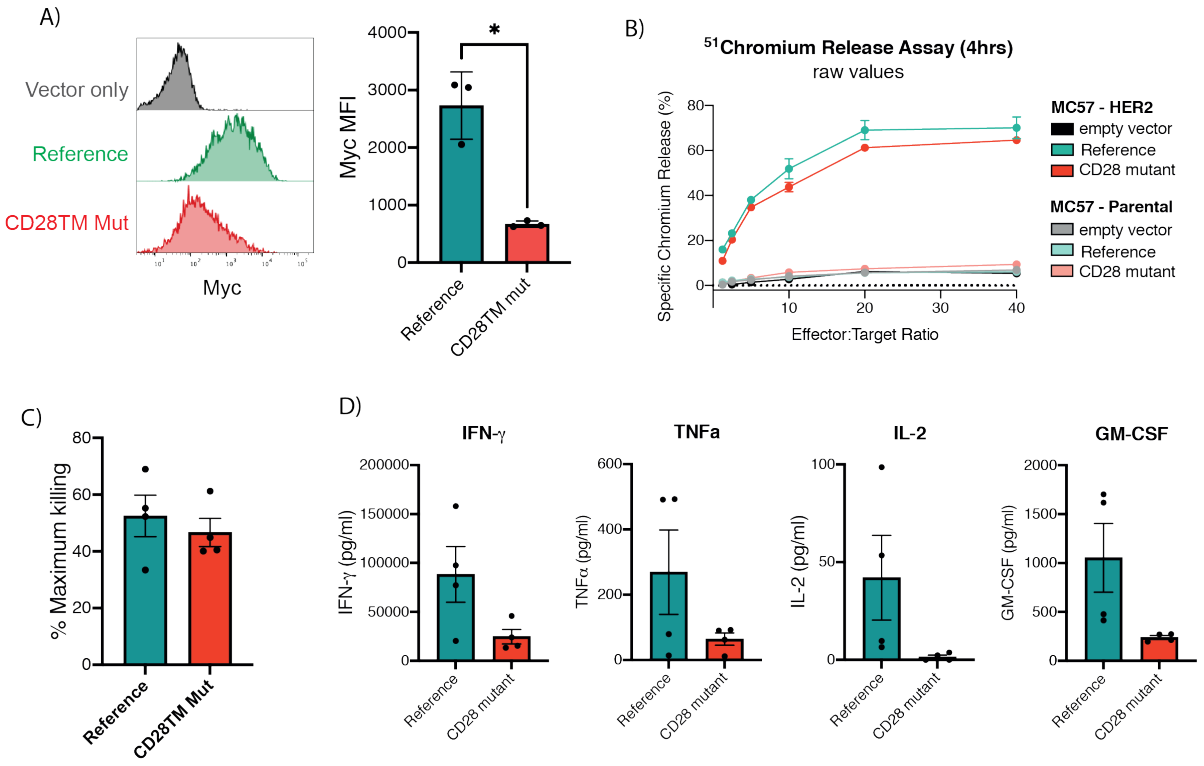

Figure 5.6. CD28TM mut supports cell killing, attenuates cytokine release. *A) Surface expression of reference vs. CD28TM mut in primary mouse T cells (anti-Myc staining) N=3, mean +/-SEM, * = P<0.05, paired student t-test. B) Representative killing curve comparing response to HER2-/+ target cells. C) Summary of cell killing in response to HER2+ target cells at 20:1 effector:target ratio. N=3, mean +/- SEM. B) Cytokine release as measured following 24-hour co-culture with MC57-HER2 target cells. N=4, mean +/- SEM. All surface staining and cytotoxicity measurement were conducted by Dr. Ashleigh Davey. Cytokine release measurements were conducted by Dr. Ashleigh Davey and Nicholas Chandler.*

Reference and CD28TM mut CAR T cells demonstrated comparable cytotoxicity against antigen-high MC57-HER2 target cells (Fig 5.6B, C); however, CD28TM mut displayed reduced release of IL-2, TNFα, IFNγ and GM-CSF in line with levels produced by proCAR T cells (Fig 5.6D).

Quantification of co-association of CAR and endogenous CD28

Once CD28TM mut had been shown to display a similar phenotype to our proCAR designs we set out to test the hypothesis that the CAR CD28TM domain was facilitating recruitment of endogenous CD28 through TM-TM interactions mediated by the YSx_3T motif. We used an co-clustering approach to probe this question, which involves crosslinking a given receptor on the surface of a lymphocyte to induce active clustering and then fixing and staining for a second receptor. Overlapping fluorescence derived from the two receptors can then be interpreted as a close interaction.

I hypothesized that if the YSx_3T motif was responsible for mediating interactions with endogenous CD28, then co-clustering with CD28 would be expected of Reference and Cys Mut constructs, whereas reduced CD28 co-clustering would be expected of CD28TM mut and proCAR constructs. To explore this hypothesis, I evaluated a subset of our CAR panel, selecting all dimeric designs to simplify the comparison: Reference, Cys Mut, proCAR2 and CD28TM mut. Primary CAR T cells expressing these constructs were generated and treated with anti-Myc and a fluorescent secondary antibody to induce CAR crosslinking and visualise CAR clusters. Cells were subsequently stained with anti-CD28 to visualise receptor co-clustering. Staining of CD28 was conducted on ice and in the presence of 0.1% sodium azide to halt cellular metabolism and minimize induced clustering of CD28. Following data collection, co-recruitment was inferred from the number of CAR clusters that co-localised with a CD28 clusters. The reference FRP5 CAR exhibited extensive CAR clustering at the cell surface as expected, with approximately 25% of CAR clusters on average per cell co-localising with a distinct cluster of CD28 (Fig 5.7A, B). FRP5 Cys Mut CAR demonstrated a subtle enhancement in its co-association with CD28 compared to reference, although this small difference did not reach statistical significance. Given the subtle difference in CD28 association of Cys Mut and reference FRP5 CARs I decided that the relevant comparisons should be made between CAR designs with equivalent stalk cysteine design (Reference vs.

CD28TM mut because both have the disulfide bond intact [Fig 5.5]; Cys Mut vs. proCAR2 because neither can form the stalk disulfide bond [Fig 4.6]).

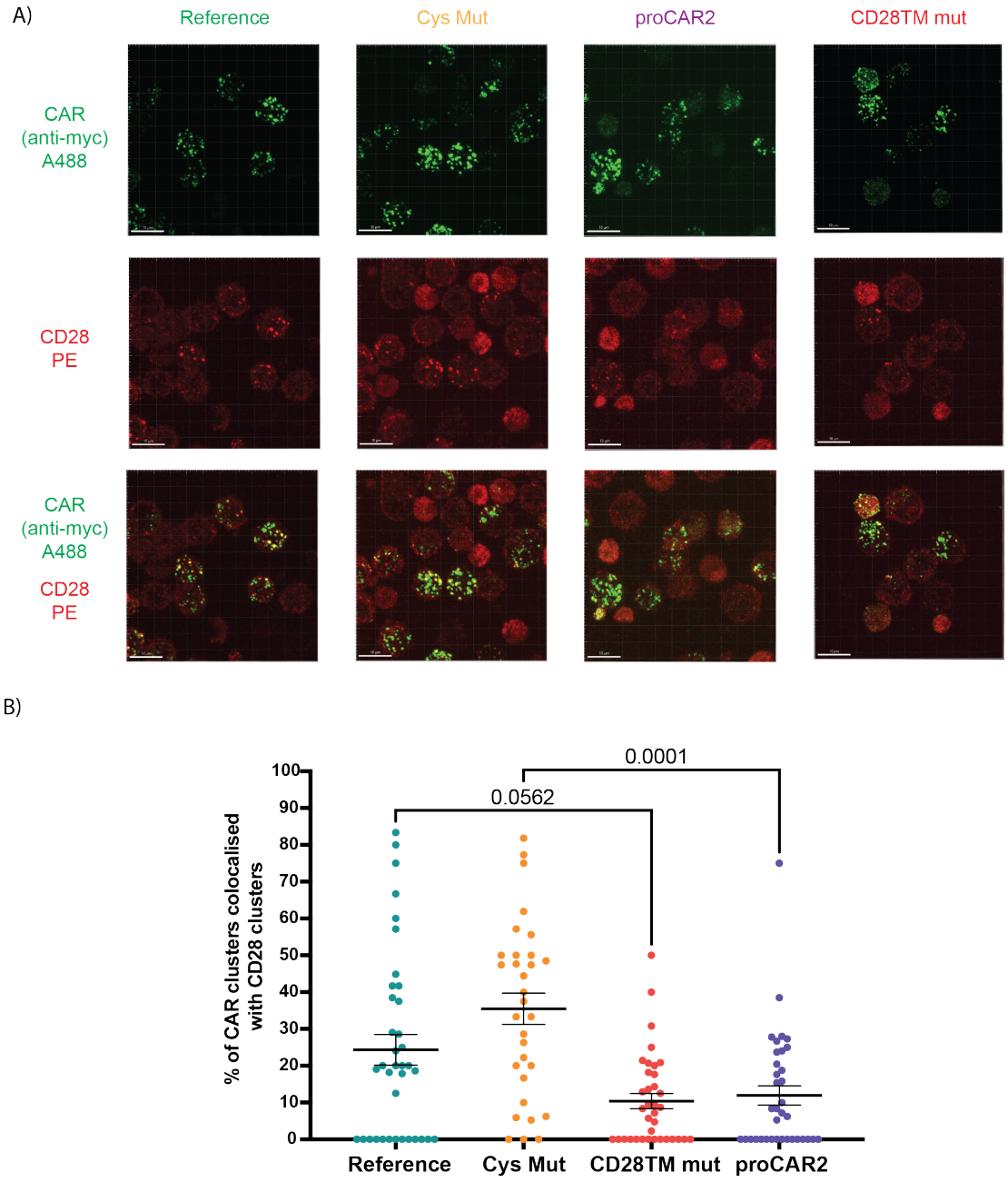

Figure 5.7 Investigation of CAR-CD28 association via co-clustering analysis. *A) Representative images of primary CAR T cells following CAR crosslinking induced clustering. Bright puncta were quantified and termed CAR or CD28 'clusters'. B) CD28 co-clustering data measured for relevant cell lines. Each dot represents the percentage of CAR clusters for a given cell that co-clustered with the respective secondary receptor. Mean+/-SEM, at least 20 cells analysed per cell line. P-values calculated using one-way Anova statistical analysis.*

Mutation of the CD28 dimerization motif (CD28TM mut) indeed caused reduced co-clustering compared to reference with a P-value trending strongly towards significance (Fig 5.7B). Additionally, proCAR2 displayed significantly less CD28 co-clustering compared to FRP5 Cys Mut CARs and was in fact very similar to CD28TM mut. From this data we concluded that the FRP5 CAR was capable of associating with CD28 at the cell surface and that this interaction was mediated at least in part by conserved CD28 YSx_3T motif.

Use of proCAR approach with a CD28TM containing, CD19-directed CAR design

To explore the wider relevance of the mechanistic link between the CD28TM dimerization motif and CAR cytokine release, I decided to incorporate proMP sequences onto the background of a different CAR that also uses the CD28TM domain. Hence, a CD19 directed CAR design was selected consisting of a CD19-specific scFv, CD28 stalk/TMD/Costimulatory tail and a CD3ζ tail. This sequence was adopted from the FDA-approved, Yescarta® CAR T cell treatment (also known as axicabtagene ciloleucel) which importantly also presented an opportunity to confirm the impact of proMP insertions in a highly clinically relevant setting.

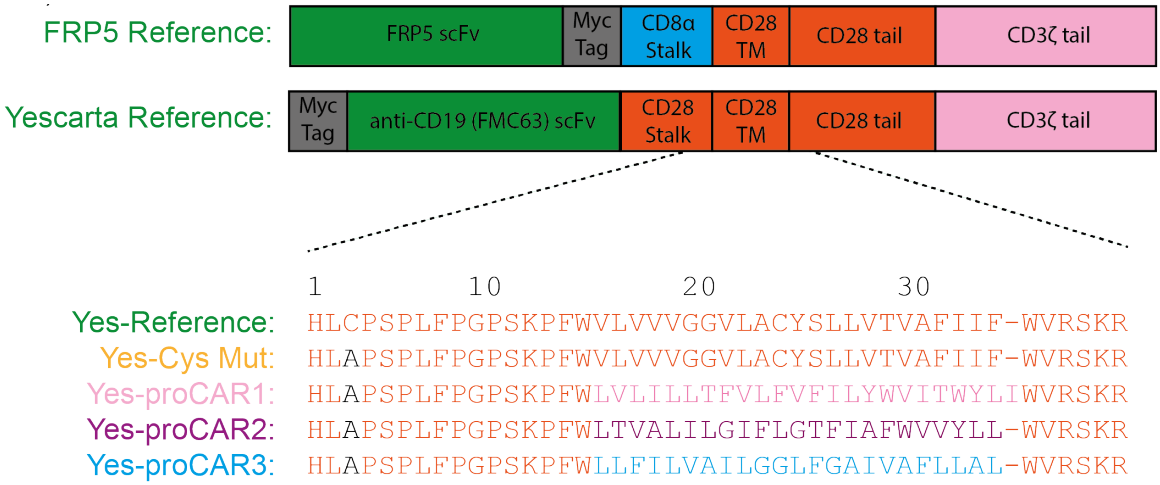

Figure 5.8. Design of the Yescarta proCAR panel. *Comparison of domain architecture of FRP5 CAR vs. that of the Yescarta CD19-specific CAR. Inset is sequence alignment of* Yescarta *CAR sequences, insertion site used in FRP5 CAR was present in* Yescarta *CAR permitting identical proMP insertion site. Stalk cysteine mutation to alanine depicted in black font.*

ProMP sequences were cloned into the CD28 TM domain of the Yescarta reference CAR (Yes-Reference) at an identical position to that of the FRP5 Reference CAR (Fig 5.8). As in the case of the design of the FRP5 proCAR panel, Yescarta proCARs were designed on the background of a construct (Yes-Cys Mut) where stalk cysteines were mutated to prevent inter-chain disulfide linkages. In contrast to the FRP5 reference CAR, the Yescarta sequence currently used clinically does not include an affinity tag, hence a myc tag was included at the N-terminus to assist in receptor detection.

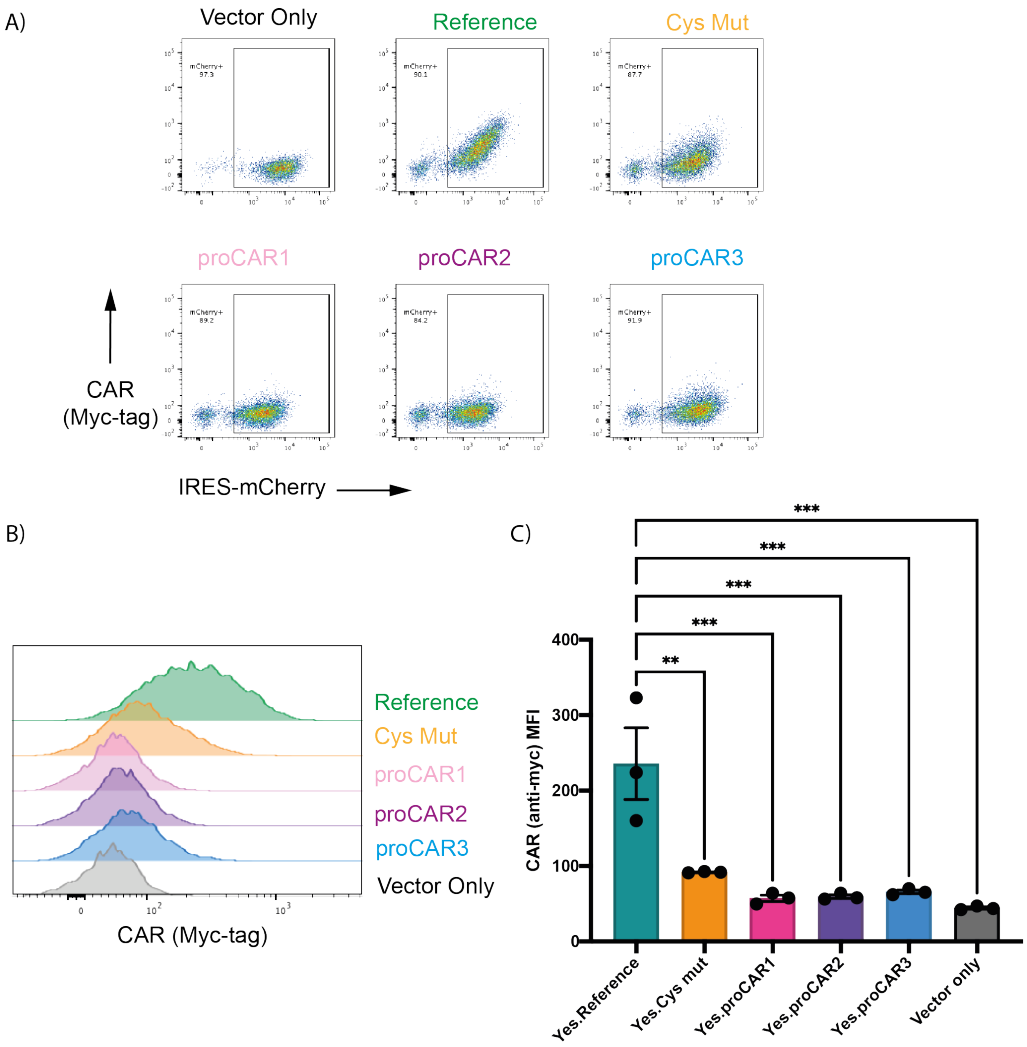

Figure 5.9. Surface expression of Yescarta proCARs. *A) Representative flow cytometry analysis of mCherry and CAR expression in the BW5147 mouse T cell line with corresponding histograms (B) of CAR surface expression. C) CAR surface expression quantified over N=3 independent experiments, mean +/- SEM. **= P<0.001, ***= P<0.0001. P-values calculated using One-way Anova statistical test.*

Upon retroviral expression in the BW5147 NFκB GFP reporter T cell line, Yes-Reference exhibited enhanced cell surface staining compared to Yes-Cys Mut (Fig 5.9C). Yes-proCAR designs exhibited even further reductions in surface expression compared to the Yes-Cys Mut receptor (Fig 5.9C).

Due to the weak surface staining of the Yescarta proCAR designs I conducted an immunoprecipitation experiment using these same cell lines to confirm their expression. Cells were first surface coated with a polyclonal-anti-IgG antibody capable of binding scFv domains and following cell lysis, the antibody-bound receptors were captured with protein-G beads. Western blot analysis confirmed that the mutation of the CD28 stalk cysteine residue was sufficient to prevent covalent dimerization. In contrast to cell surface staining, western blot analysis suggested that Yes-proCAR and Cys Mut receptors were far more similar in expression to Yes-reference (Fig 5.10). The cause of this observation was unclear, however given that different antibodies were used in flow cytometry vs. IP experiments it is possible that Myc-tag accessibility may be compromised in receptors lacking a CD28 stalk cysteine. There was also a notable absence of the lower molecular weight doublet observed in western blotting of the FRP5 proCAR designs (Fig 5.10 vs. Fig 4.6), suggesting that these bands may have been caused by extracellular sequences, given the Yescarta and FRP5 CAR tail sequences are identical (depicted in Fig 5.8). Subsequent blotting with an anti-Myc antibody gave rise to several background bands in all lanes, preventing accurate visualization of CAR proteins for comparison against CD28 blots pictured in fig 5.10A.

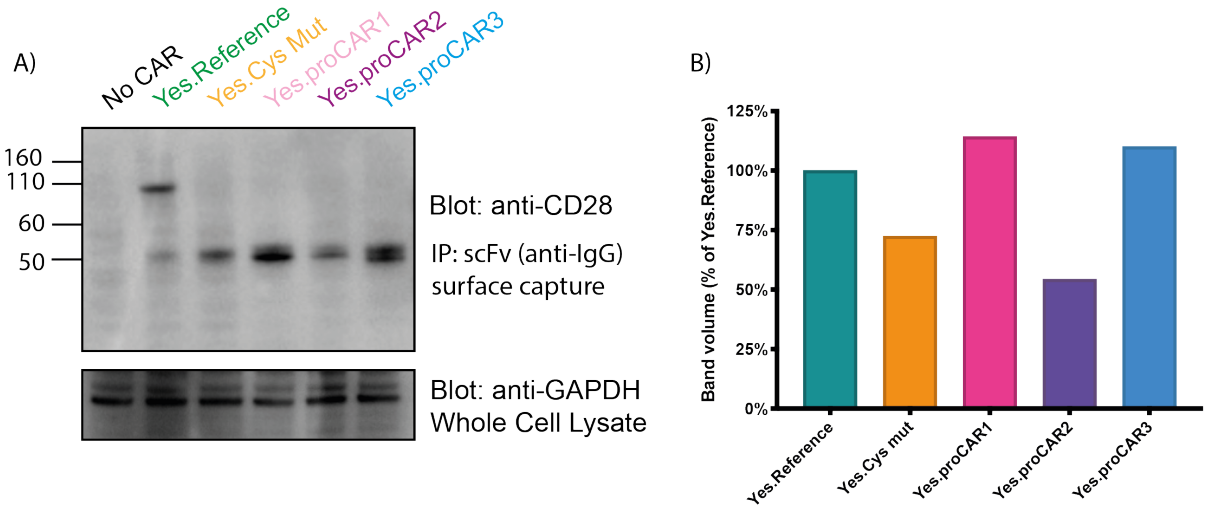

Figure 5.10. Confirming Yescarta surface expression via IP/western blotting. *A) Surface capture/IP was conducted on BW5147 mouse T cells expressing Yescarta proCAR panel. 10 million BW5147 T cells input used per lane, 5% input used for whole cell lysate controls. Theoretical MW of* Yescarta *CAR is 55kDa. B) Quantification of CAR band volume normalised against GAPDH blot of matched whole cell lysate samples. N=1.*

Following the confirmation of Yes-proCAR surface expression via surface-IP and western blotting, this panel of receptors was progressed for functional characterisation. Yes-proCAR T cells were co-cultured for 6 hours with the CD19+ Raji lymphoblastic cell line and subsequently assessed via flow cytometry for activation of NFκB and upregulation of CD69. It was immediately evident that mutation of the CD28 stalk cysteine to generate the Yes-Cys Mut construct resulted in a noticeable reduction in both CD69 and NFκB activation, although this difference only reached statistical significance in the case of CD69 upregulation (Fig 5.11). ProCAR designs by comparison exhibited a phenotype similar to Cys Mut, suggesting that their reduction in signalling capacity was likely a result of the mutation of the CD28 stalk cysteine residue also present in Yes-Cys Mut. Given that earlier experiments on the FRP5 CAR background did not identify a clear correlation between NFκB activation or CD69 upregulation and primary T cell functionality I reasoned that given the Yescarta CAR panel of designs was still signalling competent, primary T cell experiments would be worthwhile pursuing.

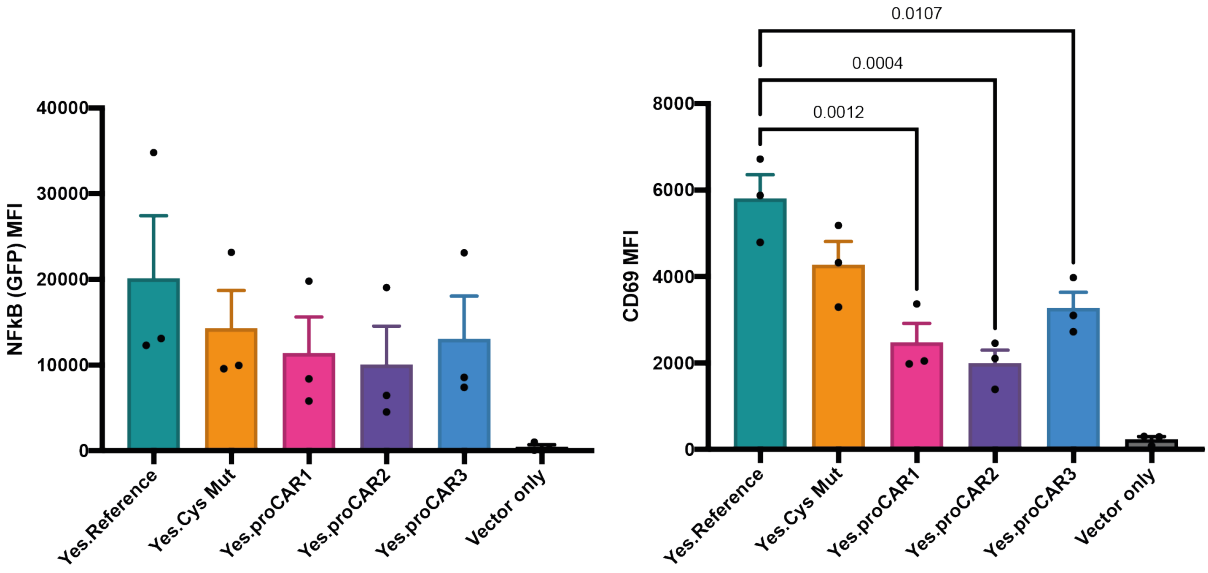

Figure 5.11. Yescarta proCAR initiate T cell signalling. *BW5147 cells expressing Yescarta proCARs were co-cultured for 6 hours with CD19+ Raji B cells. Surface staining and flow cytometry was used to quantitate CD69 expression and NFκB activation. N=3, mean +/- SEM. P-values calculated using one-way Anova statistical test.*

Preliminary evaluation of Yescarta-proCAR panel in primary mouse T cells

Yescarta Reference, Cys Mut and proCAR constructs were expressed in primary mouse T cells to assess their ability to trigger cytotoxicity and cytokine release. HEK293T cells ectopically expressing human CD19 were used as target cells, with parental HEK293T cells used as antigen-negative controls. This preliminary experiment was conducted by Dr. Ashleigh Davey, with additional replicates currently underway at the time of writing. Myc-tag surface staining indicated that expression in primary mouse T cells appears to match closely with expression levels observed in the BW5147 cell line, with Yes-reference CARs expressing at higher levels than both Yes-Cys-mut and Yes-proCAR designs (Fig 5.12A). Levels of IFNγ, IL-2 and TNFα release were lower in Yes-Cys Mut and Yes-proCAR T cells compared to Yes-Reference CAR T cells, while in the case of IFNγ and IL2 cytokine output was lower than observed in FRP5 CAR experiments (Fig 5.12C). By contrast measurement of these same CAR T cells in a cytotoxicity assay indicated that Yescarta reference and Cys-mut constructs demonstrated indistinguishable killing ability, while Yescarta proCAR2 and proCAR3 T cells appeared to present a subtle enhancement in target cell killing (Fig 5.12B).

However, these observations remain to be replicated and further experiments are currently underway to confirm these findings.

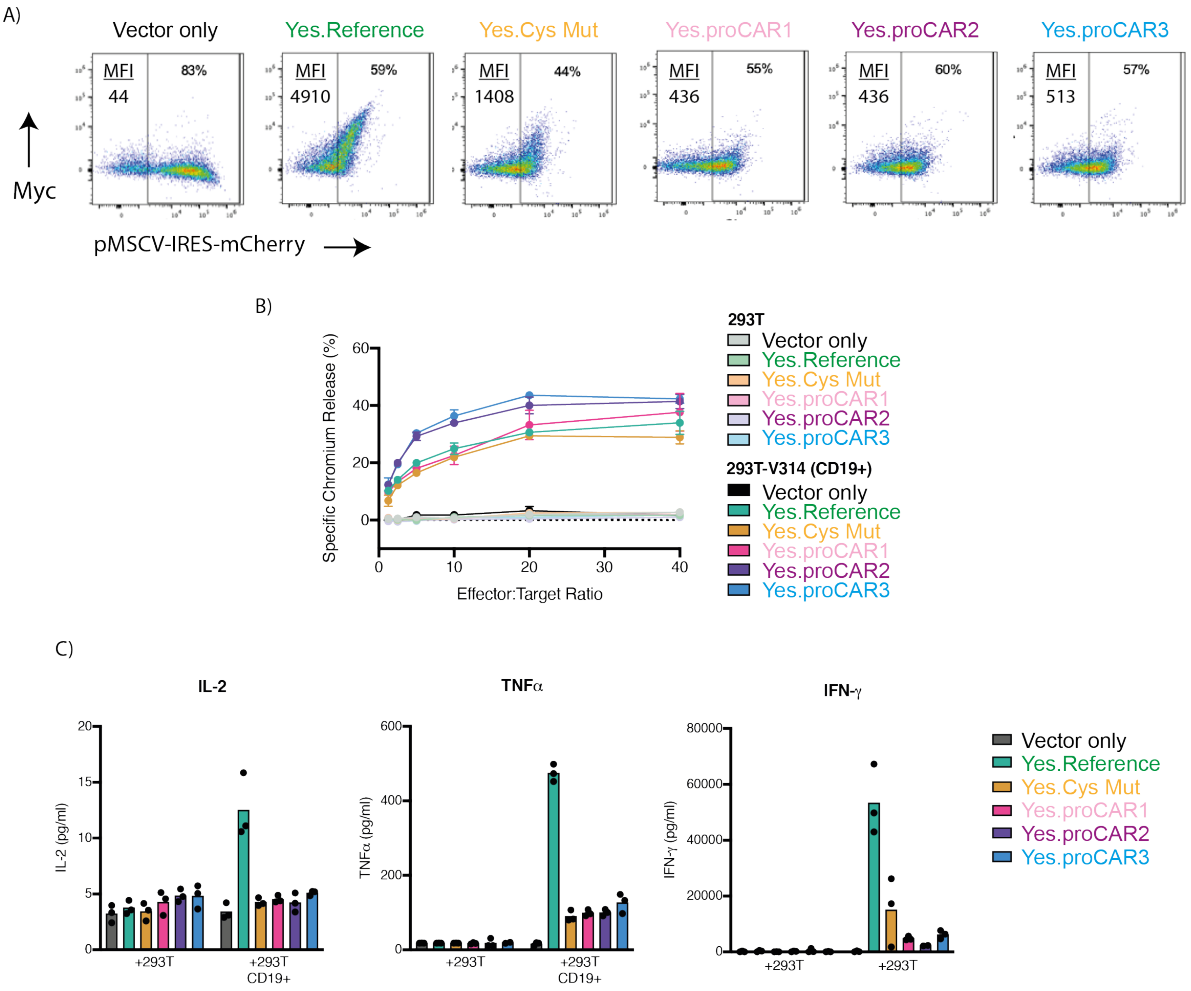

Figure 5.12. Yescarta proCARs demonstrate robust primary T cell activity. Yescarta *proCAR panel was expressed in primary mouse CD8+ T cells. A) Representative floy cytometry plots showing myc staining (Y-axis) vs. pMSCV IRES mCherry expression (x-axis). CAR T cells were subjected to either A) chromium killing assay or B) cytokine release assay via co-culture for 4-hours or 24-hours respectively, co-cultured with either CD19+ 293T cells or CD19- parental 293T cells. Experiment conducted by Dr. Ashleigh Davey.*

5.3 Discussion

CD28TM drives CAR cytokine release, not cytotoxicity

Through the rational design of mutations to a conserved dimerization motif in the CD28 TM domain we have elucidated a previously unappreciated role for lateral hetero-typic

interactions in CAR function. This CD28TM mutant exhibited a reduction in its ability to recruit endogenous CD28 when compared to Reference CAR, a phenotype that was re-capitulated in the significantly reduced co-recruitment of CD28 by proCAR2 compared to the FRP5 Cys Mut receptor. These results suggest not only that the CD28TM dimerization motif is central to the recruitment of endogenous CD28, but also that the lack of this motif in proMP sequences is also likely responsible for reducing CD28 recruitment in proCAR designs. These findings were very recently supported by a study showing that the CD28TM drove CAR interactions with endogenous CD28 that were detectable by co-IP and also required the polar dimerization motif (Muller et al., 2021). Our study extends these findings by highlighting a correlation between the CD28TM dimerization motif and CAR-induced cytokine release. The targeted mutation of this motif resulted in a dramatic reduction in release of IL-2, TNFα, IFNγ and GM-CSF, in line with the reductions observed when the CD28TM sequence was removed entirely to permit proMP insertion. In contrast, mutation of the YSx_3T motif did not affect CAR T cell cytotoxicity *in vitro*, as the CD28TM mutant displayed equivalent target cell killing to Reference FRP5 CAR. This phenotype recapitulates previous observations that ablation of CD28 signalling via mutation of canonical CD28 tail signalling motifs resulted in equivalent *in vitro* cell killing but attenuated cytokine release (Moeller et al., 2004). Our findings suggest a surprising, overlapping role for CD28TM and cytosolic motifs and suggest that the CD28 tail and TM domain both contribute significantly to CD28 signalling in the context of 2nd generation CAR constructs.

While these findings are highly suggestive of a functional role for interactions between CARs and endogenous CD28, confidence in this conclusion would be greatly enhanced by validation using orthogonal biochemical approaches. For example, a fluorescence resonance energy transfer (FRET)-based approach would be capable of detecting CAR/CD28 protein colocalization within a radius of 10nm (Algar et al., 2019), which would further support the involvement of direct protein-protein interactions between TM domains. It will also be important in subsequent studies to account for the difference in surface expression between Reference and CD28TM mutant CARs. It is unclear what impact large differences in surface expression impart upon the co-clustering analysis presented above and it is possible that the low levels of surface expression of the CD28TM mut CAR may impair the recruitment of sufficient concentrations of endogenous CD28 to be effectively visualised.

Previous studies have identified that mutation of the mouse CD28 YxxxxT motif reduces surface expression in the context of full-length CD28 (Leddon et al., 2020), suggesting that reducing expression levels of Reference CAR may serve as a more practical and relevant control for future co-clustering or FRET experiments. Such a control would also be useful in investigating the impact of receptor surface expression on CD28TM mut CAR function. Studies investigating the functional relevance of antigen density have previously observed that cytokine expression is more readily attenuated than target cell killing, in line with the observed phenotype of the CD28TM mut (Majzner et al., 2020). However, the functional relevance of surface expression by comparison does not appear to be linear or consistent between CAR designs (Walker et al., 2017) and therefore it is difficult to predict the functional implications of attenuated surface expression on the CD28TM mut CAR. Interestingly, expression of the CD28TM mut CAR appeared more comparable to Reference when expressed in the BW5147 T cell line. This observation suggests that these two systems may engender differences in CAR trafficking and/or surface stability.

The comparison of HER2 proCAR2 and reference, both dimeric receptors, clearly demonstrates that the CD28 cytosolic tail alone is insufficient to compensate for the loss of CD28 TM domain in terms of cytokine release. Furthermore, proCAR3 demonstrates that increasing the number of CD28 tails/CAR complex (3 in proCAR3 versus 2 in Reference) only partially compensates for reduced cytokine expression due to the loss the CD28 TM domain. Assuming the underlying mechanism of the CAR CD28TM is to increase the number of CD28 signalling tails (in the form of laterally associated endogenous CD28 molecules) per CAR complex, then it is possible that higher order oligomeric proCARs may be capable of elevated cytokine expression compared to proCARs1-3. This hypothesis is supported by the subtle, yet consistent enhancement of cytokine release exhibited by proCAR3 compared to proCAR1 in primary mouse T cell experiments (Fig 4.15B).

Given the proposed complexity of the CD28 signal transduction mechanism a potentially more nuanced influence of CAR CD28TM sequences on endogenous CD28 signalling should also not be discounted. The cytosolic tails of CD28 are capable of associating with the plasma membrane inner leaflet, an interaction that is disrupted upon ligand binding (Dobbins et al., 2016). It has been suggested that ligand binding induced alterations in the

CD28 TM dimer may be responsible for triggering such cytosolic tail re-arrangements. Interestingly, ligand binding induced changes in association of the cytosolic tails of CD3ζ and the inner leaflet have also been observed (Zhang et al., 2011, Aivazian and Stern, 2000). Additionally, physical re-arrangements in the CD3ζ TM dimer have been observed in response to ligand binding, (Lee et al., 2015). Given that both the CD3ζ and CD28 TM domains share the conserved Yx_4T dimerization motif it is possible that these receptors possess homologous features of signal transduction. Hence, as new data concerning the signal transduction mechanism either of these native receptors comes to hand, the relationship between CD28TM sequence and signal transduction should be carefully re-evaluated.

It was also notable that western blot analysis suggested that the CD28TM mut CAR was still capable of forming covalent homodimers at the cell surface, in spite of the ablation of potential hydrogen bonding pairs. Other reported attempts to disrupt this dimerization interface in native CD28 (Leddon et al., 2020) and CARs (Yannick. D. Muller, 2020) have utilised leucine residues, which may be more disruptive, particularly compared to the conservative TM mutations we chose (YSx_3T to FAx_3V). This may suggest that our conservative mutations still allow some degree of CD28TM dimerization, with sufficient affinity to facilitate covalent CAR dimerization. However, to test this hypothesis reproduction of previously published LLxxxL CD28TM mutations in the context of the FRP5 CAR background would be required. It is also possible that other domains within the FRP5 CAR contribute to homodimerization, for example the scFv domains via domain-swapping (Gil and Schrum, 2013) as discussed in section 4.3. Given the irreversible nature of disulfide bonds (under normal cellular conditions) it is likely that such interactions, even if weak, combined could build up to the degree of covalent dimerization observed. Most importantly, however, the co-clustering analysis indicated a notable reduction in recruitment of endogenous CD28, demonstrating that our more conservative TM mutations do interfere with heterotypic CD28-CAR association.

Untangling the proCAR phenotype from CD28 stalk cysteine mutation contributions

While experiments on the Yescarta background are ongoing, several observations can inform the development of future refinements to these CAR designs. Our preliminary

interpretation of the influence of proMP insertion is complicated by the observation that mutation of the CD28 stalk cysteine alone results in a functional profile different to that of the Yescarta reference CAR. Yescarta Cys Mut surface expression as measured by surface staining and flow cytometry was notably lower than that of reference in both primary T cells and the BW5147 T cell line. By contrast, figure 5.10 demonstrated that levels of receptor recovered via surface capture of scFv using a polyclonal anti-IgG antibody were inconsistent with results from flow cytometry data. Combined, these data make it difficult to infer the impact of proMP insertion on receptor expression and stability. For this reason, alternative affinity reagents should be considered for the quantification of Yescarta surface expression, for example protein L affinity reagents capable of robust, pan-scFv binding (Zheng et al., 2012).

CD69 expression of all Yescarta proCARs were significantly attenuated compared to Yescarta reference, however differences between the proCARs and Cys Mut were smaller and not statistically significantly. A similar trend was observed of NFκB activation, albeit variability obscured these results to a degree. This data suggested that mutation of the stalk cysteine was contributing to this attenuation of signalling. This effect may have been related to reduced surface expression levels, given that proximal CAR signalling has been observed to correlate with receptor surface expression *in vitro* (Walker et al., 2017). A solution to this issue may rest in the re-introduction of a stalk cysteine residue to the Yescarta proCAR2 design. These modifications could be reasonably expected to restore signalling deficiencies associated with stalk cysteine mutation and allow independent determination of the functional relevance of TM sequence in Yescarta CAR proximal signalling.

Interestingly, signalling deficiencies identified in the BW5147 cell line did not correlate with target cell killing measurements in primary CAR T cells. Yescarta reference, Cys Mut and proCAR1 all demonstrated comparable killing, whereas proCAR2 and proCAR3 target cell cytotoxicity was at the very least comparable if not slightly enhanced compared to Yescarta reference and Cys Mut CARs. These observations were consistent with the pattern of cytotoxicity observed of the FRP5 CAR panel, where proCAR2 and proCAR3 demonstrated enhanced target cell killing. Although repeat measurements of the Yescarta proCAR panel are required to conclusively quantitate this relationship, these preliminary results

promisingly point to a consistent phenotype of enhanced target cell killing *in vitro* by proCARs compared to reference constructs and a positive correlation between oligomeric state and cytotoxicity.

A role for lateral protein interactions in CAR function

These findings suggest a previously underappreciated function role for lateral interactions between CAR framework regions and endogenous proteins at the T cell membrane. While our study focussed directly on the role of the CD28 TM domain, it raises the possibility that other frequently used CAR hinge and TM domains may also contribute in unforeseen ways to receptor function. For example, CD8α is known to efficiently form homo- and heterodimers with CD8α and CD8β respectively, via interactions within their stalk and TM domains as well as their extracellular Ig domains (Hennecke and Cosson, 1993, Chang et al., 2005). This leaves open the possibility for CD8α stalk and TM sequences also prevalent among 2nd generation CAR architectures to facilitate interactions with these endogenous proteins at the cell surface in CD8+ T cells. Given the emerging importance of stalk and TM domains on CAR function (Majzner et al., 2020, Alabanza et al., 2017, Ying et al., 2019), determining the functional relevance of such lateral interactions will be crucial to the continued improvement of CAR T cell therapies.

Chapter 6 Concluding Remarks and Future Directions

Efforts to improve CAR construct design currently serve as one of the key pillars of advancement in the search for safer, more effective and more widely applicable CAR-T cell therapies. In addition to complex and creative efforts to completely redesign signalling circuits (Roybal and Lim, 2017, Labanieh et al., 2018), it is now clear that an improved understanding of the basic receptor biology of widely used 2nd generation CARs permits significant modulation of CAR T cell efficacy and safety. This is exemplified by recent studies that have for example uncovered the relevance of CD3ζ ITAM stoichiometry and position (Feucht et al., 2019, Majzner et al., 2020) and CAR ubiquitin-mediated downregulation (Li et al., 2020) and exploited these fundamental principles to improve CAR therapies. Our work on oligomeric proCAR designs contributes to this growing understanding of basic receptor biology of 2nd generation CARs, whilst in and of itself presenting an opportunity to immediately improve CAR safety and efficacy.

6.1 Therapeutic potential of HER2-specific proCARs

The *in vitro* and *in vivo* performance of the FRP5 proCAR panel described in Chapter 4 has the potential to drive improvements in various clinically relevant HER2-specific CAR therapy settings. One of the most promising avenues for the clinical translation of our findings is in the use of our FRP5 CARs in the treatment of glioblastoma. The safety of HER2-targeted CAR T cell treatment for glioblastoma has been established in phase 1 clinical trials (using CARs composed of FRP5 scFv-IgG1 stalk-CD28 TM-CD28 tail-CD3ζ tail), however such treatments have resulted in only modest improvements to patient outcomes (Ahmed et al., 2017, Ahmed et al., 2015). One hurdle faced in the optimization of such therapies is the incidence of neurotoxicity initiated by CAR T cell mediated activation of myeloid cells which subsequently release inflammatory cytokines within the central nervous system (Neelapu et al., 2018). Neurotoxicity is encountered frequently in CAR T cell treatments of haematological malignancies, particularly in the case of CARs containing CD28 costimulatory domains (Davey et al., 2020). For this reason, dosing of CAR T cells in the treatment of neurological malignancies has proceeded cautiously in trials thus far (Ahmed et al., 2015, Ahmed et al., 2017). There is a case to be made that proCAR-T cells may offer an advantage

compared to standard FRP5 CARs in the advancement of these therapies in light of the real concerns of neurotoxicity. Given that proCARs exhibit a dramatic reduction in cytokine release whilst still maintaining cell killing potential (proCAR3 in particular), we would propose that higher dosages of proCAR T cells may be possible compared to reference FRP5 CARs, with a lower risk of CAR T cell induced neurotoxicity. Dose escalation studies are currently planned at the time of writing with the aim of testing this hypothesis in the previously described MC38-HER2 mouse tumour model, however collaborations with A/Prof Misty Jenkins (brain cancer immunotherapy lab at WEHI) have been established with the aim of concurrently exploring this hypothesis in the context of mouse models of human brain tumours.

6.2 Translating the proCAR approach to alternative CAR architectures

Part of the intended benefit of our proCAR approach was the potential for broad application in various CAR constructs. Therefore, while investigating the utility of proMP designs in the context of the Yescarta CAR provided a means of interrogating our hypothesis of CD28TM heterotypic interactions, it also provided the first test of the broader applicability our proCAR approach. Our experience with Yescarta proCAR designs highlighted the potential for proMP sequences to facilitate expression of constructs with varied components but also to elicit a comparable primary T cell phenotype in response to different target antigens. Further experiments are required to reliably quantify the effect of proMP sequences on Yescarta function *in vitro* and *in vivo*, however the results presented in this thesis provide an encouraging sign that the results obtained in FRP5 *in vivo* models may realistically be achievable via proMP insertion into any CD28TM containing CAR.

While a large proportion of CAR designs in clinical use or undergoing clinical trials utilise CD28 stalk/TM/tail sequences, a significant number of CAR T cell therapies utilise CARs composed of a CD8α stalk/TM framework region connected to 4-1BB and CD3ζ tails. Testing the relationship between oligomeric state and the functionality of CD8α-41BB-CD3ζ CAR constructs is therefore a high priority within our lab. However, there are two notably different characteristics of CD8α-41BB-CD3ζ CARs compared to CD28TM/tail-CD3ζ CARs which suggest that slightly different results may be expected. Firstly, CD8α stalk/TM

containing CARs are associated with reduced levels of cytokine release compared to those incorporating CD28 stalk/TM/tail components (Majzner et al., 2020, Alabanza et al., 2017). Hence, the use of proMP sequences on the background of a CD8α-41BB-CD3ζ CAR may present an opportunity to assess *in vivo* advantages to higher oligomeric states on tumour control without the confounding impact of comparative reductions in cytokine output as illustrated by our preliminary *in vivo* experiments in Chapter 4. A second key consideration between these CAR designs is that the costimulatory 4-1BB tail derives from a tumour necrosis factor receptor superfamily (TNFRSF) protein of the same name. Activation of TNFR family members is regulated by alterations in oligomeric state, with TNFR tails responsible for binding trimeric signalling complexes to initiate downstream signalling (Vanamee and Faustman, 2018). Furthermore, recent publications have highlighted that in other members of the TNFR family, transitions in receptor oligomeric state from monomer to trimeric or even higher-order arrangements are associated with receptor activation (Karathanasis et al., 2020, Pan et al., 2019, Fu et al., 2016). While data surrounding the oligomeric determinants of 4-1BB signalling are currently lacking, particular care will be required when controlling 4-1BB tail containing CARs that constitutive, antigen-independent receptor activation is not initiated, in particular by trimeric TM arrangements. With these considerations in mind, proMP1, proMP2.2 and proMP3 have been cloned into the Kyrmiah clinically-approved CAR construct, possessing CD19-specific CAR-CD8α stalk/TM-4-1BB tail-CD3ζ tail at the time of writing. Additionally, a construct has been designed with CD8α TM domain in place of the CD28 TM domain of the FRP5 reference CAR (FRP5-CD8α stalk-TM-CD28 tail – CD3ζ), with the primary aim of benchmarking the cytokine release of FRP5 proCARs already described in this thesis against the relatively low levels of cytokine release expected of an FRP5 CAR with CD8α stalk/TM domains.

An important question that remains to be tested using our proCAR panel is whether increases in CAR oligomeric state correspond with increases in antigen sensitivity. Experiments conducted in BW5147 cells demonstrated that signalling and activation of all CARs was reduced in response to target cells expressing low levels of HER2, however no significant differences in signalling or activation were observed between Reference and proCARs in response to these low-antigen expressing targets (Fig 4.13). These findings warrant further investigation in primary mouse T cells, given the observations by others that

altering CAR potency can result in differential primary T cell activity according to antigen expression level (Liu et al., 2015, Majzner et al., 2020). The significance of tuning CAR sensitivity to ligand density is that it offers an opportunity to circumvent issues associated with on-target, off-tumour cytotoxicity directed at healthy tissues expressing low levels of HER2. However, reference FRP5 CAR does not display obvious signs of such autoimmunity when administered in tumour mouse models using human HER2-expressing transgenic mice (Wang et al., 2010). Instead, there are several other CAR T cell antigen targets which may represent more clinically relevant models for investigating the relationship between CAR oligomeric state and ligand density. For example, resistance to anti-CD22 CAR T cell therapy in the treatment of relapsed and refractory B-ALL has been observed due to the selection of tumour variants expressing low levels of CD22 (Fry et al., 2018). Hence, CD22-specific CARs may offer a clinically beneficial model in which improvements in CAR sensitivity to low levels of antigen via alterations in CAR oligomeric state would potentially improve targeted treatment of CD22-low relapse.

In this regard another exciting avenue of CAR T cell development involves the targeting of peptide antigens presented by MHC. Such CARs utilize scFv domains capable of binding MHC complexes presenting oncogene-associated peptide-MHC (pMHC) complexes. One of the key differences between surface proteins, such as CD19, and pMHC targets is that surface expression levels of pMHC are likely to be lower by approximately 10^3-fold (Olejniczak et al., 2006, Rammensee et al., 1993). One of the remarkable features of CD8+ cytotoxic T cells is their ability to kill target cells expressing fewer than 10 copies of cognate pMHC (Irvine et al., 2002, Purbhoo et al., 2004), but recapitulating this sensitivity represents a theoretical barrier to the success of pMHC-targeted CAR T cells (Oren et al., 2014). While preclinical evidence has validated the potential of this approach (Willemsen et al., 2001, Zhang et al., 2014, Zhao et al., 2015a, Rafiq et al., 2017), unfortunately human clinical trials are yet to materialize. There is evidence that ensuring antigen specificity of such CARs may rely on incorporating low-affinity pMHC-specific scFvs in place of high-affinity clones (Maus et al., 2016), mirroring the observation that productive pMHC:TCR interactions in nature are overwhelmingly of comparatively low affinity (with micromolar rather than nanomolar dissociation constants, in the range of 1000-fold lower) (Matsui et al., 1991, Weber et al., 1992). In this regard, controlling CAR oligomeric state via proMP TM sequences offers an

enticing opportunity to mimic another important aspect of TCR biology, that is the lateral recruitment of large numbers of signalling tails (Fig 1.3). Such an approach may be expected to increase the potency of pMHC-targeted CARs and will be a worthwhile consideration should current approaches to pMHC-targeted CARs fail to translate clinically.

6.3 Extending proMP use to answer open questions in CAR biology.

There are several interesting biological questions within the CAR-T cell field where the application of proMPs capable of dictating oligomeric state may be of particular use. For example, there is a growing understanding that membrane proximity of cytosolic CAR domains influences their functionality. Costimulatory domains situated in the N-terminal position (closer to the membrane) exhibit a dominant influence over CAR T cell phenotype in the context of both 2nd and 3rd generation CAR designs (Guedan et al., 2018, Finney et al., 1998, Hombach et al., 2012, Pule et al., 2005). Additionally, membrane proximity was shown to drive favourable T cell phenotype in 2nd generation CARs encoding only one active version of the 3 CD3ζ ITAMs (Feucht et al., 2019). These studies strongly suggest there may be an inherent advantage in multiplying signalling motifs by laterally associating CARs into stable oligomers, as opposed to linearly extending tails. This was recently demonstrated in a study comparing HIV-directed CARs where a third-generation design encoding a CD28-4-1BB-CD3ζ (dual-costimulatory sequence) tail was out-performed by T cells expressing two separate CD28-CD3ζ and 4-1BB-CD3ζ (each with a single costimulatory sequence) CAR designs (Maldini et al., 2020). In this case it appears that lateral association of two costimulatory domains located close to the membrane was superior to a configuration in which one of the two was necessarily located further from the membrane.

Modulation of CAR oligomeric state using proMP sequences may serve as a useful tool capable of extending these findings and providing added value to the next generation of CAR designs. For example, while a CAR encoding a single membrane-proximal ITAM demonstrated improved T cell phenotype (Feucht et al., 2019), the same construct was demonstrated to possess reduced cytotoxicity in response to low antigen expressing cells (Majzner et al., 2020, Feucht et al., 2019). Oligomerization of CARs encoding a single, membrane proximal ITAM may have the potential to increase CAR potency whilst also

achieving a favourable pro-survival, anti-inflammatory phenotype. Work is also underway to validate a modified proMP pipeline capable of designing heterodimeric TM assemblies, which if successful may present an opportunity to generate hetero-typic arrangements of CAR constructs each encoding a different costimulatory domain. This presents an opportunity to enhance the performance of 3rd generation CARs, by ensuring equivalent membrane proximity of several costimulatory domains in a single CAR complex. The modularity of the proCAR platform would very easily permit the experiments described above and has the potential to add value to a variety of other CAR designs currently in a preliminary stage of functional validation.

6.4 proMP sequences as receptor engineering tools

While the field of CAR protein engineering was a logical and impactful first-case use for the TM sequences generated by the proMP pipeline, several other biological applications have the potential to make use of these oligomeric tools. One of the strengths of this approach is the ability to generate several sequences capable of adopting the same oligomeric state albeit with differing packing geometries. There is a growing appreciation that structures adopted by the TM domains of many type-I receptors are dynamic and capable of influencing signalling. For example, the TM domains of Receptor Tyrosine Kinases (RTK's) such as the EGFR family have been shown capable of adopting two mutually exclusive conformation predicted to correspond with active and inactive states (Li and Hristova, 2006, Bocharov et al., 2008). A role for dynamic modulation of TM structure in signal transduction pathways has also been suggested for CD28 (Leddon et al., 2020, Sanchez-Lockhart et al., 2011, Sanchez-Lockhart et al., 2014) and CD3ζ (Lee et al., 2015). However, due to the technical complexity of determining structures of TM domains, establishing what structures correspond with active/inactive receptor states remains a significant challenge. This presents a significant opportunity for the proMP panel of *de novo* designed dimeric TM domains described in Chapter 3. These sequences exhibit a variety of predicted crossing angles and depths and are selected for the ability of each design to adopt a single conformation with a high degree of stability. By splicing such sequences into native receptors, it may be possible to characterize the TM orientations required (or otherwise) for signal transduction. Optimization of the proMP design process has also allowed the design

of a panel of trimeric TM sequences, differing in their interface motifs and geometries. These sequences could foreseeably be used to test the relationship between trimer geometry and signal activation of trimeric receptors, such as those within the Tumour Necrosis factor receptor family (TNSRF).

In recent years the *de novo* design of soluble proteins with diverse homo- and hetero-oligomeric states have rapidly advanced the concept of wholly synthetic logic gates and circuitry within cellular systems (Chen et al., 2020). ProMPs represent the first example of *de novo* designed single-pass TM oligomers and as such they are prime candidates to be used in combination with these systems in pursuit of wholly synthetic biological circuits. The fusion of proMPs with *de novo* designed catalytic subunits could foreseeably engender synthetic circuits with transmembrane signalling potential or enable simultaneous membrane targeting and oligomerisation of circuitry components.

References:

ADAMS, P. D., AFONINE, P. V., BUNKOCZI, G., CHEN, V. B., DAVIS, I. W., ECHOLS, N., HEADD, J. J., HUNG, L. W., KAPRAL, G. J., GROSSE-KUNSTLEVE, R. W., MCCOY, A. J., MORIARTY, N. W., OEFFNER, R., READ, R. J., RICHARDSON, D. C., RICHARDSON, J. S., TERWILLIGER, T. C. & ZWART, P. H. 2010. PHENIX: a comprehensive Python-based system for macromolecular structure solution. *Acta Crystallogr D Biol Crystallogr,* 66**,** 213-21.

AHMED, N., BRAWLEY, V., DIOUF, O., WAKEFIELD, A., ASHOORI, A., GHAZI, A., GERKEN, C., YI, J., LIU, H., ROONEY, C. M., DOTTI, G., GEE, A., GROSSMAN, R., KEW, Y., BASKIN, D., ZHANG, J., NEW, P., HICKS, J., POWELL, S. Z., WELS, W., BRENNER, M. K., HESLOP, H. E. & GOTTSCHALK, S. 2015. A Phase I Clinical Trial of Autologous HER2 CMV Bispecific CAR T Cells for Progressive Glioblastoma. *Molecular Therapy,* 23**,** S9-S9.

AHMED, N., BRAWLEY, V., HEGDE, M., BIELAMOWICZ, K., KALRA, M., LANDI, D., ROBERTSON, C., GRAY, T. L., DIOUF, O., WAKEFIELD, A., GHAZI, A., GERKEN, C., YI, Z. Z., ASHOORI, A., WU, M. F., LIU, H., ROONEY, C., DOTTI, G., GEE, A., SU, J., KEW, Y., BASKIN, D., ZHANG, Y. J., NEW, P., GRILLEY, B., STOJAKOVIC, M., HICKS, J., POWELL, S. Z., BRENNER, M. K., HESLOP, H. E., GROSSMAN, R., WELS, W. S. & GOTTSCHALK, S. 2017. HER2-Specific Chimeric Antigen Receptor-Modified Virus-Specific T Cells for Progressive Glioblastoma A Phase 1 Dose-Escalation Trial. *Jama Oncology,* 3**,** 1094-1101.

AIVAZIAN, D. & STERN, L. J. 2000. Phosphorylation of T cell receptor zeta is regulated by a lipid dependent folding transition. *Nat Struct Biol,* 7**,** 1023-6.

AKATSUKA, Y. 2020. TCR-Like CAR-T Cells Targeting MHC-Bound Minor Histocompatibility Antigens. *Front Immunol,* 11**,** 257.

ALABANZA, L., PEGUES, M., GELDRES, C., SHI, V., WILTZIUS, J. J. W., SIEVERS, S. A., YANG, S. & KOCHENDERFER, J. N. 2017. Function of Novel Anti-CD19 Chimeric Antigen Receptors with Human Variable Regions Is Affected by Hinge and Transmembrane Domains. *Mol Ther,* 25**,** 2452-2465.

ALGAR, W. R., HILDEBRANDT, N., VOGEL, S. S. & MEDINTZ, I. L. 2019. FRET as a biomolecular research tool - understanding its potential while avoiding pitfalls. *Nat Methods,* 16**,** 815-829.

ALTSCHUL, S. F., GISH, W., MILLER, W., MYERS, E. W. & LIPMAN, D. J. 1990. Basic local alignment search tool. *J Mol Biol,* 215**,** 403-10.

BANG, Y. J., VAN CUTSEM, E., FEYEREISLOVA, A. & INVESTIGATORS, T. T. 2010. Trastuzumab in combination with chemotherapy versus chemotherapy alone for treatment of HER2-positive advanced gastric or gastro-oesophageal junction cancer (TOGA): a phase 3, open-label, randomised controlled trial (vol 376, pg 687, 2010). *Lancet,* 376**,** 1302-1302.

BASELGA, J., ALBANELL, J., MOLINA, M. A. & ARRIBAS, J. 2001. Mechanism of action of trastuzumab and scientific update. *Semin Oncol,* 28**,** 4-11.

BERRY, R. & CALL, M. E. 2017. Modular Activating Receptors in Innate and Adaptive Immunity. *Biochemistry,* 56**,** 1383-1402.

BOCHAROV, E. V., MINEEV, K. S., VOLYNSKY, P. E., ERMOLYUK, Y. S., TKACH, E. N., SOBOL, A. G., CHUPIN, V. V., KIRPICHNIKOV, M. P., EFREMOV, R. G. & ARSENIEV, A. S. 2008. Spatial structure of the dimeric transmembrane domain of the growth factor

receptor ErbB2 presumably corresponding to the receptor active state. *Journal of Biological Chemistry,* 283**,** 6950-6956.

BOOMER, J. S. & GREEN, J. M. 2010. An enigmatic tail of CD28 signaling. *Cold Spring Harb Perspect Biol,* 2**,** a002436.

BOUCHKOUJ, N., KASAMON, Y. L., DE CLARO, R. A., GEORGE, B., LIN, X., LEE, S., BLUMENTHAL, G. M., BRYAN, W., MCKEE, A. E. & PAZDUR, R. 2019. FDA Approval Summary: Axicabtagene Ciloleucel for Relapsed or Refractory Large B-cell Lymphoma. *Clin Cancer Res,* 25**,** 1702-1708.

BRAHMER, J. R., TYKODI, S. S., CHOW, L. Q. M., HWU, W. J., TOPALIAN, S. L., HWU, P., DRAKE, C. G., CAMACHO, L. H., KAUH, J., ODUNSI, K., PITOT, H. C., HAMID, O., BHATIA, S., MARTINS, R., EATON, K., CHEN, S. M., SALAY, T. M., ALAPARTHY, S., GROSSO, J. F., KORMAN, A. J., PARKER, S. M., AGRAWAL, S., GOLDBERG, S. M., PARDOLL, D. M., GUPTA, A. & WIGGINTON, J. M. 2012. Safety and Activity of Anti-PD-L1 Antibody in Patients with Advanced Cancer. *New England Journal of Medicine,* 366**,** 2455-2465.

BRENTJENS, R. J., DAVILA, M. L., RIVIERE, I., PARK, J., WANG, X., COWELL, L. G., BARTIDO, S., STEFANSKI, J., TAYLOR, C., OLSZEWSKA, M., BORQUEZ-OJEDA, O., QU, J., WASIELEWSKA, T., HE, Q., BERNAL, Y., RIJO, I. V., HEDVAT, C., KOBOS, R., CURRAN, K., STEINHERZ, P., JURCIC, J., ROSENBLAT, T., MASLAK, P., FRATTINI, M. & SADELAIN, M. 2013. CD19-targeted T cells rapidly induce molecular remissions in adults with chemotherapy-refractory acute lymphoblastic leukemia. *Sci Transl Med,* 5**,** 177ra38.

BRENTJENS, R. J., SANTOS, E., NIKHAMIN, Y., YEH, R., MATSUSHITA, M., LA PERLE, K., QUINTAS-CARDAMA, A., LARSON, S. M. & SADELAIN, M. 2007. Genetically targeted T cells eradicate systemic acute lymphoblastic leukemia xenografts. *Clin Cancer Res,* 13**,** 5426-35.

BRIDGEMAN, J. S., HAWKINS, R. E., BAGLEY, S., BLAYLOCK, M., HOLLAND, M. & GILHAM, D. E. 2010. The optimal antigen response of chimeric antigen receptors harboring the CD3zeta transmembrane domain is dependent upon incorporation of the receptor into the endogenous TCR/CD3 complex. *J Immunol,* 184**,** 6938-49.

BROOKS, A. J., DAI, W., O'MARA, M. L., ABANKWA, D., CHHABRA, Y., PELEKANOS, R. A., GARDON, O., TUNNY, K. A., BLUCHER, K. M., MORTON, C. J., PARKER, M. W., SIERECKI, E., GAMBIN, Y., GOMEZ, G. A., ALEXANDROV, K., WILSON, I. A., DOXASTAKIS, M., MARK, A. E. & WATERS, M. J. 2014. Mechanism of activation of protein kinase JAK2 by the growth hormone receptor. *Science,* 344**,** 1249783.

BRUDNO, J. N., LAM, N., VANASSE, D., SHEN, Y. W., ROSE, J. J., ROSSI, J., XUE, A., BOT, A., SCHOLLER, N., MIKKILINENI, L., ROSCHEWSKI, M., DEAN, R., CACHAU, R., YOUKHARIBACHE, P., PATEL, R., HANSEN, B., STRONCEK, D. F., ROSENBERG, S. A., GRESS, R. E. & KOCHENDERFER, J. N. 2020. Safety and feasibility of anti-CD19 CAR T cells with fully human binding domains in patients with B-cell lymphoma. *Nat Med,* 26**,** 270-280.

BUGGE, K., LINDORFF-LARSEN, K. & KRAGELUND, B. B. 2016. Understanding single-pass transmembrane receptor signaling from a structural viewpoint-what are we missing? *FEBS J,* 283**,** 4424-4451.

CALL, M. E., PYRDOL, J., WIEDMANN, M. & WUCHERPFENNIG, K. W. 2002. The organizing principle in the formation of the T cell receptor-CD3 complex. *Cell,* 111**,** 967-79.

CALL, M. E., SCHNELL, J. R., XU, C., LUTZ, R. A., CHOU, J. J. & WUCHERPFENNIG, K. W. 2006. The structure of the zetazeta transmembrane dimer reveals features essential for its assembly with the T cell receptor. *Cell,* 127**,** 355-68.

CALL, M. E. & WUCHERPFENNIG, K. W. 2007. Common themes in the assembly and architecture of activating immune receptors. *Nat Rev Immunol,* 7**,** 841-50.

CAMILLERI-BROET, S., HARDY-BESSARD, A. C., LE TOURNEAU, A., PARAISO, D., LEVREL, O., LEDUC, B., BAIN, S., ORFEUVRE, H., AUDOUIN, J. & PUJADE-LAURAINE, E. 2004. HER-2 overexpression is an independent marker of poor prognosis of advanced primary ovarian carcinoma: a multicenter study of the GINECO group. *Annals of Oncology,* 15**,** 104-112.

CARDOSO, F., PALUCH-SHIMON, S., SENKUS, E., CURIGLIANO, G., AAPRO, M. S., ANDRE, F., BARRIOS, C. H., BERGH, J., BHATTACHARYYA, G. S., BIGANZOLI, L., BOYLE, F., CARDOSO, M. J., CAREY, L. A., CORTES, J., EL SAGHIR, N. S., ELZAYAT, M., ENIU, A., FALLOWFIELD, L., FRANCIS, P. A., GELMON, K., GLIGOROV, J., HAIDINGER, R., HARBECK, N., HU, X., KAUFMAN, B., KAUR, R., KIELY, B. E., KIM, S. B., LIN, N. U., MERTZ, S. A., NECIOSUP, S., OFFERSEN, B. V., OHNO, S., PAGANI, O., PRAT, A., PENAULT-LLORCA, F., RUGO, H. S., SLEDGE, G. W., THOMSSEN, C., VOROBIOF, D. A., WISEMAN, T., XU, B., NORTON, L., COSTA, A. & WINER, E. P. 2020. 5th ESO-ESMO international consensus guidelines for advanced breast cancer (ABC 5). *Annals of Oncology,* 31**,** 1623-1649.

CARPENITO, C., MILONE, M. C., HASSAN, R., SIMONET, J. C., LAKHAL, M., SUHOSKI, M. M., VARELA-ROHENA, A., HAINES, K. M., HEITJAN, D. F., ALBELDA, S. M., CARROLL, R. G., RILEY, J. L., PASTAN, I. & JUNE, C. H. 2009. Control of large, established tumor xenografts with genetically retargeted human T cells containing CD28 and CD137 domains. *Proc Natl Acad Sci U S A,* 106**,** 3360-5.

CHANDLER, N. J., CALL, M. J. & CALL, M. E. 2020. T Cell Activation Machinery: Form and Function in Natural and Engineered Immune Receptors. *Int J Mol Sci,* 21.

CHANG, H. C., TAN, K., OUYANG, J., PARISINI, E., LIU, J. H., LE, Y., WANG, X., REINHERZ, E. L. & WANG, J. H. 2005. Structural and mutational analyses of a CD8alphabeta heterodimer and comparison with the CD8alphaalpha homodimer. *Immunity,* 23**,** 661-71.

CHEN, Z., KIBLER, R. D., HUNT, A., BUSCH, F., PEARL, J., JIA, M., VANAERNUM, Z. L., WICKY, B. I. M., DODS, G., LIAO, H., WILKEN, M. S., CIARLO, C., GREEN, S., EL-SAMAD, H., STAMATOYANNOPOULOS, J., WYSOCKI, V. H., JEWETT, M. C., BOYKEN, S. E. & BAKER, D. 2020. De novo design of protein logic gates. *Science,* 368**,** 78-84.

CHEREZOV, V., ROSENBAUM, D. M., HANSON, M. A., RASMUSSEN, S. G., THIAN, F. S., KOBILKA, T. S., CHOI, H. J., KUHN, P., WEIS, W. I., KOBILKA, B. K. & STEVENS, R. C. 2007. High-resolution crystal structure of an engineered human beta2-adrenergic G protein-coupled receptor. *Science,* 318**,** 1258-65.

DAVEY, A. S., CALL, M. E. & CALL, M. J. 2020. The Influence of Chimeric Antigen Receptor Structural Domains on Clinical Outcomes and Associated Toxicities. *Cancers (Basel),* 13.

DOBBINS, J., GAGNON, E., GODEC, J., PYRDOL, J., VIGNALI, D. A. A., SHARPE, A. H. & WUCHERPFENNIG, K. W. 2016. Binding of the cytoplasmic domain of CD28 to the plasma membrane inhibits Lck recruitment and signaling. *Science Signaling,* 9.

DONG, ZHENG, L., LIN, J., ZHANG, B., ZHU, Y., LI, N., XIE, S., WANG, Y., GAO, N. & HUANG, Z. 2019. Structural basis of assembly of the human T cell receptor-CD3 complex. *Nature,* 573**,** 546-552.

DONG, H. D., ZHU, G. F., TAMADA, K. & CHEN, L. P. 1999. B7-H1, a third member of the B7 family, co-stimulates T-cell proliferation and interleukin-10 secretion. *Nature Medicine,* 5**,** 1365-1369.

DOURA, A. K. & FLEMING, K. G. 2004. Complex interactions at the helix-helix interface stabilize the glycophorin A transmembrane dimer. *Journal of Molecular Biology,* 343**,** 1487-1497.

DOURA, A. K., KOBUS, F. J., DUBROVSKY, L., HIBBARD, E. & FLEMING, K. G. 2004. Sequence context modulates the stability of a GxxxG-mediated transmembrane helix-helix dimer. *Journal of Molecular Biology,* 341**,** 991-998.

ELAZAR, A., WEINSTEIN, J., BIRAN, I., FRIDMAN, Y., BIBI, E. & FLEISHMAN, S. J. 2016a. Mutational scanning reveals the determinants of protein insertion and association energetics in the plasma membrane. *Elife,* 5.

ELAZAR, A., WEINSTEIN, J. J., PRILUSKY, J. & FLEISHMAN, S. J. 2016b. Interplay between hydrophobicity and the positive-inside rule in determining membrane-protein topology. *Proceedings of the National Academy of Sciences of the United States of America,* 113**,** 10340-10345.

EMSLEY, P., LOHKAMP, B., SCOTT, W. G. & COWTAN, K. 2010. Features and development of Coot. *Acta Crystallogr D Biol Crystallogr,* 66**,** 486-501.

ESHHAR, Z., WAKS, T., GROSS, G. & SCHINDLER, D. G. 1993. Specific Activation and Targeting of Cytotoxic Lymphocytes through Chimeric Single Chains Consisting of Antibody-Binding Domains and the Gamma-Subunit or Zeta-Subunit of the Immunoglobulin and T-Cell Receptors. *Proceedings of the National Academy of Sciences of the United States of America,* 90**,** 720-724.

FENG, J. W., GARRITY, D., CALL, M. E., MOFFETT, H. & WUCHERPFENNIG, K. W. 2005. Convergence on a distinctive assembly mechanism by unrelated families of activating immune receptors. *Immunity,* 22**,** 427-438.

FEUCHT, J., SUN, J., EYQUEM, J., HO, Y. J., ZHAO, Z., LEIBOLD, J., DOBRIN, A., CABRIOLU, A., HAMIEH, M. & SADELAIN, M. 2019. Calibration of CAR activation potential directs alternative T cell fates and therapeutic potency. *Nat Med,* 25**,** 82-88.

FINNEY, H. M., LAWSON, A. D., BEBBINGTON, C. R. & WEIR, A. N. 1998. Chimeric receptors providing both primary and costimulatory signaling in T cells from a single gene product. *J Immunol,* 161**,** 2791-7.

FITZER-ATTAS, C. J., SCHINDLER, D. G., WAKS, T. & ESHHAR, Z. 1998. Harnessing Syk family tyrosine kinases as signaling domains for chimeric single chain of the variable domain receptors: Optimal design for T cell activation. *Journal of Immunology,* 160**,** 145-154.

FOWLER, D. M., STEPHANY, J. J. & FIELDS, S. 2014. Measuring the activity of protein variants on a large scale using deep mutational scanning. *Nat Protoc,* 9**,** 2267-84.

FRY, T. J., SHAH, N. N., ORENTAS, R. J., STETLER-STEVENSON, M., YUAN, C. M., RAMAKRISHNA, S., WOLTERS, P., MARTIN, S., DELBROOK, C., YATES, B., SHALABI, H., FOUNTAINE, T. J., SHERN, J. F., MAJZNER, R. G., STRONCEK, D. F., SABATINO, M., FENG, Y., DIMITROV, D. S., ZHANG, L., NGUYEN, S., QIN, H., DROPULIC, B., LEE, D. W. & MACKALL, C. L. 2018. CD22-targeted CAR T cells induce remission in B-ALL that is naive or resistant to CD19-targeted CAR immunotherapy. *Nat Med,* 24**,** 20-28.

FU, Q., FU, T. M., CRUZ, A. C., SENGUPTA, P., THOMAS, S. K., WANG, S., SIEGEL, R. M., WU, H. & CHOU, J. J. 2016. Structural Basis and Functional Role of Intramembrane Trimerization of the Fas/CD95 Death Receptor. *Mol Cell,* 61**,** 602-613.

GARRITY, D., CALL, M. E., FENG, J. W. & WUCHERPFENNIG, K. W. 2005. The activating NKG2D receptor assembles in the membrane with two signaling dimers into a hexameric structure. *Proceedings of the National Academy of Sciences of the United States of America,* 102**,** 7641-7646.

GEYER, M. B. 2019. First CAR to Pass the Road Test: Tisagenlecleucel's Drive to FDA Approval. *Clin Cancer Res,* 25**,** 1133-1135.

GHORASHIAN, S., KRAMER, A. M., ONUOHA, S., WRIGHT, G., BARTRAM, J., RICHARDSON, R., ALBON, S. J., CASANOVAS-COMPANY, J., CASTRO, F., POPOVA, B., VILLANUEVA, K., YEUNG, J., VETHAROY, W., GUVENEL, A., WAWRZYNIECKA, P. A., MEKKAOUI, L., CHEUNG, G. W., PINNER, D., CHU, J., LUCCHINI, G., SILVA, J., CIOCARLIE, O., LAZAREVA, A., INGLOTT, S., GILMOUR, K. C., AHSAN, G., FERRARI, M., MANZOOR, S., CHAMPION, K., BROOKS, T., LOPES, A., HACKSHAW, A., FARZANEH, F., CHIESA, R., RAO, K., BONNEY, D., SAMARASINGHE, S., GOULDEN, N., VORA, A., VEYS, P., HOUGH, R., WYNN, R., PULE, M. A. & AMROLIA, P. J. 2019. Enhanced CAR T cell expansion and prolonged persistence in pediatric patients with ALL treated with a low-affinity CD19 CAR. *Nat Med*.

GIL, D. & SCHRUM, A. G. 2013. Strategies to stabilize compact folding and minimize aggregation of antibody-based fragments. *Adv Biosci Biotechnol,* 4**,** 73-84.

GROSS, G., WAKS, T. & ESHHAR, Z. 1989. Expression of Immunoglobulin-T-Cell Receptor Chimeric Molecules as Functional Receptors with Antibody-Type Specificity. *Proceedings of the National Academy of Sciences of the United States of America,* 86**,** 10024-10028.

GUEDAN, S., POSEY, A. D., JR., SHAW, C., WING, A., DA, T., PATEL, P. R., MCGETTIGAN, S. E., CASADO-MEDRANO, V., KAWALEKAR, O. U., URIBE-HERRANZ, M., SONG, D., MELENHORST, J. J., LACEY, S. F., SCHOLLER, J., KEITH, B., YOUNG, R. M. & JUNE, C. H. 2018. Enhancing CAR T cell persistence through ICOS and 4-1BB costimulation. *JCI Insight,* 3.

HARADA, Y., OHGAI, D., WATANABE, R., OKANO, K., KOIWAI, O., TANABE, K., TOMA, H., ALTMAN, A. & ABE, R. 2003. A single amino acid alteration in cytoplasmic domain determines IL-2 promoter activation by ligation of CD28 but not inducible costimulator (ICOS). *J Exp Med,* 197**,** 257-62.

HARWERTH, I. M., WELS, W., MARTE, B. M. & HYNES, N. E. 1992. Monoclonal antibodies against the extracellular domain of the erbB-2 receptor function as partial ligand agonists. *J Biol Chem,* 267**,** 15160-7.

HATADA, M. H., LU, X., LAIRD, E. R., GREEN, J., MORGENSTERN, J. P., LOU, M., MARR, C. S., PHILLIPS, T. B., RAM, M. K., THERIAULT, K. & ET AL. 1995. Molecular basis for interaction of the protein tyrosine kinase ZAP-70 with the T-cell receptor. *Nature,* 377**,** 32-8.

HAYNES, N. M., SNOOK, M. B., TRAPANI, J. A., CERRUTI, L., JANE, S. M., SMYTH, M. J. & DARCY, P. K. 2001. Redirecting mouse CTL against colon carcinoma: superior signaling efficacy of single-chain variable domain chimeras containing TCR-zeta vs Fc epsilon RI-gamma. *J Immunol,* 166**,** 182-7.

HAYNES, N. M., TRAPANI, J. A., TENG, M. W., JACKSON, J. T., CERRUTI, L., JANE, S. M., KERSHAW, M. H., SMYTH, M. J. & DARCY, P. K. 2002. Single-chain antigen recognition

receptors that costimulate potent rejection of established experimental tumors. *Blood,* 100**,** 3155-63.
HAYNES, N. M., TRAPANI, J. A., TENG, M. W. L., JACKSON, J. T., CERRUTI, L., JANE, S. M., KERSHAW, M. H., SMYTH, M. J. & DARCY, P. K. 2003. Rejection of syngeneic colon carcinoma by CTLs expressing single-chain antibody receptors codelivering CD28 costimulation. (vol 169, pg 5780, 2002). *Journal of Immunology,* 170**,** 3440-3440.
HEGDE, M., JOSEPH, S. K., PASHANKAR, F., DERENZO, C., SANBER, K., NAVAI, S., BYRD, T. T., HICKS, J., XU, M. L., GERKEN, C., KALRA, M., ROBERTSON, C., ZHANG, H., SHREE, A., MEHTA, B., DAKHOVA, O., SALSMAN, V. S., GRILLEY, B., GEE, A., DOTTI, G., HESLOP, H. E., BRENNER, M. K., WELS, W. S., GOTTSCHALK, S. & AHMED, N. 2020. Tumor response and endogenous immune reactivity after administration of HER2 CAR T cells in a child with metastatic rhabdomyosarcoma. *Nat Commun,* 11**,** 3549.
HENNECKE, S. & COSSON, P. 1993. Role of Transmembrane Domains in Assembly and Intracellular-Transport of the Cd8 Molecule. *Journal of Biological Chemistry,* 268**,** 26607-26612.
HESSA, T., KIM, H., BIHLMAIER, K., LUNDIN, C., BOEKEL, J., ANDERSSON, H., NILSSON, I., WHITE, S. H. & VON HEIJNE, G. 2005. Recognition of transmembrane helices by the endoplasmic reticulum translocon. *Nature,* 433**,** 377-81.
HODI, F. S., O'DAY, S. J., MCDERMOTT, D. F., WEBER, R. W., SOSMAN, J. A., HAANEN, J. B., GONZALEZ, R., ROBERT, C., SCHADENDORF, D., HASSEL, J. C., AKERLEY, W., VAN DEN EERTWEGH, A. J. M., LUTZKY, J., LORIGAN, P., VAUBEL, J. M., LINETTE, G. P., HOGG, D., OTTENSMEIER, C. H., LEBBE, C., PESCHEL, C., QUIRT, I., CLARK, J. I., WOLCHOK, J. D., WEBER, J. S., TIAN, J., YELLIN, M. J., NICHOL, G. M., HOOS, A. & URBA, W. J. 2010. Improved Survival with Ipilimumab in Patients with Metastatic Melanoma. *New England Journal of Medicine,* 363**,** 711-723.
HOFER, N., ARAGAO, D. & CAFFREY, M. 2010. Crystallizing transmembrane peptides in lipidic mesophases. *Biophys J,* 99**,** L23-5.
HOLDORF, A. D., GREEN, J. M., LEVIN, S. D., DENNY, M. F., STRAUS, D. B., LINK, V., CHANGELIAN, P. S., ALLEN, P. M. & SHAW, A. S. 1999. Proline residues in CD28 and the Src homology (SH)3 domain of Lck are required for T cell costimulation. *J Exp Med,* 190**,** 375-84.
HOMBACH, A. A., HEIDERS, J., FOPPE, M., CHMIELEWSKI, M. & ABKEN, H. 2012. OX40 costimulation by a chimeric antigen receptor abrogates CD28 and IL-2 induced IL-10 secretion by redirected CD4(+) T cells. *Oncoimmunology,* 1**,** 458-466.
HUANG, J., BRAMESHUBER, M., ZENG, X., XIE, J., LI, Q. J., CHIEN, Y. H., VALITUTTI, S. & DAVIS, M. M. 2013. A single peptide-major histocompatibility complex ligand triggers digital cytokine secretion in CD4(+) T cells. *Immunity,* 39**,** 846-57.
HUANG, P. S., BOYKEN, S. E. & BAKER, D. 2016. The coming of age of de novo protein design. *Nature,* 537**,** 320-327.
HUSSAIN, M. H., MACVICAR, G. R., PETRYLAK, D. P., DUNN, R. L., VAISHAMPAYAN, U., LARA, P. N., JR., CHATTA, G. S., NANUS, D. M., GLODE, L. M., TRUMP, D. L., CHEN, H., SMITH, D. C. & NATIONAL CANCER, I. 2007. Trastuzumab, paclitaxel, carboplatin, and gemcitabine in advanced human epidermal growth factor receptor-2/neu-positive urothelial carcinoma: results of a multicenter phase II National Cancer Institute trial. *J Clin Oncol,* 25**,** 2218-24.
IQBAL, N. & IQBAL, N. 2014. Human Epidermal Growth Factor Receptor 2 (HER2) in Cancers: Overexpression and Therapeutic Implications. *Mol Biol Int,* 2014**,** 852748.

IRVINE, D. J., PURBHOO, M. A., KROGSGAARD, M. & DAVIS, M. M. 2002. Direct observation of ligand recognition by T cells. *Nature,* 419**,** 845-9.
IRVING, B. A. & WEISS, A. 1991. The Cytoplasmic Domain of the T-Cell Receptor Zeta-Chain Is Sufficient to Couple to Receptor-Associated Signal Transduction Pathways. *Cell,* 64**,** 891-901.
ISHIDA, Y., AGATA, Y., SHIBAHARA, K. & HONJO, T. 1992. Induced Expression of Pd-1, a Novel Member of the Immunoglobulin Gene Superfamily, Upon Programmed Cell-Death. *Embo Journal,* 11**,** 3887-3895.
JAMES, J. R. 2018. Tuning ITAM multiplicity on T cell receptors can control potency and selectivity to ligand density. *Sci Signal,* 11.
JOH, N. H., WANG, T., BHATE, M. P., ACHARYA, R., WU, Y., GRABE, M., HONG, M., GRIGORYAN, G. & DEGRADO, W. F. 2014. De novo design of a transmembrane Zn(2)(+)-transporting four-helix bundle. *Science,* 346**,** 1520-4.
JUNE, C. H., O'CONNOR, R. S., KAWALEKAR, O. U., GHASSEMI, S. & MILONE, M. C. 2018. CAR T cell immunotherapy for human cancer. *Science,* 359**,** 1361-1365.
KABSCH, W. 2010. Xds. *Acta Crystallogr D Biol Crystallogr,* 66**,** 125-32.
KARATHANASIS, C., MEDLER, J., FRICKE, F., SMITH, S., MALKUSCH, S., WIDERA, D., FULDA, S., WAJANT, H., VAN WIJK, S. J. L., DIKIC, I. & HEILEMANN, M. 2020. Single-molecule imaging reveals the oligomeric state of functional TNF alpha-induced plasma membrane TNFR1 clusters in cells. *Science Signaling,* 13.
KHOURY, G. A., SMADBECK, J., KIESLICH, C. A. & FLOUDAS, C. A. 2014. Protein folding and de novo protein design for biotechnological applications. *Trends in Biotechnology,* 32**,** 99-109.
KNOBLICH, K., PARK, S., LUTFI, M., VAN 'T HAG, L., CONN, C. E., SEABROOK, S. A., NEWMAN, J., CZABOTAR, P. E., IM, W., CALL, M. E. & CALL, M. J. 2015. Transmembrane Complexes of DAP12 Crystallized in Lipid Membranes Provide Insights into Control of Oligomerization in Immunoreceptor Assembly. *Cell Reports,* 11**,** 1184-1192.
LABANIEH, L., MAJZNER, R. G. & MACKALL, C. L. 2018. Programming CAR-T cells to kill cancer. *Nature Biomedical Engineering,* 2**,** 377-391.
LANDAU, E. M. & ROSENBUSCH, J. P. 1996. Lipidic cubic phases: a novel concept for the crystallization of membrane proteins. *Proc Natl Acad Sci U S A,* 93**,** 14532-5.
LANGER, C. J., STEPHENSON, P., THOR, A., VANGEL, M., JOHNSON, D. H. & EASTERN COOPERATIVE ONCOLOGY GROUP, S. 2004. Trastuzumab in the treatment of advanced non-small-cell lung cancer: is there a role? Focus on Eastern Cooperative Oncology Group study 2598. *J Clin Oncol,* 22**,** 1180-7.
LANGOSCH, D., BROSIG, B., KOLMAR, H. & FRITZ, H. J. 1996. Dimerisation of the glycophorin A transmembrane segment in membranes probed with the ToxR transcription activator. *J Mol Biol,* 263**,** 525-30.
LEDDON, S. A., FETTIS, M. M., ABRAMO, K., KELLY, R., OLEKSYN, D. & MILLER, J. 2020. The CD28 Transmembrane Domain Contains an Essential Dimerization Motif. *Front Immunol,* 11**,** 1519.
LEE, M. S., GLASSMAN, C. R., DESHPANDE, N. R., BADGANDI, H. B., PARRISH, H. L., UTTAMAPINANT, C., STAWSKI, P. S., TING, A. Y. & KUHNS, M. S. 2015. A Mechanical Switch Couples T Cell Receptor Triggering to the Cytoplasmic Juxtamembrane Regions of CD3zetazeta. *Immunity,* 43**,** 227-39.
LEMMON, M. A., FLANAGAN, J. M., HUNT, J. F., ADAIR, B. D., BORMANN, B. J., DEMPSEY, C. E. & ENGELMAN, D. M. 1992. Glycophorin-a Dimerization Is Driven by Specific

Interactions between Transmembrane Alpha-Helices. *Journal of Biological Chemistry,* 267**,** 7683-7689.
LI, E. & HRISTOVA, K. 2006. Role of receptor tyrosine kinase transmembrane domains in cell signaling and human pathologies. *Biochemistry,* 45**,** 6241-6251.
LI, W. T., QIU, S. Z., CHEN, J., JIANG, S. T., CHEN, W. D., JIANG, J. W., WANG, F., SI, W., SHU, Y. L., WEI, P., FAN, G. F., TIAN, R. J., WU, H. T., XU, C. Q. & WANG, H. P. 2020. Chimeric Antigen Receptor Designed to Prevent Ubiquitination and Downregulation Showed Durable Antitumor Efficacy. *Immunity,* 53**,** 456-+.
LIM, W. A. & JUNE, C. H. 2017. The Principles of Engineering Immune Cells to Treat Cancer. *Cell,* 168**,** 724-740.
LIS, M. & BLUMENTHAL, K. 2006. A modified, dual reporter TOXCAT system for monitoring homodimerization of transmembrane segments of proteins. *Biochem Biophys Res Commun,* 339**,** 321-4.
LIU, L. X., SHAO, X. Y., GAO, W., BAI, J. L., WANG, R. S., HUANG, P. W., YIN, Y. M., LIU, P. & SHU, Y. Q. 2010. The Role of Human Epidermal Growth Factor Receptor 2 as a Prognostic Factor in Lung Cancer A Meta-Analysis of Published Data. *Journal of Thoracic Oncology,* 5**,** 1922-1932.
LIU, X., JIANG, S., FANG, C., YANG, S., OLALERE, D., PEQUIGNOT, E. C., COGDILL, A. P., LI, N., RAMONES, M., GRANDA, B., ZHOU, L., LOEW, A., YOUNG, R. M., JUNE, C. H. & ZHAO, Y. 2015. Affinity-Tuned ErbB2 or EGFR Chimeric Antigen Receptor T Cells Exhibit an Increased Therapeutic Index against Tumors in Mice. *Cancer Res,* 75**,** 3596-607.
LIU, X., ZHANG, N. & SHI, H. 2017. Driving better and safer HER2-specific CARs for cancer therapy. *Oncotarget,* 8**,** 62730-62741.
LONG, A. H., HASO, W. M., SHERN, J. F., WANHAINEN, K. M., MURGAI, M., INGARAMO, M., SMITH, J. P., WALKER, A. J., KOHLER, M. E., VENKATESHWARA, V. R., KAPLAN, R. N., PATTERSON, G. H., FRY, T. J., ORENTAS, R. J. & MACKALL, C. L. 2015. 4-1BB costimulation ameliorates T cell exhaustion induced by tonic signaling of chimeric antigen receptors. *Nature Medicine,* 21**,** 581-590.
LU, P., MIN, D., DIMAIO, F., WEI, K. Y., VAHEY, M. D., BOYKEN, S. E., CHEN, Z., FALLAS, J. A., UEDA, G., SHEFFLER, W., MULLIGAN, V. K., XU, W., BOWIE, J. U. & BAKER, D. 2018. Accurate computational design of multipass transmembrane proteins. *Science,* 359**,** 1042-1046.
MACKENZIE, K. R., PRESTEGARD, J. H. & ENGELMAN, D. M. 1997. A transmembrane helix dimer: Structure and implications. *Science,* 276**,** 131-133.
MAHER, J., BRENTJENS, R. J., GUNSET, G., RIVIERE, I. & SADELAIN, M. 2002. Human T-lymphocyte cytotoxicity and proliferation directed by a single chimeric TCRzeta /CD28 receptor. *Nat Biotechnol,* 20**,** 70-5.
MAJZNER, R. G. & MACKALL, C. L. 2019. Clinical lessons learned from the first leg of the CAR T cell journey. *Nat Med,* 25**,** 1341-1355.
MAJZNER, R. G., RIETBERG, S. P., SOTILLO, E., DONG, R., VACHHARAJANI, V. T., LABANIEH, L., MYKLEBUST, J. H., KADAPAKKAM, M., WEBER, E. W., TOUSLEY, A. M., RICHARDS, R. M., HEITZENEDER, S., NGUYEN, S. M., WIEBKING, V., THERUVATH, J., LYNN, R. C., XU, P., DUNN, A. R., VALE, R. D. & MACKALL, C. L. 2020. Tuning the Antigen Density Requirement for CAR T Cell Activity. *Cancer Discov*.
MALDINI, C. R., CLAIBORNE, D. T., OKAWA, K., CHEN, T., DOPKIN, D. L., SHAN, X., POWER, K. A., TRIFONOVA, R. T., KRUPP, K., PHELPS, M., VRBANAC, V. D., TANNO, S., BATESON, T., LESLIE, G. J., HOXIE, J. A., BOUTWELL, C. L., RILEY, J. L. & ALLEN, T. M. 2020. Dual

CD4-based CAR T cells with distinct costimulatory domains mitigate HIV pathogenesis in vivo. *Nature Medicine*.

MATSUI, K., BONIFACE, J. J., REAY, P. A., SCHILD, H., FAZEKAS DE ST GROTH, B. & DAVIS, M. M. 1991. Low Affinity Interaction of Peptide-Mhc Complexes with T-Cell Receptors. *Science,* 254**,** 1788-1791.

MAUDE, S. L., FREY, N., SHAW, P. A., APLENC, R., BARRETT, D. M., BUNIN, N. J., CHEW, A., GONZALEZ, V. E., ZHENG, Z., LACEY, S. F., MAHNKE, Y. D., MELENHORST, J. J., RHEINGOLD, S. R., SHEN, A., TEACHEY, D. T., LEVINE, B. L., JUNE, C. H., PORTER, D. L. & GRUPP, S. A. 2014. Chimeric antigen receptor T cells for sustained remissions in leukemia. *N Engl J Med,* 371**,** 1507-17.

MAUDE, S. L., TEACHEY, D. T., PORTER, D. L. & GRUPP, S. A. 2015. CD19-targeted chimeric antigen receptor T-cell therapy for acute lymphoblastic leukemia. *Blood,* 125**,** 4017-23.

MAUS, M. V., PLOTKIN, J., JAKKA, G., STEWART-JONES, G., RIVIERE, I., MERGHOUB, T., WOLCHOK, J., RENNER, C. & SADELAIN, M. 2016. An MHC-restricted antibody-based chimeric antigen receptor requires TCR-like affinity to maintain antigen specificity. *Molecular Therapy-Oncolytics,* 3.

MCCOY, A. J., GROSSE-KUNSTLEVE, R. W., ADAMS, P. D., WINN, M. D., STORONI, L. C. & READ, R. J. 2007. Phaser crystallographic software. *J Appl Crystallogr,* 40**,** 658-674.

MERRY, A. H., GILBERT, R. J. C., SHORE, D. A., ROYLE, L., MIROSHNYCHENKO, O., VUONG, M., WORMALD, M. R., HARVEY, D. J., DWEK, R. A., CLASSON, B. J., RUDD, P. M. & DAVIS, S. J. 2003. O-glycan sialylation and the structure of the stalk-like region of the T cell co-receptor CD8. *Journal of Biological Chemistry,* 278**,** 27119-27128.

MIOZZARI, G. F. & YANOFSKY, C. 1978. Translation of Leader Region of Escherichia-Coli Tryptophan Operon. *Journal of Bacteriology,* 133**,** 1457-1466.

MOASSER, M. M. 2007. The oncogene HER2: its signaling and transforming functions and its role in human cancer pathogenesis. *Oncogene,* 26**,** 6469-6487.

MOELLER, M., HAYNES, N. M., KERSHAW, M. H., JACKSON, J. T., TENG, M. W. L., STREET, S. E., CERUTTI, L., JANE, S. M., TRAPANI, J. A., SMYTH, M. J. & DARCY, P. K. 2005. Adoptive transfer of gene-engineered CD4(+) helper T cells induces potent primary and secondary tumor rejection. *Blood,* 106**,** 2995-3003.

MOELLER, M., HAYNES, N. M., TRAPANI, J. A., TENG, M. W., JACKSON, J. T., TANNER, J. E., CERUTTI, L., JANE, S. M., KERSHAW, M. H., SMYTH, M. J. & DARCY, P. K. 2004. A functional role for CD28 costimulation in tumor recognition by single-chain receptor-modified T cells. *Cancer Gene Ther,* 11**,** 371-9.

MOODY, A. M., CHUI, D., RECHE, P. A., PRIATEL, J. J., MARTH, J. D. & REINHERZ, E. L. 2001. Developmentally regulated glycosylation of the CD8 alpha beta coreceptor stalk modulates ligand binding. *Cell,* 107**,** 501-512.

MORGAN, R. A., YANG, J. C., KITANO, M., DUDLEY, M. E., LAURENCOT, C. M. & ROSENBERG, S. A. 2010. Case report of a serious adverse event following the administration of T cells transduced with a chimeric antigen receptor recognizing ERBB2. *Mol Ther,* 18**,** 843-51.

MORITZ, D. & GRONER, B. 1995. A Spacer Region between the Single-Chain Antibody-Chain and the Cd3 Zeta-Chain Domain of Chimeric T-Cell Receptor Components Is Required for Efficient Ligand-Binding and Signaling Activity. *Gene Therapy,* 2**,** 539-546.

MRAVIC, M., THOMASTON, J. L., TUCKER, M., SOLOMON, P. E., LIU, L. J. & DEGRADO, W. F. 2019. Packing of apolar side chains enables accurate design of highly stable membrane proteins. *Science,* 363**,** 1418-+.

MUELLER, B. K., SUBRAMANIAM, S. & SENES, A. 2014. A frequent, GxxxG-mediated, transmembrane association motif is optimized for the formation of interhelical C alpha-H hydrogen bonds. *Proceedings of the National Academy of Sciences of the United States of America,* 111**,** E888-E895.

MULLER, Y. D., NGUYEN, D. P., FERREIRA, L. M. R., HO, P., RAFFIN, C., VALENCIA, R. V. B., CONGRAVE-WILSON, Z., ROTH, T. L., EYQUEM, J., VAN GOOL, F., MARSON, A., PEREZ, L., WELLS, J. A., BLUESTONE, J. A. & TANG, Q. 2021. The CD28-Transmembrane Domain Mediates Chimeric Antigen Receptor Heterodimerization With CD28. *Front Immunol,* 12**,** 639818.

NAKAMURA, H., KAWASAKI, N., TAGUCHI, M. & KABASAWA, K. 2005. Association of HER-2 overexpression with prognosis in nonsmall cell lung carcinoma: a metaanalysis. *Cancer,* 103**,** 1865-73.

NEELAPU, S. S., TUMMALA, S., KEBRIAEI, P., WIERDA, W., GUTIERREZ, C., LOCKE, F. L., KOMANDURI, K. V., LIN, Y., JAIN, N., DAVER, N., WESTIN, J., GULBIS, A. M., LOGHIN, M. E., DE GROOT, J. F., ADKINS, S., DAVIS, S. E., REZVANI, K., HWU, P. & SHPALL, E. J. 2018. Chimeric antigen receptor T-cell therapy - assessment and management of toxicities. *Nature Reviews Clinical Oncology,* 15**,** 47-62.

NOLAN, R., ILIOPOULOU, M., ALVAREZ, L. & PADILLA-PARRA, S. 2018. Detecting protein aggregation and interaction in live cells: A guide to number and brightness. *Methods,* 140**,** 172-177.

OLEJNICZAK, S. H., STEWART, C. C., DONOHUE, K. & CZUCZMAN, M. S. 2006. A quantitative exploration of surface antigen expression in common B-cell malignancies using flow cytometry. *Immunological Investigations,* 35**,** 93-114.

OREN, R., HOD-MARCO, M., HAUS-COHEN, M., THOMAS, S., BLAT, D., DUVSHANI, N., DENKBERG, G., ELBAZ, Y., BENCHETRIT, F., ESHHAR, Z., STAUSS, H. & REITER, Y. 2014. Functional Comparison of Engineered T Cells Carrying a Native TCR versus TCR-like Antibody-Based Chimeric Antigen Receptors Indicates Affinity/Avidity Thresholds. *Journal of Immunology,* 193**,** 5733-5743.

ORLANDI, R., GUSSOW, D. H., JONES, P. T. & WINTER, G. 1989. Cloning Immunoglobulin Variable Domains for Expression by the Polymerase Chain-Reaction. *Proceedings of the National Academy of Sciences of the United States of America,* 86**,** 3833-3837.

OTWINOWSKI, Z. & MINOR, W. 1997. Processing of X-ray diffraction data collected in oscillation mode. *Macromolecular Crystallography, Pt A,* 276**,** 307-326.

PAGES, F., RAGUENEAU, M., ROTTAPEL, R., TRUNEH, A., NUNES, J., IMBERT, J. & OLIVE, D. 1994. Binding of phosphatidylinositol-3-OH kinase to CD28 is required for T-cell signalling. *Nature,* 369**,** 327-9.

PAN, L., FU, T. M., ZHAO, W., ZHAO, L., CHEN, W., QIU, C., LIU, W., LIU, Z., PIAI, A., FU, Q., CHEN, S., WU, H. & CHOU, J. J. 2019. Higher-Order Clustering of the Transmembrane Anchor of DR5 Drives Signaling. *Cell,* 176**,** 1477-1489 e14.

PETERSEN, F. N., JENSEN, M. O. & NIELSEN, C. H. 2005. Interfacial tryptophan residues: a role for the cation-pi effect? *Biophys J,* 89**,** 3985-96.

PORTER, D. L., HWANG, W. T., FREY, N. V., LACEY, S. F., SHAW, P. A., LOREN, A. W., BAGG, A., MARCUCCI, K. T., SHEN, A., GONZALEZ, V., AMBROSE, D., GRUPP, S. A., CHEW, A., ZHENG, Z., MILONE, M. C., LEVINE, B. L., MELENHORST, J. J. & JUNE, C. H. 2015.

Chimeric antigen receptor T cells persist and induce sustained remissions in relapsed refractory chronic lymphocytic leukemia. *Sci Transl Med,* 7**,** 303ra139.
PULE, M. A., STRAATHOF, K. C., DOTTI, G., HESLOP, H. E., ROONEY, C. M. & BRENNER, M. K. 2005. A chimeric T cell antigen receptor that augments cytokine release and supports clonal expansion of primary human T cells. *Molecular Therapy,* 12**,** 933-941.
PURBHOO, M. A., IRVINE, D. J., HUPPA, J. B. & DAVIS, M. M. 2004. T cell killing does not require the formation of a stable mature immunological synapse. *Nat Immunol,* 5**,** 524-30.
RAAB, M., CAI, Y. C., BUNNELL, S. C., HEYECK, S. D., BERG, L. J. & RUDD, C. E. 1995. p56Lck and p59Fyn regulate CD28 binding to phosphatidylinositol 3-kinase, growth factor receptor-bound protein GRB-2, and T cell-specific protein-tyrosine kinase ITK: implications for T-cell costimulation. *Proc Natl Acad Sci U S A,* 92**,** 8891-5.
RAFIQ, S., PURDON, T. J., DANIYAN, A. F., KONERU, M., DAO, T., LIU, C., SCHEINBERG, D. A. & BRENTJENS, R. J. 2017. Optimized T-cell receptor-mimic chimeric antigen receptor T cells directed toward the intracellular Wilms Tumor 1 antigen. *Leukemia,* 31**,** 1788-1797.
RAMMENSEE, H. G., FALK, K. & ROTZSCHKE, O. 1993. Peptides naturally presented by MHC class I molecules. *Annu Rev Immunol,* 11**,** 213-44.
ROSENBERG, S. A., PACKARD, B. S., AEBERSOLD, P. M., SOLOMON, D., TOPALIAN, S. L., TOY, S. T., SIMON, P., LOTZE, M. T., YANG, J. C., SEIPP, C. A., SIMPSON, C., CARTER, C., BOCK, S., SCHWARTZENTRUBER, D., WEI, J. P. & WHITE, D. E. 1988. Use of Tumor-Infiltrating Lymphocytes and Interleukin-2 in the Immunotherapy of Patients with Metastatic Melanoma - a Preliminary-Report. *New England Journal of Medicine,* 319**,** 1676-1680.
ROSENBERG, S. A., YANNELLI, J. R., YANG, J. C., TOPALIAN, S. L., SCHWARTZENTRUBER, D. J., WEBER, J. S., PARKINSON, D. R., SEIPP, C. A., EINHORN, J. N. & WHITE, D. E. 1994. Treatment of Patients with Metastatic Melanoma with Autologous Tumor-Infiltrating Lymphocytes and Interleukin-2. *Journal of the National Cancer Institute,* 86**,** 1159-1166.
ROYBAL, K. T. & LIM, W. A. 2017. Synthetic Immunology: Hacking Immune Cells to Expand Their Therapeutic Capabilities. *Annual Review of Immunology, Vol 35,* 35**,** 229-253.
RUSS, W. P. & ENGELMAN, D. M. 1999. TOXCAT: a measure of transmembrane helix association in a biological membrane. *Proc Natl Acad Sci U S A,* 96**,** 863-8.
SALZER, B., SCHUELLER, C. M., ZAJC, C. U., PETERS, T., SCHOEBER, M. A., KOVACIC, B., BURI, M. C., LOBNER, E., DUSHEK, O., HUPPA, J. B., OBINGER, C., PUTZ, E. M., HOLTER, W., TRAXLMAYR, M. W. & LEHNER, M. 2020. Engineering AvidCARs for combinatorial antigen recognition and reversible control of CAR function. *Nat Commun,* 11**,** 4166.
SANCHEZ-LOCKHART, M., KIM, M. & MILLER, J. 2011. Cutting edge: A role for inside-out signaling in TCR regulation of CD28 ligand binding. *J Immunol,* 187**,** 5515-9.
SANCHEZ-LOCKHART, M., ROJAS, A. V., FETTIS, M. M., BAUSERMAN, R., HIGA, T. R., MIAO, H., WAUGH, R. E. & MILLER, J. 2014. T cell receptor signaling can directly enhance the avidity of CD28 ligand binding. *PLoS One,* 9**,** e89263.
SAVOLDO, B., RAMOS, C. A., LIU, E., MIMS, M. P., KEATING, M. J., CARRUM, G., KAMBLE, R. T., BOLLARD, C. M., GEE, A. P., MEI, Z., LIU, H., GRILLEY, B., ROONEY, C. M., HESLOP, H. E., BRENNER, M. K. & DOTTI, G. 2011a. CD28 costimulation improves expansion and persistence of chimeric antigen receptor-modified T cells in lymphoma patients. *J Clin Invest,* 121**,** 1822-6.

SAVOLDO, B., RAMOS, C. A., LIU, E. L., MIMS, M. P., KEATING, M. J., CARRUM, G., KAMBLE, R. T., BOLLARD, C. M., GEE, A. P., MEI, Z. Y., LIU, H., GRILLEY, B., ROONEY, C. M., HESLOP, H. E., BRENNER, M. K. & DOTTI, G. 2011b. CD28 costimulation improves expansion and persistence of chimeric antigen receptor-modified T cells in lymphoma patients. *Journal of Clinical Investigation,* 121**,** 1822-1826.

SCHRAMM, C. A., HANNIGAN, B. T., DONALD, J. E., KEASAR, C., SAVEN, J. G., DEGRADO, W. F. & SAMISH, I. 2012. Knowledge-based potential for positioning membrane-associated structures and assessing residue-specific energetic contributions. *Structure,* 20**,** 924-35.

SENES, A., CHADI, D. C., LAW, P. B., WALTERS, R. F., NANDA, V. & DEGRADO, W. F. 2007. E(z), a depth-dependent potential for assessing the energies of insertion of amino acid side-chains into membranes: derivation and applications to determining the orientation of transmembrane and interfacial helices. *J Mol Biol,* 366**,** 436-48.

SHARMA, P., KAYWAN-LUTFI, M., KRSHNAN, L., BYRNE, E. F. X., CALL, M. J. & CALL, M. E. 2013. Production of Disulfide-stabilized Transmembrane Peptide Complexes for Structural Studies. *Jove-Journal of Visualized Experiments*.

SLAMON, D. J., CLARK, G. M., WONG, S. G., LEVIN, W. J., ULLRICH, A. & MCGUIRE, W. L. 1987. Human-Breast Cancer - Correlation of Relapse and Survival with Amplification of the Her-2 Neu Oncogene. *Science,* 235**,** 177-182.

SLANEY, C. Y., VON SCHEIDT, B., DAVENPORT, A. J., BEAVIS, P. A., WESTWOOD, J. A., MARDIANA, S., TSCHARKE, D. C., ELLIS, S., PRINCE, H. M., TRAPANI, J. A., JOHNSTONE, R. W., SMYTH, M. J., TENG, M. W., ALI, A., YU, Z., ROSENBERG, S. A., RESTIFO, N. P., NEESON, P., DARCY, P. K. & KERSHAW, M. H. 2017. Dual-specific Chimeric Antigen Receptor T Cells and an Indirect Vaccine Eradicate a Variety of Large Solid Tumors in an Immunocompetent, Self-antigen Setting. *Clin Cancer Res,* 23**,** 2478-2490.

STANCOVSKI, I., SCHINDLER, D. G., WAKS, T., YARDEN, Y., SELA, M. & ESHHAR, Z. 1993. Targeting of T-Lymphocytes to Neu/Her2-Expressing Cells Using Chimeric Single-Chain Fv Receptors. *Journal of Immunology,* 151**,** 6577-6582.

SUN, C., SHOU, P., DU, H., HIRABAYASHI, K., CHEN, Y., HERRING, L. E., AHN, S., XU, Y., SUZUKI, K., LI, G., TSAHOURIDIS, O., SU, L., SAVOLDO, B. & DOTTI, G. 2020. THEMIS-SHP1 Recruitment by 4-1BB Tunes LCK-Mediated Priming of Chimeric Antigen Receptor-Redirected T Cells. *Cancer Cell,* 37**,** 216-225 e6.

SUSA, K. J., RAWSON, S., KRUSE, A. C. & BLACKLOW, S. C. 2021. Cryo-EM structure of the B cell co-receptor CD19 bound to the tetraspanin CD81. *Science,* 371**,** 300-305.

TEESE, M. G. & LANGOSCH, D. 2015. Role of GxxxG Motifs in Transmembrane Domain Interactions. *Biochemistry,* 54**,** 5125-35.

THOMPSON, C. B., LINDSTEN, T., LEDBETTER, J. A., KUNKEL, S. L., YOUNG, H. A., EMERSON, S. G., LEIDEN, J. M. & JUNE, C. H. 1989. CD28 activation pathway regulates the production of multiple T-cell-derived lymphokines/cytokines. *Proc Natl Acad Sci U S A,* 86**,** 1333-7.

TRENKER, R., CALL, M. E. & CALL, M. J. 2015. Crystal Structure of the Glycophorin A Transmembrane Dimer in Lipidic Cubic Phase. *Journal of the American Chemical Society,* 137**,** 15676-15679.

TRENKER, R., CALL, M. J. & CALL, M. E. 2016. Progress and prospects for structural studies of transmembrane interactions in single-spanning receptors. *Current Opinion in Structural Biology,* 39**,** 115-123.

ULMSCHNEIDER, M. B., SANSOM, M. S. & DI NOLA, A. 2005. Properties of integral membrane protein structures: derivation of an implicit membrane potential. *Proteins,* 59**,** 252-65.

VALLINA, L. & HAWKINS, R. E. 1996. Antigen-specific targeting of CD28-mediated T cell co-stimulation using chimeric single-chain antibody variable fragment-CD28 receptors. *European Journal of Immunology,* 26**,** 2304-2309.

VANAMEE, E. S. & FAUSTMAN, D. L. 2018. Structural principles of tumor necrosis factor superfamily signaling. *Science Signaling,* 11.

VON SCHEIDT, B., WANG, M. Y., OLIVER, A. J., CHAN, J. D., JANA, M. K., ALI, A. I., CLOW, F., FRASER, J. D., QUINN, K. M., DARCY, P. K., KERSHAW, M. H. & SLANEY, C. Y. 2019. Enterotoxins can support CAR T cells against solid tumors. *Proceedings of the National Academy of Sciences of the United States of America,* 116**,** 25229-25235.

WALKER, A. J., MAJZNER, R. G., ZHANG, L., WANHAINEN, K., LONG, A. H., NGUYEN, S. M., LOPOMO, P., VIGNY, M., FRY, T. J., ORENTAS, R. J. & MACKALL, C. L. 2017. Tumor Antigen and Receptor Densities Regulate Efficacy of a Chimeric Antigen Receptor Targeting Anaplastic Lymphoma Kinase. *Mol Ther,* 25**,** 2189-2201.

WANG, L. X., WESTWOOD, J. A., MOELLER, M., DUONG, C. P., WEI, W. Z., MALATERRE, J., TRAPANI, J. A., NEESON, P., SMYTH, M. J., KERSHAW, M. H. & DARCY, P. K. 2010. Tumor ablation by gene-modified T cells in the absence of autoimmunity. *Cancer Res,* 70**,** 9591-8.

WATANABE, R., HARADA, Y., TAKEDA, K., TAKAHASHI, J., OHNUKI, K., OGAWA, S., OHGAI, D., KAIBARA, N., KOIWAI, O., TANABE, K., TOMA, H., SUGAMURA, K. & ABE, R. 2006. Grb2 and Gads exhibit different interactions with CD28 and play distinct roles in CD28-mediated costimulation. *J Immunol,* 177**,** 1085-91.

WEBER, S., TRAUNECKER, A., OLIVERI, F., GERHARD, W. & KARJALAINEN, K. 1992. Specific Low-Affinity Recognition of Major Histocompatibility Complex Plus Peptide by Soluble T-Cell Receptor. *Nature,* 356**,** 793-796.

WEINSTEIN, J. Y., ELAZAR, A. & FLEISHMAN, S. J. 2019. A lipophilicity-based energy function for membrane-protein modelling and design. *PLoS Comput Biol,* 15**,** e1007318.

WHITE, J., O'BRIEN, R. L. & BORN, W. K. 2020. BW5147 and Derivatives for the Study of T Cells and their Antigen Receptors. *Archivum Immunologiae Et Therapiae Experimentalis,* 68.

WILLEMSEN, R. A., DEBETS, R., HART, E., HOOGENBOOM, H. R., BOLHUIS, R. L. & CHAMES, P. 2001. A phage display selected fab fragment with MHC class I-restricted specificity for MAGE-A1 allows for retargeting of primary human T lymphocytes. *Gene Ther,* 8**,** 1601-8.

WINN, M. D., BALLARD, C. C., COWTAN, K. D., DODSON, E. J., EMSLEY, P., EVANS, P. R., KEEGAN, R. M., KRISSINEL, E. B., LESLIE, A. G. W., MCCOY, A., MCNICHOLAS, S. J., MURSHUDOV, G. N., PANNU, N. S., POTTERTON, E. A., POWELL, H. R., READ, R. J., VAGIN, A. & WILSON, K. S. 2011. Overview of the CCP4 suite and current developments. *Acta Crystallographica Section D-Structural Biology,* 67**,** 235-242.

WOLFE, M. S. 2019. Structure and Function of the gamma-Secretase Complex. *Biochemistry,* 58**,** 2953-2966.

YANNICK. D. MULLER, D. P. N., LEONARDO M.R. FERREIRA, PATRICK HO, CAROLINE RAFFIN, ROXXANA BELTRAN VALENCIA, ZION CONGRAVE-WILSON, THEODORE ROTH, JUSTIN EYQUEM, FREDERIC VAN GOOL, ALEXANDER MARSON, JAMES A. WELLS, JEFFREY A.

BLUESTONE, QIZHI TANG 2020. The CD28-transmembrane domain mediates chimeric antigen receptor
heterodimerization with CD28. *Biorxiv*.
YING, Z., HUANG, X. F., XIANG, X., LIU, Y., KANG, X., SONG, Y., GUO, X., LIU, H., DING, N., ZHANG, T., DUAN, P., LIN, Y., ZHENG, W., WANG, X., LIN, N., TU, M., XIE, Y., ZHANG, C., LIU, W., DENG, L., GAO, S., PING, L., WANG, X., ZHOU, N., ZHANG, J., WANG, Y., LIN, S., MAMUTI, M., YU, X., FANG, L., WANG, S., SONG, H., WANG, G., JONES, L., ZHU, J. & CHEN, S. Y. 2019. A safe and potent anti-CD19 CAR T cell therapy. *Nat Med,* 25**,** 947-953.
YOON, H. H., SHI, Q., SUKOV, W. R., WIKTOR, A. E., KHAN, M., SATTLER, C. A., GROTHEY, A., WU, T. T., DIASIO, R. B., JENKINS, R. B. & SINICROPE, F. A. 2012. Association of HER2/ErbB2 Expression and Gene Amplification with Pathologic Features and Prognosis in Esophageal Adenocarcinomas. *Clinical Cancer Research,* 18**,** 546-554.
ZHANG, G., WANG, L., CUI, H. L., WANG, X. M., ZHANG, G. L., MA, J., HAN, H. M., HE, W., WANG, W., ZHAO, Y. F., LIU, C. Z., SUN, M. Y. & GAO, B. 2014. Anti-melanoma activity of T cells redirected with a TCR-like chimeric antigen receptor. *Scientific Reports,* 4.
ZHANG, H., CORDOBA, S. P., DUSHEK, O. & VAN DER MERWE, P. A. 2011. Basic residues in the T-cell receptor zeta cytoplasmic domain mediate membrane association and modulate signaling. *Proc Natl Acad Sci U S A,* 108**,** 19323-8.
ZHANG, K., GEDDIE, M. L., KOHLI, N., KORNAGA, T., KIRPOTIN, D. B., JIAO, Y., RENNARD, R., DRUMMOND, D. C., NIELSEN, U. B., XU, L. H. & LUGOVSKOY, A. A. 2015. Comprehensive optimization of a single-chain variable domain antibody fragment as a targeting ligand for a cytotoxic nanoparticle. *Mabs,* 7**,** 42-52.
ZHAO, Q., AHMED, M., TASSEV, D. V., HASAN, A., KUO, T. Y., GUO, H. F., O'REILLY, R. J. & CHEUNG, N. K. V. 2015a. Affinity maturation of T-cell receptor-like antibodies for Wilms tumor 1 peptide greatly enhances therapeutic potential. *Leukemia,* 29**,** 2238-2247.
ZHAO, Z., CONDOMINES, M., VAN DER STEGEN, S. J. C., PERNA, F., KLOSS, C. C., GUNSET, G., PLOTKIN, J. & SADELAIN, M. 2015b. Structural Design of Engineered Costimulation Determines Tumor Rejection Kinetics and Persistence of CAR T Cells. *Cancer Cell,* 28**,** 415-428.
ZHENG, Z. L., CHINNASAMY, N. & MORGAN, R. A. 2012. Protein L: a novel reagent for the detection of Chimeric Antigen Receptor (CAR) expression by flow cytometry. *Journal of Translational Medicine,* 10.
ZHU, F., WEI, G., ZHANG, M., ZHAO, H., WU, W., YANG, L., HU, Y. & HUANG, H. 2020. Factors Associated with Costs in Chimeric Antigen Receptor T-Cell Therapy for Patients with Relapsed/Refractory B-Cell Malignancies. *Cell Transplant,* 29**,** 963689720919434.